ASYMPTOTIC, HOMOGENIZED SP_2 APPROXIMATIONS TO THE NEUTRON TRANSPORT EQUATION

by

Thomas Saller

A dissertation submitted in partial fulfillment
of the requirements for the degree of
Doctor of Philosophy
(Nuclear Engineering and Radiological Sciences and Scientific Computing)
in the University of Michigan
2015

Doctoral Committee:

Professor Edward W. Larsen, Co-Chair
Professor Thomas J. Downar, Co-Chair
Professor Charles R. Doering
Professor William R. Martin

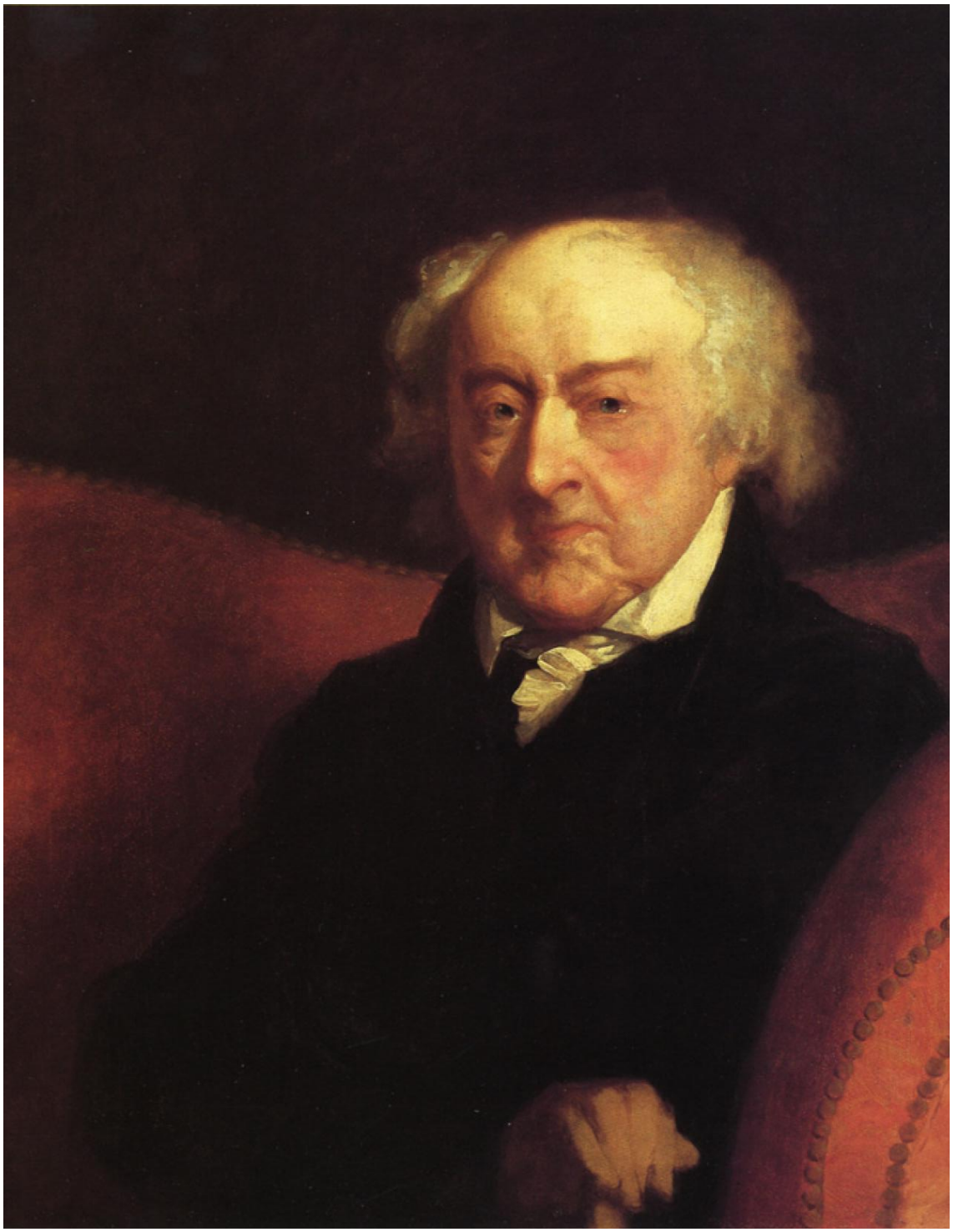

“Stop looking at me like that.”
- John Adams

2015

ACKNOWLEDGMENTS

It is impossible to properly acknowledge all of the people who helped make this document a reality, but I will try my best.

First, I would like to thank my committee:

- My co-advisors, Professors Ed Larsen and Tom Downar. It was Professor Larsen's class – NERS 644: Transport Theory – that launched my interest in asymptotic theory and its application to neutron transport. This work is largely due to his support and advice in our many, many meetings. It was Professor Downar that brought me to Michigan in the first place, and gave me the time and freedom to find out just what I wanted to do. His encouragement and guidance has been invaluable.
- The rest of my patient committee, Professors Bill Martin and Charles Doering, whose suggestions served to focus and greatly improve this work.

Next, I would like to thank everyone else at the University of Michigan that gave me support, advice, and friendship whenever I needed it:

- Andrew Hall – roommate, officemate, and friend extraordinaire.
- The MPACT team, namely Brendan Kochunas, Ben Collins, and Dan Jabaay, who introduced me to the modern world of programming.
- Travis Trahan, who helped get this whole asymptotic ball rolling, showing the world that asymptotic diffusion is great (and by extension, that asymptotic SP_2 is greater).
- The rest of the 4th floor of the Engineering Research Building, particularly Aaron Wysocki, Mitchell Young, Michael Rose, Tim Grunloh, and Andy Ward.

- Kendra Keady, who helped get me through the last few months of writing and defending my thesis. Without you and your patient kindness, the past five years might have been for naught.

I must also thank my family:

- My parents, Julie and Art, who gave me all the love, support, and good genes I needed to get where I am today.
- My siblings, Stephen, Kevin, and Katy, who will always be my best friends.
- My Ann Arbor family, Aunt Brenda, Uncle David, Hannah, and Rachel, who made my home away from home infinitely more pleasant.

The miscellaneous thanks:

- The Ann Arbor District Library, which kept me well supplied with movies, comics, and hundreds of cheap, used books my entire time in Ann Arbor.
- My Broadway housemates, who tolerated me as I lived happily in my basement for two great years.
- Professor Erich Schneider at the University of Texas, who first gave me a taste of the tantalizing world of computational neutron transport.

Finally, I would like to acknowledge my financial support these long years:

- The Department of Energy Stewardship Science Graduate Fellowship, grant number DE-FC52-08NA28752, who gave me four years of invaluable funding, wonderfully supported, as always, by the Krell Institute.
- Professors Downar and Martin, who gave me both financial support and the wonderful opportunity to experience teaching as a Graduate Student Instructor.

TABLE OF CONTENTS

LIST OF FIGURES

LIST OF TABLES

LIST OF APPENDICES

ABSTRACT

ASYMPTOTIC, HOMOGENIZED SP_2 APPROXIMATIONS TO THE NEUTRON TRANSPORT EQUATION

by

Thomas Saller

Co-Chairs:

Edward W. Larsen
Thomas J. Downar

Many current-generation reactor analysis codes use the diffusion approximation to efficiently calculate neutron fluxes. As a result, there is considerable interest in methods that provide a more accurate diffusion solution without significantly increasing computational costs. In this work, an asymptotic analysis, previously used to derive a homogenized diffusion equation for lattice-geometry systems, is generalized to derive a one-dimensional, one-group homogenized SP_2 equation as a more accurate alternative to the standard homogenized diffusion equation. This analysis results in new diffusion coefficients and an improved formula for flux reconstruction. The asymptotic SP_2 formulation is compared to standard SP_2, asymptotic diffusion, and standard diffusion for several test problems. Both the eigenvalue and reconstructed fluxes are examined. In general, the asymptotic equations are more accurate than the standard equations, and SP_2 is more accurate than diffusion theory, especially for optically small systems.

The calculation of more accurate multigroup cross sections is considered. Standard multigroup cross sections are designed to preserve both the (multigroup) infinite medium neutron spectrum and eigenvalue; this property still holds if the multigroup cross sections are modified by a multiplicative scaling factor. In this thesis, a formula for the scaling factor is derived that makes the modified multigroup cross sections satisfy the asymptotic diffusion or SP_2 limit of the neutron transport equation. Numerical simulations demonstrate that the resulting scaled multigroup cross sections yield more accurate results than standard, unscaled cross sections for multigroup eigenvalue problems in finite media.

Finally, the asymptotic analysis is then extended to a hypothesized multigroup, spatially homogenized SP_2 equation. The hypothesized equation uses standard homogenized cross section definitions, but leaves the diffusion coefficients undefined. The asymptotic analysis of the multigroup SP_2 equation results in a monoenergetic SP_2 equation, similar to the one obtained for the continuous energy transport equation. By requiring that the hypothesized multigroup SP_2 equation have the same asymptotic limit as the continuous energy transport equation, we establish a condition that the additional multigroup diffusion coefficient, $D_{2,g}$, must satisfy. Two logical definitions for $D_{2,g}$ are chosen, but numerical results indicate that they are inconsistent in their accuracy, and are frequently outperformed by both standard multigroup diffusion and SP_2.

CHAPTER 1

Introduction

In this chapter, we motivate the asymptotic derivations performed in Chapters 3, 5, and 7. We present a brief history of the simplified P_2 method and the application of asymptotic theory to neutron transport. Then we present an outline of the rest of this dissertation.

1.1 Motivation

Reactor physics, a field dedicated to calculating the distribution of reaction rates in a nuclear reactor core, involves solving the Boltzmann transport equation for neutron fluxes:

$$\begin{aligned}
&\boldsymbol{\Omega}\cdot\boldsymbol{\nabla}\psi(\boldsymbol{x},\boldsymbol{\Omega},E)+\Sigma_t(\boldsymbol{x},E)\psi(\boldsymbol{x},\boldsymbol{\Omega},E)\\
&\quad=\int_0^\infty\int_{4\pi}\Sigma_s(\boldsymbol{x},\boldsymbol{\Omega}'\to\boldsymbol{\Omega},E'\to E)\psi(\boldsymbol{x},\boldsymbol{\Omega}',E')\,d\Omega'dE' \\
&\qquad+\lambda\frac{\chi(\boldsymbol{x},E)}{4\pi}\int_0^\infty\int_{4\pi}\nu\Sigma_f(\boldsymbol{x},E')\psi(\boldsymbol{x},\boldsymbol{\Omega}',E')\,d\Omega'dE',
\end{aligned}\tag{1.1}$$

or in 1-D:

$$\begin{aligned}
&\mu\frac{\partial\psi}{\partial x}(x,\mu,E)+\Sigma_t(x,E)\psi(x,\mu,E)\\
&\quad=\int_0^\infty\int_{-1}^1\Sigma_s(x,\mu'\to\mu,E'\to E)\psi(x,\mu',E')\,d\mu'dE' \\
&\qquad+\lambda\frac{\chi(x,E)}{2}\int_0^\infty\int_{-1}^1\nu\Sigma_f(x,E')\psi(x,\mu',E')\,d\mu'dE',
\end{aligned}\tag{1.2}$$

where

$$\lambda = \frac{1}{\mathrm{k}} = 1 - \rho = \text{ eigenvalue}\,,$$

and

$$\psi(x,\mu,E) = \text{ eigenfunction}\,.$$

The neutron angular flux, $\psi(x,\mu,E)$, is a fundamental component of reactor analysis. For example, the angular integral of $\psi(x,\mu,E)$ is required to calculate fission rates that, when combined with thermal-hydraulic codes, are used to assess the safety of a core. The angular flux may also be used to estimate breeding ratios and determine fuel utilization factors.

The field of computational reactor physics can be subdivided into three classes of numerical methods: deterministic transport, Monte Carlo, and diffusion. The first two refer to methods that solve the Boltzmann equation for angular fluxes. Deterministic methods (e.g. discrete ordinates, or method-of-characteristics) discretize Eq. (1.1) in space, angle, and energy, and solve the resulting differential equation. The reactor core geometry is modeled in detail, and many energy groups are used to capture resonance effects as accurately as possible [1]. In the Monte Carlo method, individual neutrons are followed on random walks, and their average behavior is used to estimate quantities like neutron fluxes, reaction rates, or neutron currents [2].

Both deterministic and Monte Carlo methods can generate high fidelity, pin-resolved solutions. This accuracy, however, comes at a cost. The Westinghouse AP1000, for example, has 41,448 fuel pins [3], each of which must be spatially subdivided both radially and axially to be accurately simulated. The computational burden for performing a full-core, pin-resolved simulation often requires computing clusters, or even supercomputers, like the Cray XK7 Titan supercomputer at Oak Ridge [4].

In diffusion theory, the angular variable in Eq. (1.2) is eliminated by assuming that the angular flux is a linear function of angle and integrating Eq. (1.2) over all angles. This yields the approximate *neutron diffusion equation*, which is discretized only in space and energy:

$$\frac{\partial}{\partial x} J(x,E) + \Sigma_t(x,E)\phi(x,E) = \int_0^\infty \Sigma_{s,0}(x,E' \to E)\phi(x,E')dE' + \lambda\chi(x,E)\int_0^\infty \nu\Sigma_f(x,E')\phi(x,E')dE', \tag{1.3a}$$

where

$$J(x,E) = -\frac{1}{3\Sigma_{tr}(x,E)}\frac{\partial}{\partial x}\phi(x,E), \tag{1.3b}$$

and

$$\Sigma_{tr}(x,E) = \Sigma_t(x,E) - \Sigma_{s,1}(x,E). \tag{1.3c}$$

In Eqs. (1.3a) and (1.3c), $\Sigma_{s,n}(x,E)$ is the n-th Legendre moment of the differential scattering cross section.

Modern diffusion codes further reduce the number of unknowns by (i) "homogenizing" over some spatial region (typically either a fuel pin or assembly) and (ii) collapsing in energy, reducing the number of energy groups from tens or hundreds to as few as two. This involves taking a weighted average (e.g. flux weighted) of space- and energy-dependent cross sections for a specified spatial region and energy group structure. The resulting system of equations can be solved efficiently using finite difference or nodal methods, making transient calculations more tractable than with transport theory.

Fig. 1.1 illustrates the homogenization process. Each unique assembly in a core is simulated with zero-current boundary conditions. The resulting assembly flux solution is used to generate homogenized cross sections, which are used in a full-core diffusion calculation.

Due to its relatively low memory and CPU requirements, homogenized diffusion is fre-

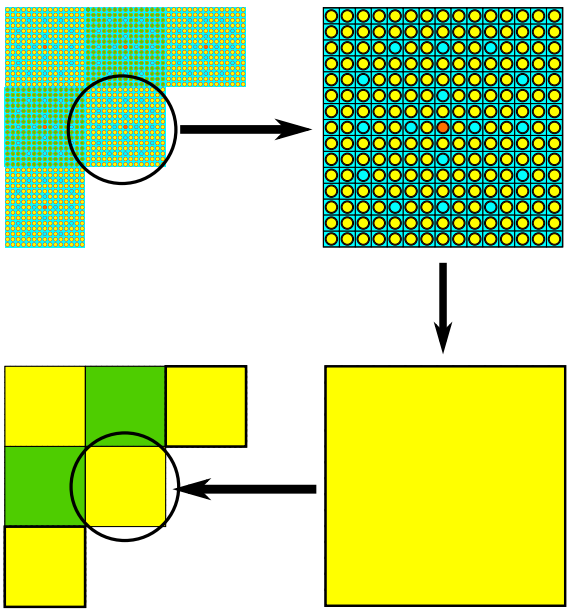

Figure 1.1: Homogenization

quently the workhorse in full core depletion and transient calculations. The commercial pressurized water reactors (PWRs) and boiling water reactors (BWRs) that have been built and operated successfully for the past 50 years have largely relied on homogenized diffusion for core analysis. However, in our current economic climate, many utilities find the cost of a new 1000 MW_e nuclear power plant prohibitive [5]. Furthermore, most developing countries do not have the infrastructure necessary to accommodate large reactors [6]. In response to these concerns, there is a push to develop Small Modular Reactors (SMRs); reactors that are smaller, less expensive, more easily manufactured, and can be assembled at a plant [5].

The linear-function-of-angle assumption made in the derivation of standard diffusion theory implies several other assumptions. One of them, the assumption that spatial flux gradients are small relative to the neutron flux, may not be valid in SMRs, where the small core leads to sharp flux gradients at the reactor core boundaries. We do not expect standard diffusion methods to treat steep flux gradients with sufficient accuracy. For this reason, there is a need for more accurate diffusion-like models of lattice-geometry neutron trans-

port that do not significantly increase the computational costs for the current generation of computing platforms. Therefore, we seek to develop more accurate diffusion-like methods that maintain the simplicity and speed of diffusion calculations while increasing accuracy. The development of such diffusion-like models is the primary theme of this thesis.

1.2 History

The use of homogenized multigroup diffusion and SP_N methods in reactor core simulations is routine today. However, the theoretical foundation of these methods is incomplete, and numerous open questions exist. Here, we briefly review the methodologies currently in practice.

The term "homogenized multigroup diffusion" indicates that approximations are made in space (homogenized), energy (multigroup), and angle (diffusion). These three general types of approximations are usually (but not always) considered separately.

1.2.1 Multigroup Approximation

Arguably, the most basic and difficult of the discretizations of the independent variables in the neutron transport problem occurs with the energy variable. In practical problems, neutron energies range over eight orders of magnitude, and over that range, neutron cross sections can vary rapidly with respect to the energy variable E. To "resolve" these rapid variations on an energy grid would require thousands, if not millions, of energy groups. Instead, a more sophisticated approach is taken, in which many fewer energy groups are used (often, 2–50), and the group constants are defined to preserve features of simpler problems that are "close to" the problem under consideration.

This procedure is not unique – and yet, the generation of "accurate" multigroup cross sections is a fundamental prerequisite for performing accurate reactor core simulations. The discretizations of the angular and spatial variables in the transport equation are, in

comparison to the discretization of the energy variable, straightforward. The discretization of E is arguably the weak link in discretizations of the transport equation for practical neutron transport problems.

Everything written in the preceding paragraph applies to each of the relevant cross sections in the Boltzmann transport equation. The multigroup approximation is a common one in reactor physics, and has been covered in many basic texts [7–9]. Often, the multigroup approximation is discussed in conjunction with the diffusion approximation [10], which is covered in Section 1.2.3.

1.2.2 Homogenization Approximation

For a "lattice" system (a periodic array of pin cells or assemblies), typically the next step after the multigroup approximation is the simplification of the multigroup transport equation by "homogenizing" the cross sections. For the original lattice system, the multigroup cross sections are periodic functions of the spatial variable, having the periodicity of the lattice. In homogenization theory, these highly space-dependent cross sections are replaced by "homogenized" cross sections, which are independent of space, but are nonetheless chosen to accurately capture the neutron flux. Often, the highly detailed cross sections within each assembly are homogenized, producing a histogram-like map of cross sections across a reactor core in which the (homogenized) cross sections are constant within each assembly, but can vary spatially between different assemblies.

Traditionally, the homogenization process is done in such a way that certain features of an idealized (e.g. infinite-medium) problem are preserved. Other than this, there is little (if any) theoretical justification for the process of homogenizing the cross sections in the multigroup Boltzmann transport equation. To say this more directly: there is no known theoretical justification for replacing the multigroup transport equation for a lattice medium by a multigroup transport equation with homogenized coefficients. Basically, this procedure is ad hoc.

Homogenization, at least for the transport equation, is infrequently covered in standard texts. Stamm'ler and Abbate briefly cover homogenization [8], as does Stacey [7]. More frequently, homogenization is considered with the diffusion approximation, discussed in the next section.

In Chapters 5 and 6 of this thesis, we address the process of homogenizing the multigroup lattice-geometry transport equation. In particular, we show in Chapter 5 that a standard homogenization method – which preserves certain features of an infinite-medium problem – can be generalized to preserve an asymptotic feature of finite homogenized transport problems. In Chapter 6, we present numerical results to demonstrate that the generalization developed in Chapter 5 is more accurate than the standard homogenization method.

1.2.3 Spherical Harmonics and Diffusion Approximations

At this point, the energy variable in the transport equation has been discretized with the multigroup approximation, and the cross sections have been spatially homogenized. We now address the discretization of the angular variable $\boldsymbol{\Omega}$. A classical method for discretizing $\boldsymbol{\Omega}$ is the spherical harmonic method. Here, the angular flux is expanded in a truncated series of spherical harmonics,

$$\begin{aligned}\psi_g(\boldsymbol{x},\boldsymbol{\Omega}) &= \sum_{n=0}^{\infty}\sum_{m=-n}^{n}\phi_{g,n,m}(\boldsymbol{x})\,Y_n^m(\boldsymbol{\Omega}) \\ &\approx \sum_{n=0}^{N}\sum_{m=-n}^{n}\phi_{g,n,m}(\boldsymbol{x})\,Y_n^m(\boldsymbol{\Omega})\,, \end{aligned} \tag{1.4}$$

where $Y_n^m(\boldsymbol{\Omega})$ are spherical harmonic functions. The spherical harmonic equations for $\phi_{g,n,m}(\boldsymbol{x})$ are obtained by introducing Eq. (1.4) into the transport equation, Eq. (1.1), and operating by:

$$\int_{4\pi} Y_{n'}^{m'*}(\boldsymbol{\Omega})(\cdot)\,d\Omega\,, \qquad 0\le n'\le N,\ -n'\le m'\le n\,. \tag{1.5}$$

In practice, the $N = 1$ (P_1) approximation is most widely used. For problems with anisotropic scattering, if a further approximation (which effectively diagonalizes the first angular moment of the group-to-group scattering matrix) is used, then the resulting approximation to the P_1 equation is called the "diffusion" approximation [8, 9].

At this point, we have derived a "homogenized multigroup diffusion approximation" to the Boltzmann transport equation. The homogenized, multigroup diffusion approximation has been repeatedly addressed in the literature [8–10], as have attempts to improve its solution (e.g. Koebke's "equivalence theory" [11], Smith's "generalized equivalence theory" [12], and "current discontinuity factors" [13]).

Remark: It is known that (i) the homogenization approximation greatly simplifies the spatial and angular dependence of the neutron flux, (ii) this simplification facilitates the use of the P_N approximation, and (iii) these approximations may not be justified in practice. This realization led to a significant amount of work that attempted to derive multigroup diffusion equations without the ad-hoc homogenization step [14–16].

1.2.4 Simplified P_N

In an attempt to generate multidimensional solutions of homogenized multigroup transport equations that are more accurate than the P_1 approximation but less expensive than the P_N approximation, $N > 1$, [which has $O(N^2)$ equations], Gelbard proposed the Simplified P_N (SP_N) approximation for the angular variable [17]. For many years, Gelbard's intuitive derivation of these equations was viewed with suspicion, but it was later found that the SP_N equations can be derived (i) asymptotically and (ii) variationally [18–24]. Today, it is widely recognized that SP_3 approximations to the homogenized multigroup transport equation are more accurate than P_1 approximations, and are often sufficiently more accurate to justify the computational cost of solving a larger system of equations.

Nevertheless, in applications of homogenized SP_N, the error associated with the ad hoc homogenization step is still present. To date, there has been no systematic attempt to extend

to SP_N the work by Gelbard, Benoist, Trahan, et al. to systematically derive homogenized multigroup diffusion equations without the ad-hoc homogenization step [15, 25].

1.3 Goals of this Thesis

Here we provide an overview of the goals of this thesis. A more detailed description follows in section 1.4.

The novel research included in this thesis consists of three parts. The first part is covered in Chapters 3 and 4. In Chapter 3, the 1-D lattice-geometry continuous energy neutron transport equation is subjected to an asymptotic expansion, which was first considered by Trahan [25]. The expansion involves a small parameter ϵ, which indicates the inverse of the thickness of the system. [$\epsilon = 0$ denotes an infinite system, while $0 < \epsilon \ll 1$ denotes a large, finite system.] If the asymptotic analysis is performed with $O\left(\epsilon^2\right)$ error, one obtains Trahan's result [15], a monoenergetic homogenized diffusion equation. In this thesis, we perform the asymptotic analysis with $O\left(\epsilon^4\right)$ error and obtain a monoenergetic homogenized SP_2 result. However, the coefficients in our SP_2 equation are very different from those in the standard SP_2 equation. In Chapter 4, we provide numerical results that confirm the validity of the asymptotic analysis in Chapter 3.

The second part of this thesis is presented in Chapters 5 and 6, which focus on the definition of multigroup transport cross sections. We show that the standard method for deriving multigroup cross sections can be generalized in a way that preserves extra physics. The primary analytic tool in Chapter 5 is an asymptotic expansion similar to that considered in Chapter 3. The difference is that in Chapter 3, the goal is to derive an asymptotic limit of the transport equation - a homogenized SP_2 equation. In Chapter 5, the goal is to improve the accuracy of the homogenized multigroup cross sections.

The third part of this thesis is detailed in Chapters 7 and 8. Here we attempt to generalize Trahan's asymptotic homogenized multigroup diffusion results to multigroup SP_2.

Thus, we *conjecture* a form of the homogenized multigroup SP_2 equations, and we design the definitions of the homogenized cross sections and diffusion coefficients in these equations so that as many exact elements of transport physics as possible are preserved. [For an infinite medium, the exact eigenvalue and homogenized eigenfunction are preserved.] The theoretical derivations of this homogenized SP_2 theory are given in Chapter 7. In Chapter 8, numerical results are presented. Unfortunately, these results do not demonstrate that the new (asymptotic, multigroup homogenized SP_2) results are a systematic improvement over Trahan's asymptotic, multigroup homogenized diffusion results. A major issue is that the prescription of the homogenized multigroup SP_2 diffusion coefficients is not unique. The prescription that Trahan used for his diffusion coefficients worked well for his problems, but similar prescriptions for the SP_2 equations do not seem to yield a systematic improvement in accuracy. Our results indicate that further work should be done before a practical homogenized SP_2 approximation could be used in practice.

1.4 Outline of the Remainder of this Thesis

A detailed description of the remainder of this thesis is as follows.

In Chapter 2, we review some of the common methods of solving the neutron transport equation. These are subdivided into deterministic transport methods, Monte Carlo methods, and homogenized diffusion-based methods.

In Chapter 3, we consider a continuous energy, spatially periodic 1-D system, comparable to a 1-D model of a reactor core. We apply an asymptotic analysis to this problem, assuming that the system is optically thick, as defined by the small parameter $\epsilon = 1/N$, where N is the number of spatial cells. The asymptotic analysis yields a result which is exact when $\epsilon = 0$ (an infinitely thick system with a periodic solution), but which is approximate when $0 < \epsilon \ll 1$ (a finite, optically thick system with a nearly-periodic solution and a weak spatial "buckling"). Our analysis is similar to that performed earlier by Trahan [15],

but we carry the analysis to higher order. In Trahan's work, a monoenergetic homogenized diffusion equation is the final result, having an $O(\epsilon^2)$ error. Our work extends the analysis to $O(\epsilon^4)$ error, which yields a more complicated homogenized P_2 equation. We also obtain a higher-order "flux reconstruction" formula, which expresses the angular flux ψ in terms of (i) specified energy-dependent functions that are spatially periodic, and (ii) the solution of the monoenergetic homogenized SP_2 equation, which is not spatially periodic. The leading-order term in this expansion of ψ is the usual "flux reconstruction" formula commonly used in reactor physics calculations. One of the higher-order terms in this expansion was derived by Trahan [15], while the others are new and unfamiliar.

Next, in Chapter 4, we consider several 1-D monoenergetic transport problems that are solved (i) directly, using the discrete ordinates approximation with diamond differencing, and (ii) using the approximate homogenized P_2 theory developed in Chapter 3. For the problems considered, numerical results demonstrate that the new asymptotic homogenized SP_2 approximation is a significant improvement over the asymptotic homogenized diffusion theory developed by Trahan. (Trahan himself showed that his asymptotic homogenized diffusion theory was an improvement over standard homogenized diffusion methods.) Overall, the numerical results presented in Chapter 4 demonstrate that for problems in which the asymptotic analysis is justified (1-D, spatially periodic, many spatial cells in width), the results of the analysis are significantly more accurate than standard homogenized diffusion and SP_2 approximations.

In Chapter 5, we consider a fundamentally different problem – that of accurately defining multigroup cross sections for multigroup transport problems. As in Chapter 3, we consider a 1-D continuous-energy transport problem and begin with the standard methodology of defining multigroup cross sections for this problem, by calculating weighted averages of the cross sections over each energy group. The "weights" are taken to be the infinite-medium neutron spectrum function (the solution of the infinite-medium problem). The resulting multigroup cross sections preserve both the infinite medium eigenvalue and the

infinite medium multigroup eigenfunction. However, it turns out that there are many other multigroup cross sections that preserve these two properties. In Chapter 5, we show that a simple modification of the multigroup cross sections - obtained by multiplying the cross sections by a group-independent scaling factor ρ - will, if ρ is chosen properly, enable the scaled multigroup transport equations to preserve an asymptotic limit of the continuous-energy transport equation. Essentially, the scaling factor ρ allows the multigroup transport equation to preserve some space-dependent transport physics that are not preserved by the standard, unscaled multigroup cross sections. In Chapter 5, we derive two explicit expressions for the scaling factor ρ.

In Chapter 6, we numerically test the theory developed in Chapter 5. We initially pose several 1-D problems hat use higher-order multigroup cross sections. Then we consider approximate transport problems, using fewer energy groups with group-collapsed cross sections, both with and without the scaling factor derived in Chapter 5. We show that for all the cases considered, (i) the inclusion of the scaling factor improves the accuracy of the few-group calculation, and (ii) the scaling factor ρ is nearly equal to unity when the number of groups is large but is not necessarily close to unity when the number of groups is small, as expected.

In Chapter 7, we apply an asymptotic analysis to a hypothesized, spatially homogenized, multigroup, 1-D SP_2 equation. The hypothesized equation uses standard homogenized cross section definitions, but leaves the diffusion coefficients undefined. To facilitate the asymptotic analysis, we again assume that the system is thick relative to the size of a single cell. The analysis is comparable to one performed by Trahan [15], but with a hypothesized multigroup SP_2 equation rather than a hypothesized multigroup diffusion equation. Indeed, we select the same definition for the multigroup diffusion coefficient ($\overline{D}_{0,g}$) that Trahan chose. The asymptotic analysis of the multigroup SP_2 equation results in a monoenergetic SP_2 equation, similar to the one obtained in Chapter 3. By requiring that the hypothesized multigroup SP_2 equation have the same asymptotic limit as the continuous

energy transport equation, we establish a condition that the other multigroup diffusion coefficient, $\overline{D}_{2,g}$, must satisfy. There are many ways to define $\overline{D}_{2,g}$, and we choose two logical definitions to be tested in Chapter 8.

In Chapter 8, the SP_2 equation hypothesized in Chapter 7 is tested for a series of homogeneous media. The multigroup SP_2 equations with asymptotically-defined coefficients are inconsistent in their accuracy, and are frequently outperformed by standard SP_2 and even diffusion. The most likely explanation for these inconsistencies is the definition of $\overline{D}_{2,g}$, as Eq. (7.31) does not lend itself to an unambiguous definition of $\overline{D}_{2,g}$. Future work is suggested to try an obtain a less ambiguous, more accurate definition for $\overline{D}_{2,g}$.

Finally, in Chapter 9, we summarize our work and numerical results, and we discuss potential future work.

CHAPTER 2

Standard Neutron Transport Methodology

Before we discuss the derivation of the asymptotic SP_2 equations, several standard reactor physics methods are first summarized. The discrete ordinates method, the method of characteristics, and the spherical harmonics method all represent deterministic transport methods. Monte Carlo characterizes stochastic transport methods. Finally, homogenized diffusion theory and homogenized simplified P_N are the two primary diffusion-based methods.

2.1 Deterministic Transport Methods

In deterministic transport methods, the neutron transport equation is discretized and solved. Common deterministic methods include discrete ordinates, the method of characteristics, and spherical harmonics.

2.1.1 Multigroup, 1-D Discrete Ordinates (S_N)

In the discrete ordinates (S_N) method [1, 2], the continuous Boltzmann equation, Eq. (1.2), is broken up into discrete angular bins, resulting in a series of differential equations for each discrete angle. If we also apply the multigroup approximation from Section 1.2.1, we

have the multigroup, 1-D discrete ordinates equations:

$$\mu_n \frac{\partial \psi_{n,g}}{\partial x}(x) + \Sigma_{t,g}(x)\psi_{n,g}(x) = \sum_{g=1}^{G}\sum_{n'=1}^{N}\Big(\Sigma_{s,g'\to g}(x,\mu_{n'}\to\mu_n)\psi_{n',g'}(x)\Big)w_{n'} + \lambda\frac{\chi_g(x)}{2}\sum_{g=1}^{G}\sum_{n'=1}^{N}\Big(\nu\Sigma_{f,g'}(x)\psi_{n',g'}(x)\Big)w_{n'}\,. \tag{2.1}$$

If we integrate Eq. (2.1) over a spatial bin ($x_{i-1/2}$ to $x_{i+1/2}$), define:

$$h_i = x_{i+1/2} - x_{i-1/2}\,, \tag{2.2a}$$

$$\psi_{i,n,g} = \frac{1}{h_i}\int_{x_{i-1/2}}^{x_{i+1/2}} \psi_g(x,\mu_n)\,dx\,, \qquad \mu \in [\mu_{n-1/2},\mu_{n+1/2}]\,, \tag{2.2b}$$

and

$$\psi_{i\pm1/2,n,g} = \psi_g(x_{i\pm1/2},\mu_n)\,, \qquad \mu \in [\mu_{n-1/2},\mu_{n+1/2}]\,, \tag{2.2c}$$

and apply the diamond difference approximation:

$$\psi_{i,n,g} = \frac{1}{2}\Big(\psi_{i+1/2,n,g} + \psi_{i-1/2,n,g}\Big), \tag{2.3}$$

Eq. (2.1) becomes:

$$\frac{\mu_n}{h_i}\Big(\psi_{i+1/2,n,g} - \psi_{i-1/2,n,g}\Big) + \Sigma_{t,i,g}\psi_{i,n,g} = \sum_{g=1}^{G}\sum_{n'=1}^{N}\Big(\Sigma_{s,i,g'\to g}(\mu_{n'}\to\mu_n)\psi_{i,n',g'}\Big)w_{n'} + \lambda\frac{\chi_g}{2}\sum_{g=1}^{G}\sum_{n'=1}^{N}\Big(\nu\Sigma_{f,i,g'}\psi_{i,n',g'}\Big)w_{n'}\,. \tag{2.4}$$

Eqs. (2.3) and (2.4) are the 1-D, multigroup, diamond-differenced, discrete ordinates equations.

The spatial index ranges from $i = 1$ to I and the angular from $n = 1$ to N. Eq. (2.3), the diamond difference auxiliary equation, provides the additional relationship necessary to solve Eq. (2.4).

Eqs. (2.3) and (2.4) are solved in a sweeping, iterative manner. The right side of Eq. (2.4) (the source) is lagged, beginning with an initial guess. For a 1-D problem, the equations can be solved starting at the left boundary and moving to the right for $n = [1, N/2]$ ($\mu_n > 0$). Then, starting from the right and moving to the left, the equations are solved for $n = [N/2+1, N]$ ($\mu_n < 0$), completing a single iteration. This is repeated, updating the source on the right side of Eq. (2.4) at the end of each iteration, until some convergence is achieved.

Deterministic methods can be as accurate as the user desires by increasing the number of angles, energy groups, and spatial bins (though non-planar geometries can get complicated). However, this is limited by the computer resources available and, as in all neutron transport calculations, the accuracy of the cross section data.

2.1.2 Method of Characteristics (MOC)

The method of characteristics (MOC) [1, 2, 9] is an "integral transport" method, in which the integro-differential transport equation is converted to an integral equation. Like S_N, the problem is split into discrete spatial regions, angles, and energy bins. Unlike S_N, the transport equation itself is not discretized. Rather, it is solved analytically in each region along a line in a single (characteristic) direction. Scalar quantities, like the neutron flux or reaction rates, are constructed by summing their individual angular components in a region.

To calculate the angular flux in a given region, Eq. (1.2) is first converted to integral

form:

$$\psi(x_0+s\mu,\mu,E) = \exp\Big(-\int_0^s \Sigma_t(x_0+s'\mu,E)\,ds'\Big)\psi(x_0,\mu,E) + \int_0^s \exp\Big(-\int_{s'}^s \Sigma_t(x_0+s''\mu,E)\,ds''\Big)q(x_0+s'\mu,\mu,E)\,ds', \tag{2.5a}$$

where

$$q(x,\mu,E) = \int_0^\infty \int_{-1}^1 \Sigma_s(x,\mu'\to\mu,E'\to E)\psi(x,\mu',E')\,d\mu'\,dE' + \lambda\frac{\chi(x,E)}{2}\int_0^\infty \int_{-1}^1 \nu\Sigma_f(x,E')\psi(x,\mu',E')\,d\mu'\,dE', \tag{2.5b}$$

and x_0 lies on the region's boundary.

Eq. (2.5a) can be analytically solved if the incoming angular flux $\psi(x_0,\mu,E)$ is known and we assume that the cross sections and source in the region are constant. The latter condition is known as the "flat source approximation," and is one of the key disadvantages of MOC. However, it is only a significant disadvantage if the flux varies rapidly in the region; if the shape of the flux is relatively flat, then this approximation has small errors.

With these assumptions, the angular flux inside a flat source region i is

$$\psi_i(x_0+s\mu,\mu,E) = e^{-\Sigma_{t,i}(E)s}\psi(x_0,\mu,E) + \frac{q_i(\mu,E)}{\Sigma_{t,i}(E)}\Big(1-e^{-\Sigma_{t,i}(E)}\Big), \tag{2.6a}$$

where

$$q_i(\mu,E) = \int_0^\infty \int_{-1}^1 \Sigma_{s,i}(\mu'\to\mu,E'\to E)\psi_i(\mu',E')\,d\mu'\,dE' + \lambda\frac{\chi_i(E)}{2}\int_0^\infty \int_{-1}^1 \nu\Sigma_{f,i}(E')\psi_i(\mu',E')\,d\mu'\,dE'. \tag{2.6b}$$

Eq. (2.6a) is solved along "rays" that overlay the entire problem, with the exiting flux from one region used as the incoming angular flux for the next region in a ray's path. A

region may contain more than one ray in a given direction; more rays in a region can lead to a more accurate solution.

These rays allow MOC to handle complex geometries more easily than S_N. Rather than trying to discretize over a complex geometry, MOC only needs to calculate the distance from one surface to another. Furthermore, MOC solutions describe a more accurate representation of the flux within a cell than S_N with diamond differencing. However, if the step characteristics auxiliary equation is chosen instead of diamond difference, S_N and MOC, at least in 1-D, will be identical.

Finally, the MOC angular quadrature is often modified for a problem to ensure that all of the rays will line up. This process is called "modularization." Without properly adjusting the angular weights, modularization can lead to errors when quantities are summed (integrated) over angle.

2.1.3 Spherical Harmonics (P_N)

In the spherical harmonic, or P_N, approximation [1,26], the angular dependence of $\psi(\boldsymbol{x}, \boldsymbol{\Omega}, E)$ is approximated by a spherical harmonics expansion:

$$\begin{aligned} \psi(\boldsymbol{x}, \boldsymbol{\Omega}, E) &= \sum_{n=0}^{\infty} \sum_{m=-n}^{n} \phi_{n,m}(\boldsymbol{x}, E)\, Y_n^m(\boldsymbol{\Omega}) \\ &\approx \sum_{n=0}^{N} \sum_{m=-n}^{n} \phi_{n,m}(\boldsymbol{x}, E)\, Y_n^m(\boldsymbol{\Omega}) \,, \end{aligned} \tag{2.7}$$

where $Y_n^m(\boldsymbol{\Omega})$ is the spherical harmonic function of order n, m.

Introducing Eq. (2.7) into the 3-D transport equation, Eq. (1.1), multiplying the result by the complex conjugate of the spherical harmonic function, $\overline{Y}_n^m(\boldsymbol{\Omega}) = Y_n^{-m}(\boldsymbol{\Omega})$, and integrating over $\boldsymbol{\Omega} \in 4\pi$ yields $(N+1)^2$ equations that are only functions of $\boldsymbol{x}$ and E.

In 1-D, planar geometry, these equations reduce to $(N+1)$ equations,

$$\frac{d}{dx}\left[\frac{n}{2n+1}\phi_{n-1}(x,E)+\frac{n+1}{2n+1}\phi_{n+1}(x,E)\right]+\Sigma_t(x,E)\phi_n(x,E) \tag{2.8}$$
$$=\int_0^\infty \Sigma_{sn}(x,E'\rightarrow E)\phi_n(x,E')dE'+Q(x,E)\delta_{n,0}\,,\ 0\le n\le N\,,$$

where $Q(x)$ is the source (fission, fixed, etc.), and

$$\phi_{-1}(x,E)=\phi_{N+1}(x,E)=0\,. \tag{2.9}$$

The P_N method has the benefit of eliminating the angular variable, but at the cost of greatly increasing the number of differential equations to be solved, especially in 3-D. For $N=1$, the P_N method yields the diffusion equation. P_N is also the basis for the simplified P_N (SP_N) method, discussed in Section 2.3.2.

2.2 Monte Carlo Transport Methods

Monte Carlo methods [2, 27, 28] are stochastic methods that do not make direct use of the neutron transport equation. Rather, they use probabilities and random numbers to simulate individual neutrons' journeys from birth (by fission, or some other source) to death (from absorption, or leaking out of the system). By simulating large numbers of neutrons (on the order of millions+), an approximate solution to the neutron transport equation is obtained. The success of Monte Carlo methods underscores that the Boltzmann equation describes the *average* behavior of a distribution of neutrons, obtained (in principle) by averaging over an infinite number of Monte Carlo particles.

The random walk of a individual neutron in a Monte Carlo method can be described as follows:

1. A neutron is generated with a random location, energy, and angle.

2. The distance the neutron travels before colliding is stochastically determined.
3. If the collision point of the neutron is still in the system, then a collision type (e.g. scattering or fission) is determined, based on the material region the collision occurred in.
4. If the neutron scatters, then a new direction and energy are calculated, and steps 2-4 are repeated.
5. If the neutron is absorbed, or leaks out of the system, then its history is terminated and any quantities of interest are tallied.

Each random event, such as the starting location, the distance to collision, or the direction of a scattered neutron, is calculated using a pseudo-random number generator and probability distribution functions (pdfs). Sampling from a pdf using a random number on $\zeta = [0, 1]$ requires calculating the cumulative distribution function (cdf) and inverting it; if a cdf is too difficult to invert, then rejection sampling may be used [28].

Monte Carlo has several advantages over deterministic transport methods. First, Monte Carlo is theoretically capable of modeling any 3-D geometry that can be described by equations. (Deterministic methods are commonly restricted to geometries with piecewise planar surfaces.) Second, Monte Carlo does not require any discretization (for space, angle, or energy), eliminating any discretization errors. The ability to sample cross sections on a continuous energy spectrum - thereby eliminating any resonance calculations - is a significant advantage. Third, at any point in a simulation the results can be tallied and used as an estimate of the variables of interest. The solution does not need to be converged before it can provide a meaningful value, as long as one takes into account the solution's standard deviation.

However, Monte Carlo also has disadvantages. The primary disadvantage is that the errors in Monte Carlo are statistical in nature, and these decrease slowly with computational effort. According to the Central Limit Theorem, the expected statistical error in the estimate of a quantity of interest is proportional to $1/\sqrt{N}$, where N is the number of histories sampled

(which is proportional to the computational effort). Therefore, to reduce the statistical error in a Monte Carlo simulation by a factor of 10, it is necessary to increase the run time of the simulation by a factor of 100!

For more information on Monte Carlo methods, we direct the reader to [2, 27, 28].

2.3 Homogenized Diffusion-Based Methods

2.3.1 Homogenized Diffusion Theory

In diffusion theory, the diffusion equation, Eq. (1.3a), is solved rather than the transport equation, Eq. (1.2). Without an angular dependence, the number of unknowns is considerably reduced. While the diffusion equation can be solved as-is with finite difference or finite element approximations in space and energy (similar to S_N), it is more frequently further simplified to what is known as *homogenized* diffusion theory.

In homogenized diffusion theory, Eq. (1.3a) is integrated over a region of interest ($L_i = [x_{i+1/2}, x_{i-1/2}]$), typically a pin or assembly, yielding:

$$\int_{L_i} \frac{\partial}{\partial x} J(x,E)\,dx + \int_{L_i} \Sigma_t(x,E)\,\phi(x,E)\,dx = \int_{L_i}\int_0^\infty \Sigma_{s,0}(x,E'\to E)\,\phi(x,E')\,dE'dx + \lambda \int_{L_i} \chi(x,E) \int_0^\infty \nu\Sigma_f(x,E')\,\phi(x,E')\,dE'dx\,, \tag{2.10a}$$

or

$$\frac{1}{h_i}\Big(J(x_{i+1/2},E) - J(x_{i-1/2},E)\Big) + \overline{\Sigma}_{t,i}(E)\,\phi_i(E) = \int_0^\infty \overline{\Sigma}_{s,0,i}(E'\to E)\,\phi_i(E')\,dE' + \lambda\overline{\chi}_i(E)\int_0^\infty \overline{\nu\Sigma}_{f,i}(E')\,\phi_i(E')\,dE'\,, \tag{2.10b}$$

where

$$\phi_i(E) = \frac{1}{h_i}\int_{x_{i-1/2}}^{x_{i+1/2}} \phi(x,E)\,dx\,, \tag{2.11a}$$

$$\overline{\Sigma}_{t,i}(E) = \frac{\int_{x_{i-1/2}}^{x_{i+1/2}} \Sigma_t(x,E)\phi(x,E)dx}{\int_{x_{i-1/2}}^{x_{i+1/2}} \phi(x,E)dx}, \tag{2.11b}$$

$$\overline{\Sigma}_{s,0,i}(E' \to E) = \frac{\int_{x_{i-1/2}}^{x_{i+1/2}} \Sigma_{s,0}(x,E' \to E)\phi(x,E)dx}{\int_{x_{i-1/2}}^{x_{i+1/2}} \phi(x,E)dx}, \tag{2.11c}$$

$$\overline{\nu\Sigma}_{f,i}(E) = \frac{\int_{x_{i-1/2}}^{x_{i+1/2}} \nu\Sigma_f(x,E)\phi(x,E)dx}{\int_{x_{i-1/2}}^{x_{i+1/2}} \phi(x,E)dx}, \tag{2.11d}$$

$$\overline{\chi}_i(E) = \frac{\int_{x_{i-1/2}}^{x_{i+1/2}} \chi(x,E)\int_0^\infty \nu\Sigma_f(x,E')\phi(x,E')dE'dx}{\int_{x_{i-1/2}}^{x_{i+1/2}} \int_0^\infty \nu\Sigma_f(x,E')\phi(x,E')dE'dx}, \tag{2.11e}$$

and

$$h_i = x_{i+1/2} - x_{i-1/2}\,. \tag{2.11f}$$

Using Eq. (1.3b) to eliminate J, Eq. (2.10b) becomes

$$\begin{aligned} -\frac{D(x_{i+1/2},E)}{h_i}\frac{\partial}{\partial x}\phi(x_{1+1/2},E) + \frac{D(x_{i-1/2},E)}{h_i}\frac{\partial}{\partial x}\phi(x_{1+1/2},E) \\ +\overline{\Sigma}_{t,i}(E)\phi_i(E) = \int_0^\infty \overline{\Sigma}_{s,0,i}(E' \to E)\phi_i(E')dE' \\ +\lambda\overline{\chi}_i(E)\int_0^\infty \overline{\nu\Sigma}_{f,i}(E')\phi_i(E')dE', \end{aligned} \tag{2.12}$$

where

$$D(x,E) = \frac{1}{3\Sigma_{tr}(x,E)}\,. \tag{2.13}$$

Eq. (2.12) can be solved in a variety of ways, including finite difference and nodal methods.

Homogenized diffusion can be alternatively derived by first homogenizing the transport equation, Eq. (1.2), rather than the diffusion equation, Eq. (1.3a), and then deriving the diffusion equation from the *homogenized* transport equation. This leads to an altogether different definition of the diffusion coefficient, D [7].

A problem with homogenized diffusion is that the "homogenized" parameters in Eqs. (2.11b-2.11d) require the core scalar flux that we are trying to solve for, $\phi(x,E)$.

In order to avoid this chicken-and-egg problem, the homogenized parameters are typically calculated with a transport calculation (e.g. S_N, or MOC) for each unique region with reflecting boundaries; this "lattice" calculation is one of the key approximations made in homogenized diffusion. The same lattice calculation can be used to generate shaping functions for flux reconstruction and discontinuity factors for a diffusion calculation.

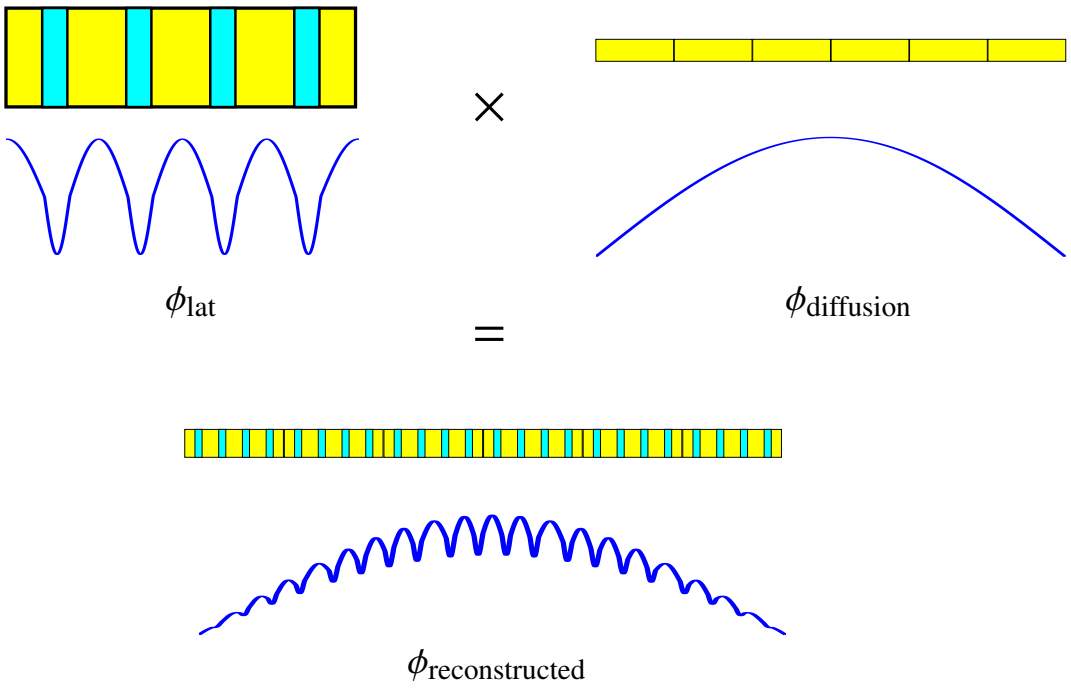

Figure 2.1: Flux Reconstruction

Fig. 2.1 illustrates the basic concept behind flux reconstruction. The detailed spatially periodic flux from a lattice calculation is combined with the non-periodic result from a full core diffusion calculation to achieve an estimate of the detailed scalar flux in the core. In standard homogenized diffusion theory,

$$\phi_{\text{core}}(x,E) = \phi_{\text{diffusion}}(x,E) \times \left[\frac{\phi_{\text{lat}}(x,E)}{<\phi_{\text{lat}}>(E)} \right], \tag{2.14}$$

where $<\phi_{\text{lat}}>(E)$ indicates that $\phi_{\text{lat}}(x,E)$ has been averaged over a cell.

Discontinuity factors are a natural extension of flux reconstruction. If we have a contin-

uous diffusion solution, $\phi_{\text{diffusion}}$, then there is no guarantee that the reconstructed solution is continuous. However, if we allow $\phi_{\text{diffusion}}$ to be discontinuous at the interface between two different homogenized regions, like in Fig. 2.2 (reproduced from [12]), then it is possible to make the reconstructed flux continuous.

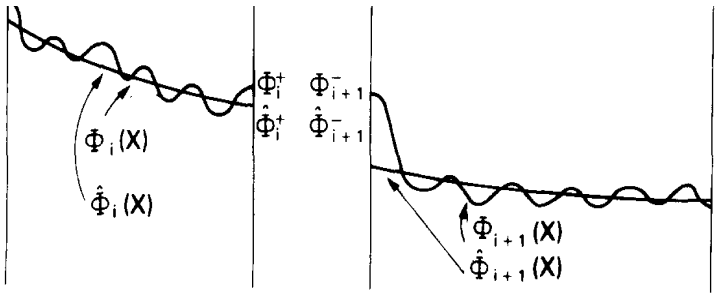

Figure 2.2: Discontinuity Factors [12]

Homogenized diffusion theory remains one of the most widely used methods in reactor physics. Its speed, combined with the accuracy provided by pin power reconstruction and discontinuity factors, make it the preferred technique for transient and burnup calculations.

2.3.2 Homogenized Simplified P_N (SP_N)

The 2-D and 3-D SP_N approximations are a further simplification of the planar 2-D and 3-D P_N equations, respectively. In the traditional derivation, the 1-D P_N equation, Eq. (2.8), is formally modified by replacing any 1-D spatial derivative by the gradient operator,

$$\frac{d}{dx}\phi(x) = \nabla\phi(\boldsymbol{x})\,, \tag{2.15a}$$

or

$$\frac{d}{dx}D\frac{d}{dx}\phi(x) = \nabla\cdot D\nabla\phi(\boldsymbol{x})\,. \tag{2.15b}$$

A downside to SP_N theory is that it, as opposed to P_N theory, does not converge to the transport solution as $N \to \infty$. Regardless, it provides a more accurate alternative to

diffusion theory with computational costs still much less than the transport methods.

It has been shown [18–23] that the SP_N equations can be derived using both asymptotic theory and variational methods. However, *homogenized* SP_N has, until this work, no theoretical justification. Homogenized SP_N is similar to homogenized diffusion theory; by averaging flux-weighted cross sections over a region of interest, a coarse grid can be used and the number of unknowns reduced. However, the choice of diffusion coefficients, already ambiguous in homogenized diffusion theory, is even more uncertain with homogenized SP_N. [As we have already discussed, this leads to practical difficulties discussed in Chapters 7 and 8.]

Current derivations of homogenized SP_N equations are as follows. First, the transport equation with spatially periodic cross sections is approximated by the transport equation with *homogenized* cross sections. (This step is ad hoc.) Second, the 1-D planar, homogenized P_N equations are obtained by approximating the angular flux for this second, homogenized transport equation with a spherical harmonics expansion. (This step is theoretically justified.) Third, the homogenized SP_N equations are obtained by applying the standard SP_N approximation, shown in Eq. (2.15), to the 1-D planar, homogenized P_N equations. (This step has also been theoretically justified by asymptotic and variational analyses.) The Achilles' heel in this current derivation of homogenized SP_N equations is the ad-hoc step of homogenizing the cross sections in the multigroup transport equation. This generally has a profound simplifying effect on the spatial and angular dependence of the transport solution. As has already been explained, the goal of this thesis is to develop methods that do not rely on the ad-hoc step of homogenizing the multigroup transport equation.

CHAPTER 3

Asymptotic Analysis of the 1-D Continuous Energy Lattice-Geometry Transport Equation

In this chapter, an asymptotic analysis is applied to the 1-D, continuous energy, lattice-geometry Boltzmann transport equation. For a large, periodic lattice system, the solution is assumed to have two length scales ℓ_1 (the width of a pin or assembly) and ℓ_2 (the width of the core). The dimensionless ratio $\epsilon = \ell_1/\ell_2 = 1/N$, where N is the number of pins or assemblies in the system, is assumed to be small (i.e. $\ll 1$). The solution is then expanded in powers of ϵ, and the Boltzmann transport equation is split into equations with equal orders of ϵ. These equations are solved sequentially for ϵ^0 to ϵ^5, and the result, obtained from the solvability conditions for ϵ^2 to ϵ^5, is a 1-D, one group simplified P_2 equation.

When $\epsilon = 0$, we have an infinite lattice with a periodic asymptotic solution, which is exact. When $0 < \epsilon \ll 1$, then the system is large, yet finite. In this case, the asymptotic solution is periodic with a small spatial "buckling." This is representative of a nuclear reactor, which contains several assemblies filled with repeating pins. The asymptotic analysis provides an expression for the angular flux that, to leading order, is identical to the standard "flux reconstruction." Higher-order terms provide corrections to standard flux reconstruction that, as shown in Chapter 4, improve the accuracy of the solution.

3.1 Asymptotic Analysis

We begin by stating the 1-D, continuous energy, anisotropically-scattering transport equation,

$$\begin{aligned}\mu\frac{\partial\psi}{\partial x}(x,\mu,E)+\Sigma_t(x,E)\psi(x,\mu,E)&\\ =\int_0^\infty\int_{-1}^1\Sigma_s(x,\mu'\to\mu,E'\to E)\psi(x,\mu',E')\,d\mu'dE'&\\ +\lambda\frac{\chi(x,E)}{2}\int_0^\infty\int_{-1}^1\nu\Sigma_f(x,E')\psi(x,\mu',E')\,d\mu'dE'\,,&\end{aligned}\tag{3.1}$$

where

$$\lambda=\frac{1}{k}=1-\rho\,.\tag{3.2}$$

To perform the asymptotic analysis, we assume that the physical system is periodic, consisting of a symmetric cell (e.g. a pin or an assembly) repeated N times, with N large enough that

$$\epsilon=1/N\ll 1\,.\tag{3.3}$$

This allows us to represent the angular flux $\psi(x,\mu,E)$ as a function of two spatial variables: one periodic "fast" variable (y) that operates on the cell (variations in the cell), and one non-periodic "slow" variable (z) that operates on the entire core (variations in the core), as seen in Fig. 3.1.

If the periodic system is infinite (i.e. $\epsilon=0$), the angular flux would be periodic, and would depend solely on the periodic "fast" spatial variable. Once we perturb the infinite system to make it finite (i.e. $\epsilon\ll 1$), we introduce a weak, non-periodic spatial dependence (the "slow" spatial variable) that we can assume is *independent* of the periodic variation.

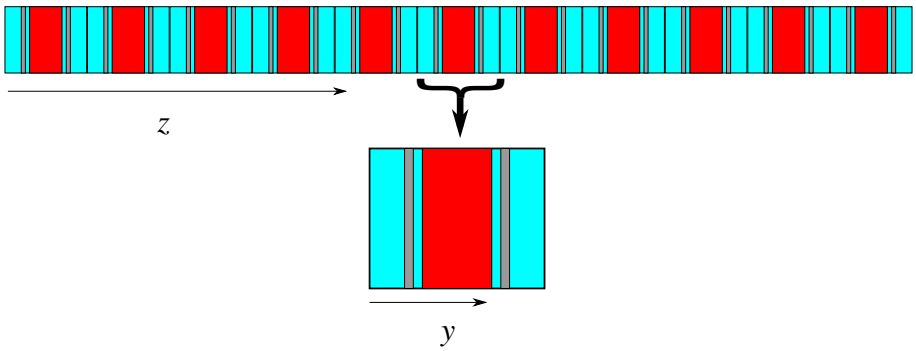

Figure 3.1: Fast versus Slow Scales

With this assumption, we rewrite $\psi(x,\mu,E)$ as:

$$\psi(x,\mu,E) = \Psi(y,z,\mu,E)\,, \tag{3.4a}$$

where

$$y = x\,, \tag{3.4b}$$

$$z = \epsilon x\,, \tag{3.4c}$$

Ψ is a periodic function of y (when y and z are independent), and

$$\frac{\partial}{\partial x}\psi(x,\mu,E) = \frac{\partial}{\partial y}\Psi(y,z,\mu,E) + \epsilon\frac{\partial}{\partial z}\Psi(y,z,\mu,E)\,. \tag{3.4d}$$

The cross sections depend solely on the fast scale in a periodic manner:

$$\Sigma_j(x,E) = \Sigma_j(y,E) = \Sigma_j(y+h,E)\,, \tag{3.5}$$

where h is the width of a single cell. If the center of a cell is at $y = 0$, then its symmetry can be expressed as

$$\Sigma_j(y,E) = \Sigma_j(-y,E)\,. \tag{3.6}$$

With these assumptions, we expand Ψ and λ in ϵ:

$$\Psi(y,z,\mu,E) = \Psi_0(y,z,\mu,E) + \epsilon\Psi_1(y,z,\mu,E) + \epsilon^2\Psi_2(y,z,\mu,E) + \dots , \tag{3.7a}$$

$$\lambda = \lambda_0 + \epsilon^2\lambda_2 . \tag{3.7b}$$

There is no $\epsilon\lambda_1$ in Eq. (3.7b) because, as shown in [25] (and Appendix A), $\lambda_1 = 0$.

Introducing Eqs. (3.4) and (3.7) into Eq. (3.1) and assuming a Legendre polynomial expansion of the differential scattering cross section, we obtain:

$$\begin{aligned}
&\mu\frac{\partial}{\partial y}\Big[\Psi_0(y,z,\mu,E) + \epsilon\Psi_1(y,z,\mu,E) + \epsilon^2\Psi_2(y,z,\mu,E) + \dots\Big] \\
&\quad + \epsilon\mu\frac{\partial}{\partial z}\Big[\Psi_0(y,z,\mu,E) + \epsilon\Psi_1(y,z,\mu,E) + \epsilon^2\Psi_2(y,z,\mu,E) + \dots\Big] \\
&\quad + \Sigma_t(y,E)\Big[\Psi_0(y,z,\mu,E) + \epsilon\Psi_1(y,z,\mu,E) + \epsilon^2\Psi_2(y,z,\mu,E) + \dots\Big] \\
&= \int_0^\infty\int_{-1}^1 \Sigma_s(y,\mu'\to\mu,E'\to E)[\Psi_0(y,z,\mu',E') + \epsilon\Psi_1(y,z,\mu',E') + \dots]d\mu' dE' \\
&\quad + \lambda\frac{\chi(y,E)}{2}\int_0^\infty \nu\Sigma_f(y,E')\int_{-1}^1 [\Psi_0(y,z,\mu',E') + \epsilon\Psi_1(y,z,\mu',E') + \dots]d\mu' dE' .
\end{aligned} \tag{3.8}$$

We now equate the coefficients of the different powers of ϵ:

ϵ^0:

$$L\Psi_0(y,z,\mu,E) = 0 , \tag{3.9a}$$

ϵ^1:

$$L\Psi_1(y,z,\mu,E) = -\mu\frac{\partial}{\partial z}\Psi_0(y,z,\mu,E) , \tag{3.9b}$$

ϵ^n for $n \geq 2$:

$$L\Psi_n(y,z,\mu,E) = -\mu\frac{\partial}{\partial z}\Psi_{n-1}(y,z,\mu,E) + \lambda_2\frac{\chi(y,E)}{2}\int_0^\infty \nu\Sigma_f(y,E')\int_{-1}^1 \Psi_{n-2}(y,z,\mu',E')\,d\mu'dE', \tag{3.9c}$$

where L is the "infinite-lattice" transport operator:

$$\begin{aligned} L\Psi(y,z,\mu,E) = \mu\frac{\partial}{\partial y}\Psi(y,z,\mu,E) + \Sigma_t(y,E)\Psi(y,z,\mu,E) \\ - \int_0^\infty\int_{-1}^1 \Sigma_s(y,\mu'\to\mu,E'\to E)\Psi(y,z,\mu',E')\,d\mu'dE' \\ - \lambda_0\frac{\chi(y,E)}{2}\int_0^\infty \nu\Sigma_f(y,E')\int_{-1}^1 \Psi(y,z,\mu',E')\,d\mu'dE'. \end{aligned} \tag{3.10}$$

The properties of L are detailed in Appendix B and summarized here:

1. L acts only on y, μ, and E. It is independent of the slow spatial operator z.

2. L is symmetry-preserving. If $g(y,\mu,E)$ is symmetric,

$$g(y,\mu,E) = g(-y,-\mu,E), \tag{3.11}$$

then Lg is symmetric,

$$Lg(y,\mu,E) = Lg(-y,-\mu,E). \tag{3.12}$$

Likewise, if $g(y,\mu)$ is antisymmetric,

$$g(y,\mu,E) = -g(-y,-\mu,E), \tag{3.13}$$

then Lg is antisymmetric,

$$Lg(y,\mu,E) = -Lg(-y,-\mu,E). \tag{3.14}$$

3. The solution of

$$\boxed{Lf_0(y,\mu,E)=0} \tag{3.15}$$

is the infinite-medium lattice solution (with λ_0 equal to the infinite-lattice eigenvalue, chosen so that the solution f_0 is positive). f_0 is both a periodic function of y and a symmetric function of y and μ.

4. The inner product of two periodic (in y) functions $g(y,\mu,E)$ and $h(y,\mu,E)$,

$$(g,h)=\int_0^h\int_0^\infty\int_{-1}^1 g(y,\mu,E)\,h(y,\mu,E)\,d\mu dE dy\,, \tag{3.16}$$

has the property

$$(g,Lh)=(L^*g,h)\,. \tag{3.17}$$

Here the integral $\int_0^h(\cdot)dy$ denotes a spatial integral over a single cell, and L^* is the adjoint operator.

5. The adjoint operator L^* is defined by:

$$\begin{aligned} Lg(y,\mu,E) = &-\mu\frac{\partial}{\partial y}g(y,\mu,E)+\Sigma_t(y,E)\,g(y,\mu,E)\\ &-\int_0^\infty\int_{-1}^1\Sigma_s(y,\mu\to\mu',E\to E')\,g(y,\mu',E')\,d\mu' dE'\\ &-\lambda_0\frac{\nu\Sigma_f(y,E)}{2}\int_0^\infty\chi(y,E')\int_{-1}^1 g(y,\mu',E')\,d\mu' dE'\,. \end{aligned} \tag{3.18}$$

6. The solution of $L^*f_0^*(y,\mu,E)=0$ is the adjoint infinite-medium lattice solution, and it is also a periodic function of y and a symmetric function of y and μ. For one group in 1-D, $f_0^*(y,\mu)=f_0(y,-\mu)$.

Eqs. (3.9) are solved sequentially, beginning with Eq. (3.9a). Because L acts solely on the angular variable μ, the fast spatial variable y, and the energy variable E, the general solution of Eq. (3.9a) is the solution of the infinite-lattice problem multiplied by an

unspecified function of z, $A_0(z)$:

$$\boxed{\Psi_0(y,z,\mu,E) = f_0(y,\mu,E)A_0(z)\,.} \tag{3.19}$$

Introducing Eq. (3.19) into Eq. (3.9b), we use the Fredholm Alternative theorem (FAT) [29], discussed in detail in Appendix A, to ensure that a solution $\Psi_1(y,z,\mu,E)$ exists. As seen in Appendix A, this requires taking the inner product of $f_0^*(y,\mu)$ with Eq. (3.9b):

$$\left(f_0^*(y,\mu,E), L\Psi_1(y,z,\mu,E)\right) = \left(f_0^*(y,\mu,E), \left(-\mu\frac{\partial}{\partial z}\Psi_0(y,z,\mu,E)\right)\right). \tag{3.20}$$

The left side of Eq. (3.20) is equal to zero by the definition of the inner product and L^*:

$$\begin{aligned}\left(f_0^*(y,\mu,E), L\Psi_1(y,z,\mu,E)\right) &= \left(L^* f_0^*(y,\mu,E), \Psi_1(y,z,\mu,E)\right)\\ &= \left(0, \Psi_1(y,z,\mu,E)\right)\\ &= 0\,.\end{aligned} \tag{3.21}$$

Therefore, the right side must also equal zero:

$$\begin{aligned}&\left(f_0^*(y,\mu,E), \left(-\mu\frac{\partial}{\partial z}\Psi_0(y,z,\mu,E)\right)\right)\\ &\quad= \int_0^h\int_0^\infty\int_{-1}^1 f_0^*(y,\mu,E)\left(-\mu\frac{\partial}{\partial z}\Psi_0(y,z,\mu,E)\right)d\mu dE dy\\ &\quad= -\int_0^h\int_0^\infty\int_{-1}^1 f_0^*(y,\mu,E)\left(\mu\frac{\partial}{\partial z}\Big(f_0(y,\mu,E)A_0(z)\Big)\right)d\mu dE dy\\ &\quad= -\left(\frac{\partial}{\partial z}A_0(z)\right)\int_0^h\int_0^\infty\int_{-1}^1 \mu f_0^*(y,\mu,E)\,f_0(y,\mu,E)\,d\mu dE dy\,.\end{aligned} \tag{3.22}$$

Both $f_0(y,\mu,E)$ and $f_0^*(y,\mu,E)$ are symmetric functions of y and μ, while μ is antisymmetric. The integrand in Eq. (3.22) is therefore antisymmetric, so the integral is equal to

zero (see Appendix B for details):

$$\begin{aligned}
&\left(f_0^*(y,\mu,E),\left(-\mu\frac{\partial}{\partial z}\Psi_0(y,z,\mu,E)\right)\right) \\
&\qquad = -\left(\frac{\partial}{\partial z}A_0(z)\right)\int_0^h\int_0^\infty\int_{-1}^1 \mu f_0^*(y,\mu,E)\, f_0(y,\mu,E)\, d\mu dE dy \\
&\qquad = -\left(\frac{\partial}{\partial z}A_0(z)\right)\int_0^h\int_0^\infty\int_{-1}^1 (\text{antisymmetric})(\text{symmetric})(\text{symmetric})\, d\mu dE dy \\
&\qquad = -\left(\frac{\partial}{\partial z}A_0(z)\right)\int_0^h\int_0^\infty\int_{-1}^1 (\text{antisymmetric})\, d\mu dE dy \\
&\qquad = 0\,. \qquad (3.23)
\end{aligned}$$

By Eq. (3.23), the solvability condition is satisfied, so by the FAT a particular solution of Eq. (3.9b) exists:

$$\begin{aligned}
\Psi_{1,particular}(y,z,\mu,E) &= L^{-1}\left[-\mu\frac{\partial}{\partial z}f_0(y,\mu,E)A_0(z)\right] \\
&= -L^{-1}\left[\mu f_0(y,\mu,E)\right]\frac{\partial}{\partial z}A_0(z) \qquad (3.24) \\
&= -f_1(y,\mu,E)\frac{\partial}{\partial z}A_0(z)\,,
\end{aligned}$$

where L^{-1} is the pseudo-inverse, and

$$\boxed{f_1(y,\mu,E) = L^{-1}\left[\mu f_0(y,\mu,E)\right].} \qquad (3.25)$$

In Eqs. (3.24) and (3.25), $f(y,\mu,E) = L^{-1}[g(y,\mu,E)]$ is the unique solution to the fixed source lattice transport problem with an external source $g(y,\mu,E)$, defined by:

$$Lf(y,\mu,E) = g(y,\mu)\,, \qquad (3.26)$$

where $g(y,\mu)$ and $f(y,\mu)$ both satisfy

$$\left(f_0^*(y,\mu,E), g(y,\mu,E)\right) = 0\,, \tag{3.27a}$$

$$\left(f_0^*(y,\mu,E), f(y,\mu,E)\right) = 0\,. \tag{3.27b}$$

Eq. (3.27a) ensures that f exists, and Eq. (3.27b) ensures that f is unique.

The solution to Eq. (3.9b) is the sum of the particular solution, Eq. (3.24), and the solution to the homogeneous problem $L\Psi_{1,homog}(y,z,\mu,E) = 0$. As with Ψ_0, the solution to the homogeneous problem is the product of f_0 with another as-yet undefined function of z, $A_1(z)$:

$$\Psi_{1,homog}(y,z,\mu,E) = f_0(y,\mu,E)A_1(z)\,. \tag{3.28}$$

Combining Eqs. (3.24) and (3.28) yields a final solution for Ψ_1:

$$\boxed{\Psi_1(y,z,\mu,E) = f_0(y,\mu,E)A_1(z) - f_1(y,\mu,E)\frac{\partial}{\partial z}A_0(z)\,.} \tag{3.29}$$

Here $f_0(y,\mu,E)$ and $f_1(y,\mu,E)$ are specified periodic functions of y and μ, and $A_0(z)$ and $A_1(z)$ are as-yet unspecified functions of z.

The methodology for solving Eq. (3.9c) ($n = 2$) is similar to the $n = 1$ case just treated. We begin by taking the inner product of both sides with $f_0^*(y,\mu,E)$:

$$\begin{aligned}\left(f_0^*(y,\mu,E), L\Psi_2(y,z,\mu,E)\right)&\\ = \Bigg(f_0^*(y,\mu,E), -\mu\frac{\partial}{\partial z}\Psi_1(y,z,\mu,E)&\\ + \lambda_2\frac{\chi(y,E)}{2}\int_0^\infty \nu\Sigma_f(y,E')\int_{-1}^1 \Psi_0(y,z,\mu',E')\,d\mu'\,dE'\Bigg)&.\end{aligned} \tag{3.30}$$

As before, the left side is equal to zero:

$$\begin{aligned}\left(f_0^*(y,\mu,E), L\Psi_2(y,z,\mu,E)\right) &= \left(L^* f_0^*(y,\mu,E), \Psi_2(y,z,\mu,E)\right) \\ &= \left(0, \Psi_2(y,z,\mu,E)\right) \\ &= 0\,,\end{aligned} \tag{3.31}$$

so the right side of Eq. (3.30) must also equal zero. Introducing Eqs. (3.19), (3.29), and (3.31) into Eq. (3.30) we obtain the condition:

$$\begin{aligned}0 &= \left(f_0^*(y,\mu,E), -\mu\frac{\partial}{\partial z}\left(f_0(y,\mu,E)A_1(z) - f_1(y,\mu,E)\frac{\partial}{\partial z}A_0(z)\right)\right. \\ &\qquad \left. + \lambda_2\frac{\chi(y,E)}{2}\int_0^\infty \nu\Sigma_f(y,E')\int_{-1}^1 f_0(y,\mu',E')A_0(z)\,d\mu'\,dE'\right) \\ &= \left(f_0^*(y,\mu,E), -\mu f_0(y,\mu,E)\frac{\partial}{\partial z}A_1(z) + \mu f_1(y,\mu,E)\frac{\partial^2}{\partial z^2}A_0(z)\right. \\ &\qquad \left. + \lambda_2\frac{\chi(y,E)}{2}A_0(z)\int_0^\infty \nu\Sigma_f(y,E')\int_{-1}^1 f_0(y,\mu',E')\,d\mu'\,dE'\right) \\ &= -\left(f_0^*(y,\mu,E), \mu f_0(y,\mu,E)\right)\frac{\partial}{\partial z}A_1 + \left(f_0^*(y,\mu,E), \mu f_1(y,\mu,E)\right)\frac{\partial^2}{\partial z^2}A_0(z) \\ &\qquad + \lambda_2\left(f_0^*(y,\mu,E), \frac{\chi(y,E)}{2}\int_0^\infty \nu\Sigma_f(y,E')\int_{-1}^1 f_0(y,\mu',E')\,d\mu'\,dE'\right)A_0(z)\,.\end{aligned} \tag{3.32}$$

From Eq. (3.23), $\left(f_0^*(y,\mu,E), \mu f_0(y,\mu,E)\right) = 0$, yielding:

$$\begin{aligned}0 =& \left(f_0^*(y,\mu,E), \mu f_1(y,\mu,E)\right)\frac{\partial^2}{\partial z^2}A_0(z) \\ &+ \lambda_2\left(f_0^*(y,\mu,E), \frac{\chi(y,E)}{2}\int_0^\infty \nu\Sigma_f(y,E')\int_{-1}^1 f_0(y,\mu',E')\,d\mu'\,dE'\right)A_0(z)\,.\end{aligned} \tag{3.33}$$

This is the solvability condition for Eq. (3.9c) ($n = 2$) that must be satisfied for Eq. (3.9c) ($n = 2$) to have a solution.

To obtain a particular solution for Ψ_2, we multiply Eq. (3.33) by

$$\frac{f_0(y,\mu,E)}{\left(f_0^*(y',\mu',E'),f_0(y',\mu',E')\right)}$$

and subtract the result from Eq. (3.9c) ($n=2$). The resulting equation, Eq. (3.34), automatically satisfies the solvability equation:

$$\begin{aligned}
L\Psi_2(y,z,\mu,E) &= -\mu\frac{\partial}{\partial z}\Psi_1(y,z,\mu,E)\\
&\quad+\lambda_2\frac{\chi(y,E)}{2}\int_0^\infty \nu\Sigma_f(y,E')\int_{-1}^1 \Psi_0(y,z,\mu',E')\,d\mu'dE'\\
&\quad-\frac{f_0(y,\mu,E)}{\left(f_0^*(y',\mu',E'),f_0(y',\mu',E')\right)}\times\Bigg[\left(f_0^*(y,\mu,E),\mu f_1(y,\mu,E)\right)\frac{\partial^2}{\partial z^2}A_0(z)\\
&\qquad+\lambda_2\left(f_0^*(y,\mu,E),\frac{\chi(y,E)}{2}\int_0^\infty \nu\Sigma_f(y,E')\int_{-1}^1 f_0(y,\mu',E')\,d\mu'dE'\right)A_0(z)\Bigg]\\
&=-\mu\frac{\partial}{\partial z}\left(f_0(y,\mu,E)A_1(z)-f_1(y,\mu,E)\frac{\partial}{\partial z}A_0(z)\right)\\
&\quad+\lambda_2\frac{\chi(y,E)}{2}\int_0^\infty \nu\Sigma_f(y,E')\int_{-1}^1 f_0(y,\mu',E')A_0(z)\,d\mu'dE'\\
&\quad-\frac{f_0(y,\mu,E)}{\left(f_0^*(y',\mu',E'),f_0(y',\mu',E')\right)}\times\Bigg[\left(f_0^*(y,\mu,E),\mu f_1(y,\mu,E)\right)\frac{\partial^2}{\partial z^2}A_0(z)\\
&\qquad+\lambda_2\left(f_0^*(y,\mu,E),\frac{\chi(y,E)}{2}\int_0^\infty \nu\Sigma_f(y,E')\int_{-1}^1 f_0(y,\mu',E')\,d\mu'dE'\right)A_0(z)\Bigg].
\end{aligned}\tag{3.34}$$

Defining the "identity" operator I, $Ig(y,\mu,E)=g(y,\mu,E)$, and the "projection" operator P,

$$Pg(y,\mu,E)=\frac{f_0(y,\mu,E)}{\left(f_0^*(y',\mu',E'),f_0(y',\mu',E')\right)}\left(f_0^*(y',\mu',E'),g(y',\mu',E')\right),\tag{3.35}$$

Eq. (3.34) becomes:

$$\begin{aligned}
L\Psi_2(y,z,\mu,E) &= -\left(\mu f_0(y,\mu,E)\right)\frac{\partial}{\partial z}A_1(z)+\left((I-P)\mu f_1(y,\mu,E)\right)\frac{\partial^2}{\partial z^2}A_0(z)\\
&\quad+\lambda_2\left((I-P)\frac{\chi(y,E)}{2}\int_0^\infty \nu\Sigma_f(y,E')F_0(y,E')\,dE'\right)A_0(z)\,,
\end{aligned}\tag{3.36}$$

where

$$F_0(y,E) = \int_{-1}^{1} f_0(y,\mu',E)\,d\mu' \,. \tag{3.37}$$

Eq. (3.36) now automatically satisfies the solvability condition. Therefore, by the FAT, a solution $\Psi_2(y,z,\mu,E)$ of Eq. (3.36) exists. As with Eqs. (3.9a) and (3.9b), $\Psi_2(y,z,\mu,E)$ consists of the sum of the homogeneous solution to $L\Psi_2(y,z,\mu,E) = 0$ and the particular solution to Eq. (3.36):

$$\begin{aligned}
\Psi_2(y,z,\mu,E) =& f_0(y,\mu,E)A_2(z) + L^{-1}\Bigg[-\Big(\mu f_0(y,\mu,E)\Big)\frac{\partial}{\partial z}A_1(z) \\
&+ \Big((I-P)\mu f_1(y,\mu,E)\Big)\frac{\partial^2}{\partial z^2}A_0(z) \\
&+ \lambda_2\Big((I-P)\frac{\chi(y,E)}{2}\int_0^\infty \nu\Sigma_f(y,E')F_0(y,E')\,dE'\Big)A_0(z)\Bigg] \\
=& f_0(y,\mu,E)A_2(z) - L^{-1}\Big[\mu f_0(y,\mu,E)\Big]\frac{\partial}{\partial z}A_1(z) \\
&+ L^{-1}\Big[(I-P)\mu f_1(y,\mu,E)\Big]\frac{\partial^2}{\partial z^2}A_0(z) \\
&+ \lambda_2 L^{-1}\Big[(I-P)\frac{\chi(y,E)}{2}\int_0^\infty \nu\Sigma_f(y,E')F_0(y,E')\,dE'\Big]A_0(z)\,,
\end{aligned} \tag{3.38}$$

or

$$\boxed{\begin{aligned}
\Psi_2(y,z,\mu,E) = f_0(y,\mu,E)A_2(z) - f_1(y,\mu,E)\frac{\partial}{\partial z}A_1(z) \\
+ f_3(y,\mu,E)\frac{\partial^2}{\partial z^2}A_0(z) + \lambda_2 f_2(y,\mu,E)A_0(z)\,.
\end{aligned}} \tag{3.39}$$

Here $f_2(y,\mu,E)$ and $f_3(y,\mu,E)$ are new lattice functions defined as

$$f_2(y,\mu,E) = L^{-1}\Big[(I-P)\frac{\chi(y,E)}{2}\int_0^\infty \nu\Sigma_f(y,E')F_0(y,E')\,dE'\Big], \tag{3.40a}$$

and

$$f_3(y,\mu,E) = L^{-1}\Big[(I-P)\mu f_1(y,\mu,E)\Big]. \tag{3.40b}$$

Next, we perform the same analysis for Eq. (3.9c) ($n = 3$). First, we take the inner

product of both sides with $f_0^*(y,\mu,E)$ to obtain the solvability condition:

$$\begin{aligned}\left(f_0^*(y,\mu,E), L\Psi_3(y,z,\mu,E)\right) &= \left(f_0^*(y,\mu,E), -\mu\frac{\partial}{\partial z}\Psi_2(y,z,\mu,E)\right) \\ &+ \lambda_2\left(f_0^*(y,\mu,E), \frac{\chi(y,E)}{2}\int_0^\infty \nu\Sigma_f(y,E')\int_{-1}^1 \Psi_1(y,z,\mu',E')\,d\mu'dE'\right).\end{aligned} \tag{3.41}$$

As before, the left side is equal to zero:

$$\begin{aligned}\left(f_0^*(y,\mu,E), L\Psi_3(y,z,\mu,E)\right) &= \left(L^* f_0^*(y,\mu,E), \Psi_3(y,z,\mu,E)\right) \\ &= \left(0, \Psi_3(y,z,\mu,E)\right) \\ &= 0\,.\end{aligned} \tag{3.42}$$

The right side of Eq. (3.41) must therefore also equal zero. Introducing Eqs. (3.29) and (3.39), we obtain the condition:

$$\begin{aligned}0 =& \left(f_0^*(y,\mu,E), -\mu\frac{\partial}{\partial z}\left(f_0(y,\mu,E)A_2(z) - f_1(y,\mu,E)\frac{\partial}{\partial z}A_1(z)\right.\right. \\ &\left. + f_3(y,\mu,E)\frac{\partial^2}{\partial z^2}A_0(z) + \lambda_2 f_2(y,\mu,E)A_0(z)\right) \\ &\left. + \lambda_2\frac{\chi(y,E)}{2}\int_0^\infty \nu\Sigma_f(y,E')\int_{-1}^1\left(f_0(y,\mu',E')A_1(z) - f_1(y,\mu',E')\frac{\partial}{\partial z}A_0(z)\right)d\mu'dE'\right) \\ =& -\left(f_0^*(y,\mu,E), \mu f_0(y,\mu,E)\right)\frac{\partial}{\partial z}A_2(z) + \left(f_0^*(y,\mu,E), \mu f_1(y,\mu,E)\right)\frac{\partial^2}{\partial z^2}A_1(z) \\ &- \lambda_2\left(f_0^*(y,\mu,E), \mu f_3(y,\mu,E)\right)\frac{\partial^3}{\partial z^3}A_0(z) - \left(f_0^*(y,\mu,E), \mu f_2(y,\mu,E)\right)\frac{\partial}{\partial z}A_0(z) \\ &+ \lambda_2\left(f_0^*(y,\mu,E), \frac{\chi(y,E)}{2}\int_0^\infty \nu\Sigma_f(y,E')F_0(y,E')\,dE'\right)A_1(z) \\ &- \lambda_2\left(f_0^*(y,\mu,E), \frac{\chi(y,E)}{2}\int_0^\infty \nu\Sigma_f(y,E')\int_{-1}^1 f_1(y,\mu',E')\,d\mu'dE'\right)\frac{\partial}{\partial z}A_0(z)\,.\end{aligned} \tag{3.43}$$

To simplify Eq. (3.43), we recognize that $f_0(y,\mu,E)$, $f_2(y,\mu,E)$ and $f_3(y,\mu,E)$ are symmetric functions, while $f_1(y,\mu,E)$ is antisymmetric (see Appendix B). With that in mind, the first, third, fourth, and sixth terms in Eq. (3.43) contain antisymmetric integrands that

integrate to zero, leaving us with:

$$0 = \left(f_0^*(y,\mu,E), \mu f_1(y,\mu,E) \right) \frac{\partial^2}{\partial z^2} A_1(z) + \lambda_2 \left(f_0^*(y,\mu,E), \frac{\chi(y,E)}{2} \int_0^\infty \nu\Sigma_f(y,E') F_0(y,E') dE' \right) A_1(z) . \tag{3.44}$$

Eq. (3.44) is identical to the solvability condition for $\Psi_2(y,z,\mu,E)$, Eq. (3.33), but with $A_1(z)$ instead of $A_0(z)$. As with $\Psi_2(y,z,\mu,E)$, we subtract

$$\frac{f_0(y,\mu,E)}{(f_0^*(y',\mu',E'), f_0(y',\mu',E'))}$$

times Eq. (3.44) from Eq. (3.9c) ($n = 3$) to obtain an equation for Ψ_3 that automatically satisfies the solvability condition:

$$\begin{aligned} L\Psi_3(y,z,\mu,E) = &- \left(\mu f_0(y,\mu,E) \right) \frac{\partial}{\partial z} A_2(z) + \left((I-P)\mu f_1(y,\mu,E) \right) \frac{\partial^2}{\partial z^2} A_1(z) \\ &- \left(\mu f_3(y,\mu,E) \right) \frac{\partial^3}{\partial z^3} A_0(z) - \lambda_2 \left(\mu f_2(y,\mu,E) \right) \frac{\partial}{\partial z} A_0(z) \\ &+ \lambda_2 \left((I-P) \frac{\chi(y,E)}{2} \int_0^\infty \nu\Sigma_f(y,E') F_0(y,E') dE' \right) A_1(z) \\ &- \lambda_2 \left(\frac{\chi(y,E)}{2} \int_0^\infty \nu\Sigma_f(y,E') \int_{-1}^1 f_1(y,\mu',E') d\mu' dE' \right) \frac{\partial}{\partial z} A_0(z) . \end{aligned} \tag{3.45}$$

The exact solution to Ψ_3 is the sum of the particular solution to Eq. (3.45) and the

homogeneous solution to $L\Psi_3(y,z,\mu,E)=0$:

$$\begin{aligned}
\Psi_3(y,z,\mu,E) =& f_0(y,\mu,E)A_3(z)+L^{-1}\Big[-\Big(\mu f_0(y,\mu,E)\Big)\frac{\partial}{\partial z}A_2(z)\\
&+\Big((I-P)\mu f_1(y,\mu,E)\Big)\frac{\partial^2}{\partial z^2}A_1(z)\\
&-\Big(\mu f_3(y,\mu,E)\Big)\frac{\partial^3}{\partial z^3}A_0(z)-\lambda_2\Big(\mu f_2(y,\mu,E)\Big)\frac{\partial}{\partial z}A_0(z)\\
&+\lambda_2\Big((I-P)\frac{\chi(y,E)}{2}\int_0^\infty \nu\Sigma_f(y,E')F_0(y,E')\,dE'\Big)A_1(z)\\
&-\lambda_2\Big(\frac{\chi(y,E)}{2}\int_0^\infty \nu\Sigma_f(y,E')\int_{-1}^1 f_1(y,\mu',E')\,d\mu'\,dE'\Big)\frac{\partial}{\partial z}A_0(z)\Big]\\
=& f_0(y,\mu,E)A_3(z)-L^{-1}\Big[\mu f_0(y,\mu,E)\Big]\frac{\partial}{\partial z}A_2(z)\\
&+L^{-1}\Big[(I-P)\mu f_1(y,\mu,E)\Big]\frac{\partial^2}{\partial z^2}A_1(z)-L^{-1}\Big[\mu f_3(y,\mu,E)\Big]\frac{\partial^3}{\partial z^3}A_0(z)\\
&-\lambda_2 L^{-1}\Big[\mu f_2(y,\mu,E)\Big]\frac{\partial}{\partial z}A_0(z)\\
&+\lambda_2 L^{-1}\Big[(I-P)\frac{\chi(y,E)}{2}\int_0^\infty \nu\Sigma_f(y,E')F_0(y,E')\,dE'\Big]A_1(z)\\
&-\lambda_2 L^{-1}\Big[\frac{\chi(y,E)}{2}\int_0^\infty \nu\Sigma_f(y,E')\int_{-1}^1 f_1(y,\mu',E')\,d\mu'\,dE'\Big]\frac{\partial}{\partial z}A_0(z)\,,
\end{aligned}\tag{3.46}$$

or:

$$\boxed{\begin{aligned}
\Psi_3(y,z,\mu,E) =& f_0(y,\mu,E)A_3(z)-f_1(y,\mu,E)\frac{\partial}{\partial z}A_2(z)\\
&+f_3(y,\mu,E)\frac{\partial^2}{\partial z^2}A_1(z)-f_6(y,\mu,E)\frac{\partial^3}{\partial z^3}A_0(z)\\
&-\lambda_2 f_5(y,\mu,E)\frac{\partial}{\partial z}A_0(z)+\lambda_2 f_2(y,\mu,E)A_1(z)\\
&-\lambda_2 f_4(y,\mu,E)\frac{\partial}{\partial z}A_0(z)\,.
\end{aligned}}\tag{3.47}$$

Here we have defined

$$f_4(y,\mu,E)=L^{-1}\Big[\frac{\chi(y,E)}{2}\int_0^\infty \nu\Sigma_f(y,E')\int_{-1}^1 f_1(y,\mu',E')\,d\mu'\,dE'\Big],\tag{3.48a}$$

$$f_5(y,\mu,E)=L^{-1}\Big[\mu f_2(y,\mu,E)\Big],\tag{3.48b}$$

and

$$f_6(y,\mu,E) = L^{-1}\Big[\mu f_3(y,\mu,E)\Big]. \tag{3.48c}$$

We perform the same analysis for Eq. (3.9c) ($n = 4$):

$$\begin{aligned} L\Psi_4(y,z,\mu,E) = &-\mu\frac{\partial}{\partial z}\Psi_3(y,z,\mu,E) \\ &+\lambda_2\frac{\chi(y,E)}{2}\int_0^\infty \nu\Sigma_f(y,E')\int_{-1}^1 \Psi_2(y,z,\mu',E')\,d\mu'dE', \end{aligned} \tag{3.49}$$

or

$$\begin{aligned} L\Psi_4(y,z,\mu,E) = -\mu\frac{\partial}{\partial z}\Bigg[& f_0(y,\mu,E)A_3(z) - f_1(y,\mu,E)\frac{\partial}{\partial z}A_2(z) \\ &+ f_3(y,\mu,E)\frac{\partial^2}{\partial z^2}A_1(z) - f_6(y,\mu,E)\frac{\partial^3}{\partial z^3}A_0(z) - \lambda_2 f_5(y,\mu,E)\frac{\partial}{\partial z}A_0(z) \\ &+ \lambda_2 f_2(y,\mu,E)A_1(z) - \lambda_2 f_4(y,\mu,E)\frac{\partial}{\partial z}A_0(z)\Bigg] \\ &+\lambda_2\frac{\chi(y,E)}{2}\int_0^\infty \nu\Sigma_f(y,E')\int_{-1}^1\Bigg[f_0(y,\mu',E')A_2(z) - f_1(y,\mu',E')\frac{\partial}{\partial z}A_1(z) \\ &+ f_3(y,\mu',E')\frac{\partial^2}{\partial z^2}A_0(z) + \lambda_2 f_2(y,\mu',E')A_0(z)\Bigg]d\mu'dE'. \end{aligned} \tag{3.50}$$

Performing the same steps as before, we obtain a solvability condition for $\Psi_4(y,z,\mu,E)$:

$$\begin{aligned} 0 = &\Big(f_0^*(y,\mu,E),\mu f_1(y,\mu,E)\Big)\frac{\partial^2}{\partial z^2}A_2(z) \\ &+\Big(f_0^*(y,\mu,E),\mu f_6(y,\mu,E)\Big)\frac{\partial^4}{\partial z^4}A_0(z) \\ &+\lambda_2\Big(f_0^*(y,\mu,E),\mu f_5(y,\mu,E)\Big)\frac{\partial^2}{\partial z^2}A_0(z) \\ &+\lambda_2\Big(f_0^*(y,\mu,E),\frac{\chi(y,E)}{2}\int_0^\infty \nu\Sigma_f(y,E')F_0(y,E')\,dE'\Big)A_2(z) \\ &+\lambda_2\Big(f_0^*(y,\mu,E),\frac{\chi(y,E)}{2}\int_0^\infty \nu\Sigma_f(y,E')\int_{-1}^1 f_3(y,\mu',E')\,d\mu'dE'\Big)\frac{\partial^2}{\partial z^2}A_0(z) \\ &+\lambda_2^2\Big(f_0^*(y,\mu,E),\frac{\chi(y,E)}{2}\int_0^\infty \nu\Sigma_f(y,E')\int_{-1}^1 f_2(y,\mu',E')\,d\mu'dE'\Big)A_0(z), \end{aligned} \tag{3.51}$$

and the final equation for Ψ_4:

$$
\begin{aligned}
\Psi_4(y,z,\mu,E) = {} & f_0(y,\mu,E)A_4(z) - L^{-1}\Big[\mu f_0(y,\mu,E)\Big]\frac{\partial}{\partial z}A_3(z) \\
& + L^{-1}\Big[(I-P)\mu f_1(y,\mu,E)\Big]\frac{\partial^2}{\partial z^2}A_2(z,) \\
& - L^{-1}\Big[\mu f_3(y,\mu,E)\Big]\frac{\partial^3}{\partial z^3}A_1(z) \\
& + L^{-1}\Big[(I-P)\mu f_6(y,\mu,E)\Big]\frac{\partial^4}{\partial z^4}A_0(z) \\
& + \lambda_2 L^{-1}\Big[(I-P)\mu f_5(y,\mu,E)\Big]\frac{\partial^2}{\partial z^2}A_0(z) \\
& - \lambda_2 L^{-1}\Big[\mu f_2(y,\mu,E)\Big]\frac{\partial}{\partial z}A_1(z) \\
& + \lambda_2 L^{-1}\Big[\mu f_4(y,\mu,E)\Big]\frac{\partial^2}{\partial z^2}A_1(z) \\
& + \lambda_2 L^{-1}\Big[(I-P)\frac{\chi(y,E)}{2}\int_0^\infty \nu\Sigma_f(y,E')F_0(y,E')dE'\Big]A_2(z) \\
& - \lambda_2 L^{-1}\Big[\frac{\chi(y,E)}{2}\int_0^\infty \nu\Sigma_f(y,E')\int_{-1}^1 f_1(y,\mu',E')d\mu' dE'\Big]\frac{\partial}{\partial z}A_1(z) \\
& + \lambda_2 L^{-1}\Big[(I-P)\frac{\chi(y,E)}{2}\int_0^\infty \nu\Sigma_f(y,E')\int_{-1}^1 f_3(y,\mu',E')d\mu' dE'\Big]\frac{\partial^2}{\partial z^2}A_0(z) \\
& + \lambda_2^2 L^{-1}\Big[(I-P)\frac{\chi(y,E)}{2}\int_0^\infty \nu\Sigma_f(y,E')\int_{-1}^1 f_2(y,\mu',E')d\mu' dE'\Big]A_0(z)\,.
\end{aligned}
\tag{3.52}
$$

This simplifies to:

$$
\boxed{
\begin{aligned}
\Psi_4(y,z,\mu,E) = {} & f_0(y,\mu,E)A_4(z) - f_1(y,\mu,E)\frac{\partial}{\partial z}A_3(z) \\
& + f_3(y,\mu,E)\frac{\partial^2}{\partial z^2}A_2(z,) - f_6(y,\mu,E)\frac{\partial^3}{\partial z^3}A_1(z) \\
& + f_{11}(y,\mu,E)\frac{\partial^4}{\partial z^4}A_0(z) + \lambda_2 f_{10}(y,\mu,E)\frac{\partial^2}{\partial z^2}A_0(z) \\
& - \lambda_2 f_5(y,\mu,E)\frac{\partial}{\partial z}A_1(z) + \lambda_2 f_9(y,\mu,E)\frac{\partial^2}{\partial z^2}A_1(z) \\
& + \lambda_2 f_2(y,\mu,E)A_2(z) - \lambda_2 f_4(y,\mu,E)\frac{\partial}{\partial z}A_1(z) \\
& + \lambda_2 f_8(y,\mu,E)\frac{\partial^2}{\partial z^2}A_0(z) + \lambda_2^2 f_7(y,\mu,E)A_0(z)\,,
\end{aligned}
}
\tag{3.53}
$$

where the new lattice functions are:

$$f_7(y,\mu,E) = L^{-1}\left[(I-P)\frac{\chi(y,E)}{2}\int_0^\infty \nu\Sigma_f(y,E')\,F_2(y,E')\,dE'\right], \tag{3.54a}$$

$$f_8(y,\mu,E) = L^{-1}\left[(I-P)\frac{\chi(y,E)}{2}\int_0^\infty \nu\Sigma_f(y,E')\,F_3(y,E')\,dE'\right], \tag{3.54b}$$

$$f_9(y,\mu,E) = L^{-1}\Big[\mu f_4(y,\mu,E)\Big], \tag{3.54c}$$

$$f_{10}(y,\mu,E) = L^{-1}\Big[(I-P)\mu f_5(y,\mu,E)\Big], \tag{3.54d}$$

$$f_{11}(y,\mu,E) = L^{-1}\Big[(I-P)\mu f_6(y,\mu,E)\Big], \tag{3.54e}$$

and

$$F_n(y,E) = \int_{-1}^{1} f_n(y,\mu',E)\,d\mu'\,. \tag{3.55}$$

For $\Psi_5(y,z,\mu,E)$, we are only interested in the solvability condition, which is identical to Eq. (3.51), but with $A_1(z)$ instead of $A_0(z)$, and $A_3(z)$ instead of $A_2(z)$:

$$\begin{aligned}
0 =&\Big(f_0^*(y,\mu,E),\mu f_1(y,\mu,E)\Big)\frac{\partial^2}{\partial z^2}A_3(z)\\
&+\Big(f_0^*(y,\mu,E),\mu f_6(y,\mu,E)\Big)\frac{\partial^4}{\partial z^4}A_1(z)\\
&+\lambda_2\Big(f_0^*(y,\mu,E),\mu f_5(y,\mu,E)\Big)\frac{\partial^2}{\partial z^2}A_1(z)\\
&+\lambda_2\Big(f_0^*(y,\mu,E),\frac{\chi(y,E)}{2}\int_0^\infty \nu\Sigma_f(y,E')\,F_0(y,E')\,dE'\Big)A_3(z)\\
&+\lambda_2\Big(f_0^*(y,\mu,E),\frac{\chi(y,E)}{2}\int_0^\infty \nu\Sigma_f(y,E')\,F_3(y,E')\,dE'\Big)\frac{\partial^2}{\partial z^2}A_1(z)\\
&+\lambda_2^2\Big(f_0^*(y,\mu,E),\frac{\chi(y,E)}{2}\int_0^\infty \nu\Sigma_f(y,E')\,F_2(y,E')\,dE'\Big)A_1(z)\,.
\end{aligned} \tag{3.56}$$

We now have all the pieces necessary to derive the monoenergetic asymptotic homogenized diffusion and SP_2 equations and their associated flux reconstruction formulas. While the number of lattice functions (11) may seem large, we will see that only the first two are required for asymptotic diffusion, and only the first five for asymptotic SP_2.

3.2 Asymptotic Diffusion

To derive a homogenized diffusion equation, we first multiply Eq. (3.33) by ϵ^2, use Eq. (3.7b) to eliminate λ_2, and rearrange, to obtain

$$\begin{aligned} 0 =& \left(f_0^*(y,\mu,E), \mu f_1(y,\mu,E)\right)\epsilon^2 \frac{\partial^2}{\partial z^2} A_0(z) \\ &+ (\lambda-\lambda_0)\left(f_0^*(y,\mu,E), \frac{\chi(y,E)}{2}\int_0^\infty \nu\Sigma_f(y,E') F_0(y,E')\, dE'\right) A_0(z)\,, \end{aligned} \tag{3.57}$$

or

$$\begin{aligned} 0 =& \left(\int_0^h \int_0^\infty \int_{-1}^1 \mu f_0^*(y,\mu,E) f_1(y,\mu,E)\, d\mu dE dy\right)\epsilon^2 \frac{\partial^2}{\partial z^2} A_0(z) \\ &+ (\lambda-\lambda_0)\left(\int_0^h \int_0^\infty F_0^*(y,E)\frac{\chi(y,E)}{2}\int_0^\infty \nu\Sigma_f(y,E') F_0(y,E')\, dE' dE dy\right) A_0(z)\,, \end{aligned} \tag{3.58}$$

where

$$F_0^*(y,E) = \int_{-1}^1 f_0^*(y,\mu',E)\, d\mu'\,. \tag{3.59}$$

To obtain an expression for λ_0, we integrate Eq. (3.15):

$$\begin{aligned} Lf_0(y,\mu,E) =& \mu\frac{\partial}{\partial y} f_0(y,\mu,E) + \Sigma_t(y,E) f_0(y,\mu,E) \\ &- \int_0^\infty \int_{-1}^1 \Sigma_s(y,\mu'\to\mu, E'\to E) f_0(y,\mu',E')\, d\mu' dE' \\ &- \lambda_0 \frac{\chi(y,E)}{2}\int_0^\infty \nu\Sigma_f(y,E') \int_{-1}^1 f_0(y,\mu',E')\, d\mu' dE' \\ =& 0 \end{aligned}$$

over a cell, all angles, and all energies, to obtain:

$$0 = \int_0^h \int_0^\infty \int_{-1}^1 \Bigg(\mu \frac{\partial}{\partial y} f_0(y,\mu,E) + \Sigma_t(y,E) f_0(y,\mu,E) - \int_0^\infty \int_{-1}^1 \Sigma_{s,n}(y,\mu' \to \mu, E' \to E) f_0(y,\mu',E') dE' - \lambda_0 \frac{\chi(y,E)}{2} \int_0^\infty \nu\Sigma_f(y,E') F_0(y,E') dE' \Bigg) d\mu dE dy . \tag{3.60}$$

The symmetry of $f_0(y,\mu,E)$ (see Section 3.1 and Appendix B) and reflecting boundary conditions at $x = 0$ and $x = h$ imply that $f_0(0,\mu,E) = f_0(h,\mu,E)$. Therefore:

$$\int_0^h \mu \frac{\partial}{\partial y} f_0(y,\mu,E) dy = \mu \Big[f_0(h,\mu,E) - f_0(0,\mu,E) \Big] = 0 , \tag{3.61}$$

and Eq. (3.60) becomes

$$0 = \int_0^h \int_0^\infty \int_{-1}^1 \Bigg(\Sigma_t(y,E) f_0(y,\mu,E) - \int_0^\infty \int_{-1}^1 \Sigma_s(y,\mu' \to \mu, E' \to E) f_0(y,\mu',E') dE' - \lambda_0 \frac{\chi(y,E)}{2} \int_0^\infty \nu\Sigma_f(y,E') F_0(y,E') dE' \Bigg) d\mu dE dy , \tag{3.62}$$

or

$$0 = \int_0^h \Bigg(\int_0^\infty \Sigma_t(y,E) F_0(y,E) dE - \int_0^\infty \int_0^\infty \Sigma_{s,0}(y,E' \to E) F_0(y,E') dE' dE - \lambda_0 \int_0^\infty \chi(y,E) \int_0^\infty \nu\Sigma_f(y,E') F_0(y,E') dE' dE \Bigg) dy . \tag{3.63}$$

Also, if we recognize that:

$$\Sigma_{s,0}(E') = \int_0^\infty \Sigma_{s,0}(E' \to E) dE , \tag{3.64a}$$

$$\Sigma_t(E) = \Sigma_{s,0}(E) + \Sigma_a(E)\,, \tag{3.64b}$$

and

$$\int_0^\infty \chi(y,E)dE = 1\,, \tag{3.64c}$$

then Eq. (3.63) can be simplified further as:

$$\begin{aligned} 0 = \int_0^h \Bigg(& \int_0^\infty \Sigma_a(y,E)\,F_0(y,E)\,dE \\ & - \lambda_0 \int_0^\infty \nu\Sigma_f(y,E')\,F_0(y,E')\,dE'dE \Bigg) d\mu dy\,. \end{aligned} \tag{3.65}$$

Solving Eq. (3.65) for λ_0, we obtain

$$\boxed{\lambda_0 = \frac{\int_0^h \int_0^\infty \Sigma_a(y,E)\,F_0(y,E)\,dEdy}{\int_0^h \int_0^\infty \nu\Sigma_f(y,E)\,F_0(y,E)\,dEdy} = \frac{\overline{\Sigma}_a}{\overline{\nu\Sigma}_f}\,,} \tag{3.66}$$

where

$$\boxed{\overline{\Sigma}_a = \frac{\int_0^h \int_0^\infty \Sigma_a(y,E)\,F_0(y,E)\,dEdy}{\int_0^h \int_0^\infty F_0(y,E)\,dEdy}\,,} \tag{3.67a}$$

and

$$\boxed{\overline{\nu\Sigma}_f = \frac{\int_0^h \int_0^\infty \nu\Sigma_f(y,E)\,F_0(y,E)\,dEdy}{\int_0^h \int_0^\infty F_0(y,E)\,dEdy}\,.} \tag{3.67b}$$

Introducing Eq. (3.66) into Eq. (3.58) yields

$$\begin{aligned} 0 = & \left(\int_0^h \int_0^\infty \int_{-1}^1 \mu f_0^*(y,\mu,E)\,f_1(y,\mu,E)\,d\mu dEdy \right) \epsilon^2 \frac{\partial^2}{\partial z^2} A_0(z) \\ & + \left(\lambda - \frac{\int_0^h \int_0^\infty \Sigma_a(y,E)\,F_0(y,E)\,dEdy}{\int_0^h \int_0^\infty \nu\Sigma_f(y,E)\,F_0(y,E)\,dEdy} \right) \\ & \times \left(\int_0^h \int_0^\infty F_0^*(y,E) \frac{\chi(y,E)}{2} \int_0^\infty \nu\Sigma_f(y,E')\,F_0(y,E')\,dE'dEdy \right) A_0(z)\,. \end{aligned} \tag{3.68}$$

To put Eq. (3.68) in a more familiar form, we multiply through by

$$\frac{\int_0^h \int_0^\infty \nu\Sigma_f(y,E)\,F_0(y,E)\,dEdy}{\int_0^h \int_0^\infty F_0(y,E)\,dEdy} \times \frac{2}{\int_0^h \int_0^\infty F_0^*(y,E)\chi(y,E)\int_0^\infty \nu\Sigma_f(y,E')\,F_0(y,E')\,dE'dEdy}$$

to obtain

$$-\overline{D}_0\epsilon^2\frac{\partial^2}{\partial z^2}A_0(z) + \overline{\Sigma_a}A_0(z) = \lambda\overline{\nu\Sigma_f}A_0(z)\,. \tag{3.69}$$

Here $\overline{\Sigma}_a$ and $\overline{\nu\Sigma}_f$ are the standard flux-weighted homogenized absorption and nu-fission cross sections defined in Eqs. (3.67), and

$$\boxed{\overline{D_0} = \frac{\int_0^h \int_0^\infty \nu\Sigma_f(y,E)\,F_0(y,E)\,dEdy}{\int_0^h \int_0^\infty F_0(y,E)\,dEdy} \times \frac{\int_0^h \int_0^\infty \int_{-1}^1 \mu f_0^*(y,\mu,E)\,f_1(y,\mu,E)\,d\mu dEdy}{\int_0^h \int_0^\infty F_0^*(y,E)\,\frac{1}{2}\chi(y,E)\int_0^\infty \nu\Sigma_f(y,E')\,F_0(y,E')\,dE'dEdy}\,.} \tag{3.70}$$

We perform the same steps for Eq. (3.44) to yield an identical equation for $A_1(z)$:

$$-\overline{D}_0\epsilon^2\frac{\partial^2}{\partial z^2}A_1(z) + \overline{\Sigma_a}A_1(z) = \lambda\overline{\nu\Sigma_f}A_1(z)\,. \tag{3.71}$$

Adding ϵ times Eq. (3.71) to Eq. (3.69), we obtain:

$$-\overline{D}_0\epsilon^2\frac{\partial^2}{\partial z^2}\Phi_0(z) + \overline{\Sigma_a}\Phi_0(z) = \lambda\overline{\nu\Sigma_f}\Phi_0(z)\,, \tag{3.72}$$

where

$$\Phi_0(z) = A_0(z) + \epsilon A_1(z)\,. \tag{3.73}$$

Finally, we return to the original spatial variable x:

$$\epsilon^2 \frac{\partial^2}{\partial z^2}\Phi_0(z) = \frac{\partial^2}{\partial x^2}\phi_0(x)\,, \tag{3.74a}$$

$$\Phi_0(z) = \phi_0(x)\,. \tag{3.74b}$$

Substituting Eqs. (3.74) into Eq. (3.72), we obtain the following 1-D, monoenergetic, asymptotic homogenized diffusion equation:

$$\boxed{-\overline{D}_0 \frac{\partial^2}{\partial x^2}\phi_0(x) + \overline{\Sigma_a}\phi_0(x) = \lambda\overline{\nu\Sigma_f}\phi_0(x)\,,} \tag{3.75}$$

with constants described by Eqs. (3.67) and (3.70).

The asymptotic analysis also provides an estimate for the reconstructed angular flux, Eq. (3.7a). Taking the first two terms in the expansion, we have

$$\Psi(y,z,\mu,E) = \Psi_0(y,z,\mu,E) + \epsilon\Psi_1(y,z,\mu,E) + O\left(\epsilon^2\right). \tag{3.76}$$

Substituting Eqs. (3.19) and (3.29) into Eq. (3.76), we have

$$\begin{aligned}\Psi(y,z,\mu,E) =& f_0(y,\mu,E)A_0(z)\\ &+ \epsilon\left(f_0(y,\mu,E)A_1(z) - f_1(y,\mu,E)\frac{\partial}{\partial z}A_0(z)\right) + O\left(\epsilon^2\right)\\ =& f_0(y,\mu,E)\left(A_0(z) + \epsilon A_1(z)\right)\\ &- f_1(y,\mu,E)\,\epsilon\frac{\partial}{\partial z}A_0(z) + O\left(\epsilon^2\right).\end{aligned} \tag{3.77}$$

Because Eq. (3.77) is $O\left(\epsilon^2\right)$, we can add an $O\left(\epsilon^2\right)$ term without increasing the asymptotic

order of the error:

$$\begin{aligned}\Psi(y,z,\mu,E) =& f_0(y,\mu,E)\Big(A_0(z)+\epsilon A_1(z)\Big)\\ &- f_1(y,\mu,E)\,\epsilon\frac{\partial}{\partial z}\Big(A_0(z)+\epsilon A_1(z)\Big)+O\left(\epsilon^2\right)\\ =& f_0(y,\mu,E)\,\Phi_0(z)-f_1(y,\mu,E)\,\epsilon\frac{\partial}{\partial z}\Phi_0(z)+O\left(\epsilon^2\right).\end{aligned} \tag{3.78}$$

Returning to the original spatial variable x, we substitute Eq. (3.74), Eq. (3.4a),

$$f_n(y,\mu,E) = f_n(x,\mu,E)\,, \tag{3.79a}$$

and

$$\epsilon\frac{\partial}{\partial z}\Phi_0(z) = \frac{\partial}{\partial x}\phi_0(x)\,, \tag{3.79b}$$

into Eq. (3.78) to obtain

$$\boxed{\psi(x,\mu,E) = f_0(x,\mu,E)\,\phi_0(x) - f_1(x,\mu,E)\,\frac{\partial}{\partial x}\phi_0(x)+O\left(\epsilon^2\right).} \tag{3.80}$$

In traditional homogenized diffusion theory, the reconstructed flux includes only the first term in Eq. (3.80). Therefore, Eq. (3.80) represents an $O(\epsilon)$ correction to standard flux reconstruction.

Eqs. (3.75) and (3.80) were previously derived by Trahan [25]. In the following section, these results are generalized to higher order.

3.3 Asymptotic SP_2

To derive an asymptotic SP_2 equation, we build on the results from Section 3.2. By generalizing the previous derivation to higher order, we achieve a correction to asymptotic diffusion theory.

We begin by adding ϵ times Eq. (3.56) to Eq. (3.51):

$$\begin{aligned}
0 =& \left(f_0^*(y,\mu,E),\mu f_1(y,\mu,E)\right)\frac{\partial^2}{\partial z^2}\Phi_2(z) \\
&+\left(f_0^*(y,\mu,E),\mu f_6(y,\mu,E)\right)\frac{\partial^4}{\partial z^4}\Phi_0(z) \\
&+\lambda_2\left(f_0^*(y,\mu,E),\mu f_5(y,\mu,E)\right)\frac{\partial^2}{\partial z^2}\Phi_0(z) \\
&+\lambda_2\left(f_0^*(y,\mu,E),\frac{\chi(y,E)}{2}\int_0^\infty \nu\Sigma_f(y,E')F_0(y,E')dE'\right)\Phi_2(z) \\
&+\lambda_2\left(f_0^*(y,\mu,E),\frac{\chi(y,E)}{2}\int_0^\infty \nu\Sigma_f(y,E')F_3(y,E')dE'\right)\frac{\partial^2}{\partial z^2}\Phi_0(z) \\
&+\lambda_2^2\left(f_0^*(y,\mu,E),\frac{\chi(y,E)}{2}\int_0^\infty \nu\Sigma_f(y,E')F_2(y,E')dE'\right)\Phi_0(z)\,,
\end{aligned} \tag{3.81}$$

or

$$\begin{aligned}
0 =& \left[\int_0^h\int_0^\infty\int_{-1}^1 f_0^*(y,\mu,E)\mu f_1(y,\mu,E)\,d\mu dE dy\right]\frac{\partial^2}{\partial z^2}\Phi_2(z) \\
&+\left[\int_0^h\int_0^\infty\int_{-1}^1 f_0^*(y,\mu,E)\mu f_6(y,\mu,E)\,d\mu dE dy\right]\frac{\partial^4}{\partial z^4}\Phi_0(z) \\
&+\lambda_2\left[\int_0^h\int_0^\infty\int_{-1}^1 f_0^*(y,\mu,E)\mu f_5(y,\mu,E)\,d\mu dE dy\right]\frac{\partial^2}{\partial z^2}\Phi_0(z) \\
&+\lambda_2\left[\int_0^h\int_0^\infty F_0^*(y,\mu,E)\frac{\chi(y,E)}{2}\int_0^\infty \nu\Sigma_f(y,E')F_0(y,E')\,dE'dEdy\right]\Phi_2(z) \\
&+\lambda_2\left[\int_0^h\int_0^\infty F_0^*(y,\mu,E)\frac{\chi(y,E)}{2}\int_0^\infty \nu\Sigma_f(y,E')F_3(y,E')\,dE'dEdy\right]\frac{\partial^2}{\partial z^2}\Phi_0(z) \\
&+\lambda_2^2\left[\int_0^h\int_0^\infty F_0^*(y,\mu,E)\frac{\chi(y,E)}{2}\int_0^\infty \nu\Sigma_f(y,E')F_2(y,E')\,dE'dEdy\right]\Phi_0(z)\,,
\end{aligned} \tag{3.82}$$

where $\Phi_0(z)$ is defined as in Eq. (3.73), and

$$\Phi_2(z) = A_2(z) + \epsilon A_3(z)\,. \tag{3.83}$$

To simplify the notation in Eq. (3.82), we multiply this equation by

$$\epsilon^4 \frac{\int_0^h \int_0^\infty \nu\Sigma_f(y,E)\,F_0(y,E)\,dEdy}{\int_0^h \int_0^\infty F_0(y,E)\,dEdy} \times \frac{2}{\int_0^h \int_0^\infty F_0^*(y,E)\chi(y,E) \int_0^\infty \nu\Sigma_f(y,E')\,F_0(y,E')\,dE'dEdy}$$

and use Eq. (3.66) to get

$$\begin{aligned} 0 = {} & \overline{D}_0\epsilon^2 \frac{\partial^2}{\partial z^2}\epsilon^2\Phi_2(z) + \overline{D}_1\epsilon^4 \frac{\partial^4}{\partial z^4}\Phi_0(z) + \left(\lambda\overline{\nu\Sigma_f} - \overline{\Sigma_a}\right)\epsilon^2\Phi_2(z) \\ & + \left(\lambda\overline{\nu\Sigma_f} - \overline{\Sigma_a}\right)\left(\overline{\Sigma}_{f,0} + \overline{\Sigma}_{f,1}\right)\epsilon^2 \frac{\partial^2}{\partial z^2}\Phi_0(z) + \left(\lambda\overline{\nu\Sigma_f} - \overline{\Sigma_a}\right)^2 \overline{\Sigma}_{f,2}\Phi_0(z)\,. \end{aligned} \tag{3.84}$$

Here $\overline{D}_0$ is defined in Eq. (3.70),

$$\boxed{\overline{D}_1 = \frac{\int_0^h \int_0^\infty \nu\Sigma_f(y,E)\,F_0(y,E)\,dEdy}{\int_0^h \int_0^\infty F_0(y,E)\,dEdy} \times \frac{\int_0^h \int_0^\infty \int_{-1}^1 \mu f_0^*(y,\mu,E)\,f_6(y,\mu,E)\,d\mu dEdy}{\int_0^h \int_0^\infty F_0^*(y,E)\,\frac{1}{2}\chi(y,E) \int_0^\infty \nu\Sigma_f(y,E')\,F_0(y,E')\,dE'dEdy}\,,} \tag{3.85a}$$

$$\boxed{\overline{\Sigma}_{f,0} = \frac{\int_0^h \int_0^\infty \int_{-1}^1 \mu f_0^*(y,\mu,E)\,f_5(y,\mu,E)\,d\mu dEdy}{\int_0^h \int_0^\infty F_0^*(y,E)\,\frac{1}{2}\chi(y,E) \int_0^\infty \nu\Sigma_f(y,E')\,F_0(y,E')\,dE'dEdy}\,,} \tag{3.85b}$$

$$\boxed{\overline{\Sigma}_{f,1} = \frac{\int_0^h \int_0^\infty F_0^*(y,\mu,E)\,\frac{1}{2}\chi(y,E) \int_0^\infty \nu\Sigma_f(y,E')\,F_3(y,E')\,dE'dEdy}{\int_0^h \int_0^\infty F_0^*(y,E)\,\frac{1}{2}\chi(y,E) \int_0^\infty \nu\Sigma_f(y,E')\,F_0(y,E')\,dE'dEdy}\,,} \tag{3.85c}$$

and

$$\boxed{\overline{\Sigma}_{f,2} = \frac{1}{\overline{\nu\Sigma_f}} \frac{\int_0^h \int_0^\infty F_0^*(y,\mu,E)\,\frac{\chi(y,E)}{2} \int_0^\infty \nu\Sigma_f(y,E')\,F_2(y,E')\,dE'dEdy}{\int_0^h \int_0^\infty F_0^*(y,E)\,\frac{1}{2}\chi(y,E) \int_0^\infty \nu\Sigma_f(y,E')\,F_0(y,E')\,dE'dEdy}\,.} \tag{3.85d}$$

Eqs. (3.84) and (3.72) are combined in the following steps to obtain an SP_2-like equa-

tion.

1. We eliminate $\frac{\partial^4}{\partial z^4}\Phi_0(z)$ from Eq. (3.84) by taking $\frac{\partial^2}{\partial z^2}$ times Eq. (3.72), solving for $\frac{\partial^4}{\partial z^4}\Phi_0(z)$,

$$\frac{\partial^4}{\partial z^4}\Phi_0(z) = -\frac{\left(\lambda\overline{\nu\Sigma_f} - \overline{\Sigma_a}\right)}{\epsilon^2\overline{D}_0}\frac{\partial^2}{\partial z^2}\Phi_0(z)\,, \tag{3.86}$$

and substituting the result into Eq. (3.84):

$$\begin{aligned} 0 = {} & \overline{D}_0\epsilon^2\frac{\partial^2}{\partial z^2}\epsilon^2\Phi_2(z) - \overline{D}_1\epsilon^2\frac{\left(\lambda\overline{\nu\Sigma_f} - \overline{\Sigma_a}\right)}{\overline{D}_0}\frac{\partial^2}{\partial z^2}\Phi_0(z) \\ & + \left(\lambda\overline{\nu\Sigma_f} - \overline{\Sigma_a}\right)\epsilon^2\Phi_2(z) + \left(\lambda\overline{\nu\Sigma_f} - \overline{\Sigma_a}\right)\left(\overline{\Sigma}_{f,0} + \overline{\Sigma}_{f,1}\right)\epsilon^2\frac{\partial^2}{\partial z^2}\Phi_0(z) \\ & + \left(\lambda\overline{\nu\Sigma_f} - \overline{\Sigma_a}\right)^2\overline{\Sigma}_{f,2}\Phi_0(z)\,. \end{aligned} \tag{3.87}$$

2. We eliminate $\left(\lambda\overline{\nu\Sigma_f} - \overline{\Sigma_a}\right)^2\overline{\Sigma}_{f,2}\Phi(z)$ by introducing Eq. (3.72) into Eq. (3.87):

$$\begin{aligned} 0 = {} & \overline{D}_0\epsilon^2\frac{\partial^2}{\partial z^2}\epsilon^2\Phi_2(z) - \overline{D}_1\epsilon^2\frac{\left(\lambda\overline{\nu\Sigma_f} - \overline{\Sigma_a}\right)}{\overline{D}_0}\frac{\partial^2}{\partial z^2}\Phi_0(z) + \left(\lambda\overline{\nu\Sigma_f} - \overline{\Sigma_a}\right)\epsilon^2\Phi_2(z) \\ & + \left(\lambda\overline{\nu\Sigma_f} - \overline{\Sigma_a}\right)\left(\overline{\Sigma}_{f,0} + \overline{\Sigma}_{f,1}\right)\epsilon^2\frac{\partial^2}{\partial z^2}\Phi_0(z) - \left(\lambda\overline{\nu\Sigma_f} - \overline{\Sigma_a}\right)\overline{\Sigma}_{f,2}\overline{D}_0\epsilon^2\frac{\partial^2}{\partial z^2}\Phi_0(z)\,. \end{aligned} \tag{3.88}$$

3. We add Eqs. (3.72) and (3.88) together:

$$\begin{aligned} 0 = {} & \overline{D}_0\epsilon^2\frac{\partial^2}{\partial z^2}\left[\Phi_0(z) + \epsilon^2\Phi_2(z)\right] - \left(\lambda\overline{\nu\Sigma_f} - \overline{\Sigma_a}\right)\frac{\overline{D}_1}{\overline{D}_0}\epsilon^2\frac{\partial^2}{\partial z^2}\Phi_0(z) \\ & + \left(\lambda\overline{\nu\Sigma_f} - \overline{\Sigma_a}\right)\left[\Phi_0(z) + \epsilon^2\Phi_2(z)\right] \\ & + \left(\lambda\overline{\nu\Sigma_f} - \overline{\Sigma_a}\right)\left(\overline{\Sigma}_{f,0} + \overline{\Sigma}_{f,1}\right)\epsilon^2\frac{\partial^2}{\partial z^2}\Phi_0(z) \\ & - \left(\lambda\overline{\nu\Sigma_f} - \overline{\Sigma_a}\right)\overline{\Sigma}_{f,2}\overline{D}_0\epsilon^2\frac{\partial^2}{\partial z^2}\Phi_0(z)\,. \end{aligned} \tag{3.89}$$

4. Because Eq. (3.89) has an error of $O\left(\epsilon^6\right)$, we can add terms of $O\left(\epsilon^6\right)$ without increasing the asymptotic order of the error. Recognizing that $\left(\lambda\overline{\nu\Sigma_f} - \overline{\Sigma_a}\right) = O\left(\epsilon^2\right)$, we add

three $\frac{\partial^2}{\partial z^2}\epsilon^2\Phi_2(z)$ terms to Eq. (3.89), yielding

$$\begin{aligned}0 =&\overline{D}_0\epsilon^2\frac{\partial^2}{\partial z^2}\Big[\Phi_0(z)+\epsilon^2\Phi_2(z)\Big]-\Big(\lambda\overline{\nu\Sigma_f}-\overline{\Sigma_a}\Big)\frac{\overline{D}_1}{\overline{D}_0}\epsilon^2\frac{\partial^2}{\partial z^2}\Big[\Phi_0(z)+\epsilon^2\Phi_2(z)\Big]\\&+\Big(\lambda\overline{\nu\Sigma_f}-\overline{\Sigma_a}\Big)\Big[\Phi_0(z)+\epsilon^2\Phi_2(z)\Big]\\&+\Big(\lambda\overline{\nu\Sigma_f}-\overline{\Sigma_a}\Big)\Big(\overline{\Sigma}_{f,0}+\overline{\Sigma}_{f,1}\Big)\epsilon^2\frac{\partial^2}{\partial z^2}\Big[\Phi_0(z)+\epsilon^2\Phi_2(z)\Big]\\&+\Big(\lambda\overline{\nu\Sigma_f}-\overline{\Sigma_a}\Big)\overline{\Sigma}_{f,2}\overline{D}_0\epsilon^2\frac{\partial^2}{\partial z^2}\Big[\Phi_0(z)+\epsilon^2\Phi_2(z)\Big],\end{aligned}\tag{3.90}$$

or

$$\begin{aligned}0 =&\overline{D}_0\epsilon^2\frac{\partial^2}{\partial z^2}\Phi(z)-\Big(\lambda\overline{\nu\Sigma_f}-\overline{\Sigma_a}\Big)\frac{\overline{D}_1}{\overline{D}_0}\epsilon^2\frac{\partial^2}{\partial z^2}\Phi(z)\\&+\Big(\lambda\overline{\nu\Sigma_f}-\overline{\Sigma_a}\Big)\Phi(z)+\Big(\lambda\overline{\nu\Sigma_f}-\overline{\Sigma_a}\Big)\Big(\overline{\Sigma}_{f,0}+\overline{\Sigma}_{f,1}\Big)\epsilon^2\frac{\partial^2}{\partial z^2}\Phi(z)\\&-\Big(\lambda\overline{\nu\Sigma_f}-\overline{\Sigma_a}\Big)\overline{\Sigma}_{f,2}\overline{D}_0\epsilon^2\frac{\partial^2}{\partial z^2}\Phi(z)\,,\end{aligned}\tag{3.91}$$

where

$$\Phi(z)=\Phi_0(z)+\epsilon^2\Phi_2(z)\,.\tag{3.92}$$

5. Rearranging, we obtain:

$$\begin{aligned}-\Bigg[\overline{D}_0+&\Big(\lambda\overline{\nu\Sigma_f}-\overline{\Sigma_a}\Big)\Big(-\frac{\overline{D}_1}{\overline{D}_0}+\overline{\Sigma}_{f,0}+\overline{\Sigma}_{f,1}-\overline{\Sigma}_{f,2}\overline{D}_0\Big)\Bigg]\epsilon^2\frac{\partial^2}{\partial z^2}\Phi(z)\\&+\overline{\Sigma_a}\Phi(z)=\lambda\overline{\nu\Sigma_f}\Phi(z)\,,\end{aligned}\tag{3.93}$$

or

$$-\Bigg[\overline{D}_0+\Big(\lambda\overline{\nu\Sigma_f}-\overline{\Sigma_a}\Big)\overline{D}_2\Bigg]\epsilon^2\frac{\partial^2}{\partial z^2}\Phi(z)+\overline{\Sigma_a}\Phi(z)=\lambda\overline{\nu\Sigma_f}\Phi(z)\,,\tag{3.94}$$

where

$$\boxed{\overline{D}_2=-\frac{\overline{D}_1}{\overline{D}_0}+\overline{\Sigma}_{f,0}+\overline{\Sigma}_{f,1}-\overline{\Sigma}_{f,2}\overline{D}_0\,.}\tag{3.95}$$

6. Returning to the original spatial variable x, we obtain:

$$\boxed{-\left[\overline{D}_0+\left(\lambda\overline{\nu\Sigma_f}-\overline{\Sigma_a}\right)\overline{D}_2\right]\frac{\partial^2}{\partial x^2}\phi(x)+\overline{\Sigma_a}\phi(x)=\lambda\overline{\nu\Sigma_f}\phi(x)\,.} \tag{3.96}$$

This is the homogenized asymptotic SP_2 equation, with constants defined in Eqs. (3.67), (3.70), and (3.95).

It must be noted that calling Eq. (3.96) a SP_2 equation is misleading. In 1-D, SP_N and P_N are generally equivalent. However, Eq. (3.96) includes constants that have been integrated over all energies. Standard P_2 is continuous-energy (or monoenergetic if one begins with a monoenergetic transport equation). We therefore refer to Eq. (3.96) as "SP_2" because, for general energy-dependent problems, it does not depend on energy, whereas the conventional P_2 equation does depend on energy. [However, for mono-energetic problems, Eq. (3.96) and the standard P_2 equation are identical; we show this later.]

For the reconstructed flux, we keep the first three terms of the expansion in Eq. (3.7a):

$$\Psi(y,z,\mu,E)=\Psi_0(y,z,\mu,E)+\epsilon\Psi_1(y,z,\mu,E)+\epsilon^2\Psi_2(y,z,\mu,E)+O\left(\epsilon^3\right). \tag{3.97}$$

Substituting Eqs. (3.19), (3.29), and (3.39) into Eq. (3.97), we obtain:

$$\begin{aligned}\Psi(y,z,\mu,E)=&f_0(y,\mu,E)A_0(z)+\epsilon\left(f_0(y,\mu,E)A_1(z)-f_1(y,\mu,E)\frac{\partial}{\partial z}A_0(z)\right)\\&+\epsilon^2\left(f_0(y,\mu,E)A_2(z)-f_1(y,\mu,E)\frac{\partial}{\partial z}A_1(z)\right.\\&\left.+f_3(y,\mu,E)\frac{\partial^2}{\partial z^2}A_0(z)+\lambda_2 f_2(y,\mu,E)A_0(z)\right)+O\left(\epsilon^3\right)\\=&f_0(y,\mu,E)\left(A_0(z)+\epsilon A_1(z)+\epsilon^2A_2(z)\right)\\&-f_1(y,\mu,E)\epsilon\frac{\partial}{\partial z}\left(A_0(z)+\epsilon A_1(z)\right)\\&+f_3(y,\mu,E)\epsilon^2\frac{\partial^2}{\partial z^2}A_0(z)+\epsilon^2\lambda_2 f_2(y,\mu,E)A_0(z)+O\left(\epsilon^3\right).\end{aligned} \tag{3.98}$$

Adding $O\left(\epsilon^3\right)$ and higher order terms, we get:

$$\begin{aligned}\Psi(y,z,\mu,E) =& f_0(y,\mu,E)\left(A_0(z)+\epsilon A_1(z)+\epsilon^2(A_2(z)+\epsilon A_3(z))\right)\\ &-f_1(y,\mu,E)\,\epsilon\frac{\partial}{\partial z}\left(A_0(z)+\epsilon A_1(z)+\epsilon^2(A_2(z)+\epsilon A_3(z))\right)\\ &+f_3(y,\mu,E)\,\epsilon^2\frac{\partial^2}{\partial z^2}\left(A_0(z)+\epsilon A_1(z)+\epsilon^2(A_2(z)+\epsilon A_3(z))\right)\\ &+\epsilon^2\lambda_2 f_2(y,\mu,E)\left(A_0(z)+\epsilon A_1(z)+\epsilon^2(A_2(z)+\epsilon A_3(z))\right)+O\left(\epsilon^3\right)\\ =& f_0(y,\mu,E)\,\Phi(z)-f_1(y,\mu)\,\epsilon\frac{\partial}{\partial z}\Phi(z)\\ &+f_3(y,\mu,E)\,\epsilon^2\frac{\partial^2}{\partial z^2}\Phi(z)+\epsilon^2\lambda_2 f_2(y,\mu,E)\,\Phi(z)+O\left(\epsilon^3\right),\end{aligned} \tag{3.99}$$

and returning to the original spatial variable x yields:

$$\begin{aligned}\psi(x,\mu,E) =& f_0(x,\mu,E)\,\phi(x)-f_1(x,\mu,E)\frac{\partial}{\partial x}\phi(x)+f_3(x,\mu,E)\frac{\partial^2}{\partial x^2}\phi(x)\\ &+(\lambda-\lambda_0)f_2(x,\mu,E)\,\phi(x)+O\left(\epsilon^3\right).\end{aligned} \tag{3.100}$$

In practice, it can be difficult to accurately calculate $\frac{\partial^2}{\partial x^2}\phi(x)$ without an extremely fine mesh. To avoid this possible source of error, we eliminate the second derivative term using Eq. (3.96):

$$\boxed{\begin{aligned}\psi(x,\mu,E) =& f_0(x,\mu,E)\,\phi(x)-f_1(x,\mu,E)\frac{\partial}{\partial x}\phi(x)\\ &-f_3(x,\mu,E)\left(\frac{\lambda\overline{\nu\Sigma_f}-\overline{\Sigma}_a}{\overline{D}_0+\overline{D}_2\left(\overline{\nu\Sigma_f}-\overline{\Sigma}_a\right)}\right)\phi(x)\\ &+(\lambda-\lambda_0)f_2(x,\mu,E)\,\phi(x)+O\left(\epsilon^3\right).\end{aligned}} \tag{3.101}$$

If we set every lattice function other than $f_0(x,\mu,E)$ and $f_1(x,\mu,E)$ equal to zero, then $\overline{D}_2$ reduces to zero, and our homogenized SP_2 equation, Eq. (3.96), reduces to the homogenized diffusion equation, Eq. (3.75). Likewise, the SP_2 flux reconstruction, Eq. (3.101), reduces to the diffusion reconstructed flux, Eq. (3.80). This is equivalent to setting higher order terms [ϵ^4 in Eq. (3.96) and ϵ^2 in Eq. (3.101)] to zero, confirming that the SP_2 equations

represent a higher order correction to the diffusion approximation defined in Section 3.2 [Eqs. (3.75) and (3.80)].

3.4 Monoenergetic, Homogeneous Medium

In a monoenergetic, homogeneous medium, many of the expressions from Sections 3.2 and 3.3 reduce to simple functions of y and μ. For a monoenergetic, homogeneous medium, the infinite-lattice operator L becomes:

$$Lf(y,\mu) = \Sigma_t f(y,\mu) - \left(\Sigma_s + \lambda_0 \nu\Sigma_f\right) \int_{-1}^{1} f(y,\mu')\, d\mu' , \tag{3.102}$$

and the adjoint infinite-lattice operator L^* equivalent to L:

$$\begin{aligned} L^* f^*(y,\mu) =& \Sigma_t f^*(y,\mu) - \left(\Sigma_s + \lambda_0 \nu\Sigma_f\right) \int_{-1}^{1} f^*(y,\mu')\, d\mu' \\ =& Lf(y,\mu) . \end{aligned} \tag{3.103}$$

The solution to $Lf_0(y,\mu) = 0$ is now independent of y and μ, and therefore must be a constant. The same is true of $f_0^*(y,\mu)$. If we propose the normalization

$$F_0(y) = \int_{-1}^{1} f_0(y,\mu)\, d\mu = 1 , \tag{3.104a}$$

and

$$F_0^*(y) = \int_{-1}^{1} f_0^*(y,\mu)\, d\mu = 1 , \tag{3.104b}$$

then

$$f_0(y,\mu) = f_0^*(y,\mu) = \frac{1}{2} . \tag{3.105a}$$

Thus, λ_0 reduces to:

$$\lambda_0 = \frac{\nu\Sigma_f}{\Sigma_t - \Sigma_s} = \frac{\nu\Sigma_f}{\Sigma_a} . \tag{3.106}$$

If we hypothesize that $f_1(y,\mu)$, the solution to

$$Lf_1(y,\mu) = \Sigma_t f_1(y,\mu) - \left(\Sigma_s + \lambda_0 \nu \Sigma_f\right) \int_{-1}^{1} f_1(y,\mu')\, d\mu' = \mu f_0(y,\mu) = \frac{1}{2}\mu\,, \tag{3.107}$$

is a linear function of μ, then introducing our ansatz $f_1(y,\mu) = C\mu$ into Eq. (3.107), we find that:

$$f_1(y,\mu) = \frac{\mu}{2\Sigma_t}\,. \tag{3.108}$$

For $Lf_2(y,\mu)$, we note that the source $(I-P)\frac{\nu\Sigma_f}{2}F_0(y) = 0$, yielding $Lf_2(y,\mu) = 0$. By Eq. (3.27b), we have

$$\begin{aligned}\int_0^h \int_{-1}^{1} f_0^*(y,\mu)\, f_2(y,\mu)\, d\mu dy &= \int_0^h \int_{-1}^{1} \frac{1}{2} f_2(y,\mu) \\ &= 0\,,\end{aligned} \tag{3.109}$$

which implies that

$$f_2(y,\mu) = 0\,. \tag{3.110}$$

Following the same analysis for f_3, f_4, f_5, and f_6, we obtain:

$$f_3(y,\mu) = L^{-1}\Big[(I-P)\mu f_1(y,\mu)\Big] = \frac{3\mu^2 - 1}{2\Sigma_t^2}\,, \tag{3.111a}$$

$$f_4(y,\mu) = L^{-1}\Big[\frac{\nu\Sigma_f}{2}F_1(y)\Big] = 0\,, \tag{3.111b}$$

$$f_5(y,\mu) = L^{-1}\Big[\mu f_2(y,\mu)\Big] = 0\,, \tag{3.111c}$$

and

$$f_6(y,\mu) = L^{-1}\Big[\mu f_3(y,\mu)\Big] = \frac{3\mu^3 - \mu}{2\Sigma_t^3}\,. \tag{3.111d}$$

Converting back to x and substituting Eqs. (3.105), (3.108), (3.110), and (3.111) into

Eqs. (3.70) and (3.95), we find that

$$\overline{D}_0 = \frac{1}{3\Sigma_t}\,, \tag{3.112a}$$

and

$$\overline{D}_2 = -\frac{4}{15\Sigma_t^2}\,. \tag{3.112b}$$

The diffusion equation, Eq. (3.75), then reduces to

$$-\frac{1}{3\Sigma_t}\frac{\partial^2}{\partial x^2}\phi_0(x) + \overline{\Sigma_a}\phi_0(x) = \lambda\overline{\nu\Sigma_f}\phi_0(x)\,, \tag{3.113}$$

the standard (isotropic scattering) diffusion equation, while the diffusion expression for flux reconstruction, Eq. (3.80), becomes

$$\psi(x,\mu) = \frac{1}{2}\phi_0(x) - \frac{\mu}{2\Sigma_t}\frac{\partial}{\partial x}\phi_0(x) + O\left(\epsilon^2\right), \tag{3.114}$$

the standard 1-D, monoenergetic P_1 approximation for the angular flux.

Likewise, Eq. (3.96) reduces to

$$-\left[\frac{1}{3\Sigma_t} - \frac{4}{15\Sigma_t^2}\left(\lambda\overline{\nu\Sigma_f} - \overline{\Sigma_a}\right)\right]\frac{\partial^2}{\partial x^2}\phi(x) + \overline{\Sigma_a}\phi(x) = \lambda\overline{\nu\Sigma_f}\phi(x)\,, \tag{3.115}$$

the standard SP_2 equation, with flux reconstruction given by

$$\psi(x,\mu) = \frac{1}{2}\phi(x) - \frac{\mu}{2\Sigma_t}\frac{\partial}{\partial x}\phi(x) + \frac{3\mu^2-1}{2\Sigma_t^2}\frac{\partial^2}{\partial x^2}\phi(x)\,, \tag{3.116}$$

the standard 1-D, monoenergetic P_2 prescription for the angular flux.

This implies that, for one energy group in a homogeneous medium, the asymptotic equations derived in Sections 3.2 and 3.3 are equivalent to the standard P_1 and P_2 approximations. While this does not fully justify previous applications of diffusion and P_2 theory, it presents

a case that their derivations are valid in certain circumstances.

3.5 Summary

In this chapter, we applied an asymptotic analysis to the 1-D, continuous energy, lattice-geometry, Boltzmann transport equation. In this analysis, we defined six important lattice functions [Eqs. (3.15), (3.25), (3.40), and (3.48)]:

$$Lf_0(x,\mu,E) = 0\,, \tag{3.117a}$$

$$f_1(x,\mu,E) = L^{-1}\Big[\mu f_0(x,\mu,E)\Big], \tag{3.117b}$$

$$f_2(x,\mu,E) = L^{-1}\left[(I-P)\frac{\chi(x,E)}{2}\int_0^\infty \nu\Sigma_f(x,E')F_0(x,E')\right], \tag{3.117c}$$

$$f_3(x,\mu,E) = L^{-1}\Big[(I-P)\mu f_1(x,\mu,E)\Big], \tag{3.117d}$$

$$f_4(x,\mu,E) = L^{-1}\left[\frac{\chi(x,E)}{2}\int_0^\infty \nu\Sigma_f(x,E')F_1(x,E')dE'\right], \tag{3.117e}$$

$$f_5(x,\mu,E) = L^{-1}\Big[\mu f_2(x,\mu,E)\Big], \tag{3.117f}$$

and

$$f_6(x,\mu,E) = L^{-1}\Big[\mu f_3(x,\mu,E)\Big]. \tag{3.117g}$$

In Eqs. (3.117), L^{-1} is the *pseudo-inverse*.

The lattice functions were used to define the homogenized parameters [Eqs. (3.67)]:

$$\overline{\Sigma_a} = \frac{\int_0^h\int_0^\infty \Sigma_a(x,E)F_0(x,E)dEdx}{\int_0^h\int_0^\infty F_0(x,E)dEdx}\,, \tag{3.118a}$$

and

$$\overline{\nu\Sigma_f} = \frac{\int_0^h\int_0^\infty \nu\Sigma_f(x,E)F_0(x,E)dEdx}{\int_0^h\int_0^\infty F_0(x,E)dEdx}\,, \tag{3.118b}$$

as well as the asymptotic diffusion coefficients [Eq (3.70)]:

$$\overline{D_0} = \frac{\int_0^h \int_0^\infty \nu\Sigma_f(x,E) F_0(x,E) dEdx}{\int_0^h \int_0^\infty F_0(x,E) dEdx} \times \frac{\int_0^h \int_0^\infty \int_{-1}^1 \mu f_0^*(x,\mu,E) f_1(x,\mu,E) d\mu dEdx}{\int_0^h \int_0^\infty F_0^*(x,E) \frac{1}{2}\chi(x,E) \int_0^\infty \nu\Sigma_f(x,E') F_0(x,E') dE' dEdx}, \tag{3.119}$$

and [Eq (3.95)]

$$\overline{D}_2 = -\frac{\overline{D}_1}{\overline{D}_0} + \overline{\Sigma}_{f,0} + \overline{\Sigma}_{f,1} - \overline{\Sigma}_{f,2}\overline{D}_0 . \tag{3.120}$$

Here

$$\overline{D}_1 = \frac{\int_0^h \int_0^\infty \nu\Sigma_f(x,E) F_0(x,E) dEdx}{\int_0^h \int_0^\infty F_0(x,E) dEdx} \times \frac{\int_0^h \int_0^\infty \int_{-1}^1 \mu f_0^*(x,\mu,E) f_6(x,\mu,E) d\mu dEdx}{\int_0^h \int_0^\infty F_0^*(x,E) \frac{1}{2}\chi(x,E) \int_0^\infty \nu\Sigma_f(x,E') F_0(x,E') dE' dEdx}, \tag{3.121a}$$

$$\overline{\Sigma}_{f,0} = \frac{\int_0^h \int_0^\infty \int_{-1}^1 \mu f_0^*(x,\mu,E) f_5(x,\mu,E) d\mu dEdx}{\int_0^h \int_0^\infty F_0^*(x,E) \frac{1}{2}\chi(x,E) \int_0^\infty \nu\Sigma_f(x,E') F_0(x,E') dE' dEdx}, \tag{3.121b}$$

$$\overline{\Sigma}_{f,1} = \frac{\int_0^h \int_0^\infty F_0^*(x,\mu,E) \frac{1}{2}\chi(x,E) \int_0^\infty \nu\Sigma_f(x,E') F_3(x,E') dE' dEdx}{\int_0^h \int_0^\infty F_0^*(x,E) \frac{1}{2}\chi(x,E) \int_0^\infty \nu\Sigma_f(x,E') F_0(x,E') dE' dEdx}, \tag{3.121c}$$

and

$$\overline{\Sigma}_{f,2} = \frac{1}{\overline{\nu\Sigma_f}} \frac{\int_0^h \int_0^\infty F_0^*(x,\mu,E) \frac{\chi(x,E)}{2} \int_0^\infty \nu\Sigma_f(x,E') F_2(x,E') dE' dEdx}{\int_0^h \int_0^\infty F_0^*(x,E) \frac{1}{2}\chi(x,E) \int_0^\infty \nu\Sigma_f(x,E') F_0(x,E') dE' dEdx}. \tag{3.121d}$$

The homogenized parameters are then used in the 1-D, homogenized, asymptotic SP_2 equation [Eq. (3.96]:

$$-\left[\overline{D}_0 + \left(\lambda\overline{\nu\Sigma_f} - \overline{\Sigma_a}\right)\overline{D}_2\right]\frac{\partial^2}{\partial x^2}\phi(x) + \overline{\Sigma_a}\phi(x) = \lambda\overline{\nu\Sigma_f}\phi(x) , \tag{3.122}$$

with the corresponding flux reconstruction formula (Eq. (3.101):

$$\begin{aligned}\psi(x,\mu,E) =& f_0(x,\mu,E)\phi(x) - f_1(x,\mu,E)\frac{\partial}{\partial x}\phi(x) \\ &- f_3(x,\mu,E)\left(\frac{\lambda\overline{\nu\Sigma_f} - \overline{\Sigma}_a}{\overline{D}_0 + \overline{D}_2\left(\overline{\nu\Sigma_f} - \overline{\Sigma}_a\right)}\right)\phi(x) \\ &+ (\lambda - \lambda_0) f_2(x,\mu,E)\phi(x) + O\left(\epsilon^3\right).\end{aligned} \tag{3.123}$$

We have not discussed boundary conditions, instead saving that for Chapter 4, when we discuss the numerical implementation of Eq. (3.122).

CHAPTER 4

Asymptotic Analysis of the 1-D Continuous Energy Lattice-Geometry Transport Equation – Numerical Results

In this chapter, we numerically evaluate the 1-D, monoenergetic, homogenized SP_2 equation derived in Chapter 3. Because any evaluation of SP_N is incomplete without also including discontinuity factors, we first present a brief discussion and derivation of discontinuity factors for 1-D asymptotic SP_2. Our numerical results show that the asymptotic SP_2 equation significantly reduces the scalar flux errors within the core, but not necessarily in the reflector region. This improvement in accuracy is particularly evident in small problems with steep flux gradients, in which the diffusion approximation is less valid.

4.1 Discontinuity Factors

During the past thirty years, one of the most important innovations in diffusion codes for LWR analysis has been the application of discontinuity factors (DFs) [12], which are based on Equivalence Theory [11]. DFs were introduced to ensure that angular moments of the reconstructed angular flux would be continuous at an interface, while allowing the diffusion solution to be discontinuous.

The same idea can be applied to the asymptotic diffusion and SP_2 equations, which

have (i) a diffusion form, and (ii) a reconstructed angular flux that is easily suited to calculating angular integrals. The fact that the classic SP_2 solution is discontinuous at material interfaces is irrelevant, since DFs will be used at these locations anyway.

In this section, we obtain DFs at an interface for the diffusion and SP_2 equation by setting angular integrals (angular moments) of the reconstructed flux equal to each other at that interface (x_0):

$$\int_{-1}^{1} g(\mu)\psi\left(x_0^-,\mu\right)d\mu = \int_{-1}^{1} g(\mu)\psi\left(x_0^+,\mu\right)d\mu\,, \tag{4.1}$$

where

$$x_0^+ = \lim_{\epsilon\to 0}\left[x_0+\varepsilon\right], \tag{4.2a}$$

$$x_0^- = \lim_{\epsilon\to 0}\left[x_0-\varepsilon\right], \tag{4.2b}$$

and $g(\mu)$ can be any function of μ. The choice $g(\mu) = 1$ is equivalent to requiring the reconstructed scalar flux to be continuous, and the choice $g(\mu) = \mu$ is equivalent to requiring the reconstructed current to be continuous. In this section, both $g(\mu) = 1$ and $g(\mu) = \mu$ are used to obtain *two* sets of DFs. A similar approach can be used to derive DFs with $g(\mu) = \mu^2$. While we derive DFs for the monoenergetic problem, the same process can be extended to energy-dependent problems.

4.1.1 Diffusion

To obtain discontinuity factors for the asymptotic diffusion equation defined in Section 3.2 [Eq. (3.75)], we use the reconstructed flux defined in that same section, Eq. (3.80).

Introducing Eq. (3.80) into Eq. (4.1), we obtain

$$\begin{aligned}\int_{-1}^{1} g(\mu)\left[f_0^-\left(x_0^-,\mu\right)\phi_0\left(x_0^-\right) - f_1^-\left(x_0^-,\mu\right)\frac{\partial}{\partial x}\phi_0\left(x_0^-\right)\right]d\mu \\ = \int_{-1}^{1} g(\mu)\left[f_0^+\left(x_0^+,\mu\right)\phi_0\left(x_0^+\right) - f_1^+\left(x_0^+,\mu\right)\frac{\partial}{\partial x}\phi_0\left(x_0^+\right)\right]d\mu\,,\end{aligned} \tag{4.3}$$

where $f_n^{\pm}(x)$ corresponds to the n-th lattice function of the assembly to the right (+) or left (-) of the interface. In Section 3.1 and Appendix B, we saw that $f_0(x_0,\mu)$ is an even function of μ and $f_1(x_0,\mu)$ is an odd function of μ. Therefore, for $g(\mu) = 1$, Eq. (4.1) simplifies to

$$\left(\int_{-1}^{1} f_0^{-}\left(x_0^{-},\mu\right)d\mu\right)\phi_0\left(x_0^{-}\right) = \left(\int_{-1}^{1} f_0^{+}\left(x_0^{+},\mu\right)d\mu\right)\phi_0\left(x_0^{+}\right), \tag{4.4}$$

or

$$\alpha^{-}\phi_0\left(x_0^{-}\right) = \alpha^{+}\phi_0\left(x_0^{+}\right), \tag{4.5}$$

where the *flux discontinuity* factors are defined as:

$$\alpha^{\pm} = \int_{-1}^{1} f_0^{\pm}\left(x_0^{\pm},\mu\right)d\mu. \tag{4.6}$$

For $g(\mu) = \mu$, Eq. (4.3) reduces to

$$-\left(\int_{-1}^{1} \mu f_1^{-}\left(x_0^{-},\mu\right)d\mu\right)\frac{\partial}{\partial x}\phi_0\left(x_0^{-}\right) = -\left(\int_{-1}^{1} \mu f_1^{+}\left(x_0^{+},\mu\right)d\mu\right)\frac{\partial}{\partial x}\phi_0\left(x_0^{+}\right). \tag{4.7}$$

From Eq. (4.7), we can obtain an expression for discontinuity factors for the derivative of the flux. In practice, however, we are interested in an expression for the diffusion current:

$$J_{diffusion} = -\overline{D}_0\frac{\partial}{\partial x}\phi_0(x). \tag{4.8}$$

Combining Eqs. (4.7) and (4.8) yields an equation for continuity of the diffusion current:

$$-\beta^{-}\overline{D}_0^{-}\frac{\partial}{\partial x}\phi_0\left(x_0^{-}\right) = \beta^{+}\overline{D}_0^{+}\frac{\partial}{\partial x}\phi_0\left(x_0^{+}\right), \tag{4.9}$$

where the *current discontinuity factors* are defined as:

$$\beta^{\pm} = \frac{1}{\overline{D}_0^{\pm}}\int_{-1}^{1} \mu f_1^{\pm}\left(x_0^{\pm},\mu\right)d\mu. \tag{4.10}$$

Eq. (4.6) is the standard diffusion flux discontinuity factor. Most modern diffusion codes, however, do not include any form of discontinuity factor for the current. Therefore Eq. (4.10), first introduced in Trahan's work [15], is unique to these asymptotic derivations.

4.1.2 SP_2

To derive asymptotic SP_2 DFs, we perform the same analysis as in Section 4.1.1, but with the SP_2 expression for the reconstructed angular flux. Introducing Eq. (3.100) into Eq. (4.1), we obtain

$$\begin{aligned}
&\int_{-1}^{1} g(\mu)\Big[f_0^-\left(x_0^-,\mu\right)\phi_0\left(x_0^-\right) - f_1^-\left(x_0^-,\mu\right)\frac{\partial}{\partial x}\phi_0\left(x_0^-\right) \\
&\quad + f_3^-\left(x_0^-,\mu\right)\frac{\partial^2}{\partial x^2}\phi_0\left(x_0^-\right) + (\lambda-\lambda_0^-)f_2^-(x,\mu)\phi_0\left(x_0^-\right)\Big]d\mu \\
&\quad = \int_{-1}^{1} g(\mu)\Big[f_0^+\left(x_0^+,\mu\right)\phi_0\left(x_0^+\right) - f_1^+\left(x_0^+,\mu\right)\frac{\partial}{\partial x}\phi_0\left(x_0^+\right) \\
&\qquad + f_3^+\left(x_0^+,\mu\right)\frac{\partial^2}{\partial x^2}\phi\left(x_0^+\right) + (\lambda-\lambda_0^+)f_2^+\left(x_0^+,\mu\right)\phi\left(x_0^+\right)\Big]d\mu\,,
\end{aligned} \tag{4.11}$$

or, from Eq. (3.101),

$$\begin{aligned}
&\int_{-1}^{1} g(\mu)\Big[f_0^-\left(x_0^-,\mu\right)\phi_0\left(x_0^-\right) - f_1^-\left(x_0^-,\mu\right)\frac{\partial}{\partial x}\phi_0\left(x_0^-\right) \\
&\quad + f_3^-\left(x_0^-,\mu\right)\left(\frac{\lambda\overline{\nu\Sigma_f}-\overline{\Sigma}_a}{\overline{D}_0+\overline{D}_2\left(\overline{\nu\Sigma_f}-\overline{\Sigma}_a\right)}\right)^-\phi_0\left(x_0^-\right) \\
&\quad + (\lambda-\lambda_0^-)f_2^-(x,\mu)\phi_0\left(x_0^-\right)\Big]d\mu \\
&\quad = \int_{-1}^{1} g(\mu)\Big[f_0^+\left(x_0^+,\mu\right)\phi_0\left(x_0^+\right) - f_1^+\left(x_0^+,\mu\right)\frac{\partial}{\partial x}\phi_0\left(x_0^+\right) \\
&\qquad + f_3^+\left(x_0^+,\mu\right)\left(\frac{\lambda\overline{\nu\Sigma_f}-\overline{\Sigma}_a}{\overline{D}_0+\overline{D}_2\left(\overline{\nu\Sigma_f}-\overline{\Sigma}_a\right)}\right)^+\phi\left(x_0^+\right) \\
&\qquad + (\lambda-\lambda_0^+)f_2^+\left(x_0^+,\mu\right)\phi\left(x_0^+\right)\Big]d\mu\,,
\end{aligned} \tag{4.12}$$

where $f_n^{\pm}\left(x_0^{\pm}\right)$ again corresponds to the n-th lattice function of the assembly to the right (+) or left (-) of the interface, $\lambda_0^{\pm}$ corresponds to the infinite lattice eigenvalue for the right or left cell, and $\left(\frac{\lambda\overline{\nu\Sigma_f}-\overline{\Sigma}_a}{\overline{D}_0+\overline{D}_2\left(\overline{\nu\Sigma_f}-\overline{\Sigma}_a\right)}\right)^{\pm}$ indicates whether the homogenized parameters are from the cell to the right or left.

In Section 3.1 and Appendix B, it was shown that $f_0(x_0,\mu)$, $f_2(x_0,\mu)$, and $f_3(x_0,\mu)$ are even functions of μ, and $f_1(x_0,\mu)$ is an odd function of μ. Therefore, for $g(\mu)=1$, Eq. (4.1) simplifies to

$$\begin{aligned}\int_{-1}^{1}\Bigg[f_0^-\left(x_0^-,\mu\right)+f_3^-\left(x_0^-,\mu\right)\left(\frac{\lambda\overline{\nu\Sigma_f}-\overline{\Sigma}_a}{\overline{D}_0+\overline{D}_2\left(\overline{\nu\Sigma_f}-\overline{\Sigma}_a\right)}\right)^-\\ +(\lambda-\lambda_0^-)f_2^-\left(x_0^-,\mu\right)\Bigg]d\mu\phi_0\left(x_0^-\right)\\ =\int_{-1}^{1}\Bigg[f_0^+\left(x_0^+,\mu\right)+f_3^+\left(x_0^+,\mu\right)\left(\frac{\lambda\overline{\nu\Sigma_f}-\overline{\Sigma}_a}{\overline{D}_0+\overline{D}_2\left(\overline{\nu\Sigma_f}-\overline{\Sigma}_a\right)}\right)^+\\ +(\lambda-\lambda_0^+)f_2^+\left(x_0^+,\mu\right)\Bigg]d\mu\phi_0\left(x_0^+\right),\end{aligned} \tag{4.13}$$

or

$$\alpha^-\phi_0\left(x_0^-\right)=\alpha^+\phi_0\left(x_0^+\right), \tag{4.14}$$

where the SP_2 flux discontinuity factors are defined as:

$$\begin{aligned}\alpha^{\pm}=\int_{-1}^{1}\Bigg[f_0^{\pm}\left(x_0^{\pm},\mu\right)+f_3^{\pm}\left(x_0^{\pm},\mu\right)\left(\frac{\lambda\overline{\nu\Sigma_f}-\overline{\Sigma}_a}{\overline{D}_0+\overline{D}_2\left(\overline{\nu\Sigma_f}-\overline{\Sigma}_a\right)}\right)^{\pm}\\ +(\lambda-\lambda_0^{\pm})f_2^{\pm}\left(x_0^{\pm},\mu\right)\Bigg]d\mu.\end{aligned} \tag{4.15}$$

For $g(\mu)=\mu$, we obtain

$$-\left(\int_{-1}^{1}\mu f_1^-\left(x_0^-,\mu\right)d\mu\right)\frac{\partial}{\partial x}\phi_0\left(x_0^-\right)=-\left(\int_{-1}^{1}\mu f_1^+\left(x_0^+,\mu\right)d\mu\right)\frac{\partial}{\partial x}\phi_0\left(x_0^+\right). \tag{4.16}$$

Again, Eq. (4.16) only gives us an expression for discontinuity factors for the derivative of

the flux. However, we are interested in an expression for the SP_2 current:

$$J_{SP_2} = -\left[\overline{D}_0 + \left(\lambda\overline{\nu\Sigma_f} - \overline{\Sigma}_a\right)\overline{D}_2\right]\frac{\partial}{\partial x}\phi_0(x)\,. \tag{4.17}$$

Combining Eqs. (4.16) and (4.17) yields an equation for continuity of the diffusion current:

$$\begin{aligned} -\beta^-\left[\overline{D}_0 + \left(\lambda\overline{\nu\Sigma_f} - \overline{\Sigma}_a\right)\overline{D}_2\right]^- \frac{\partial}{\partial x}\phi_0\left(x_0^-\right) \\ = \beta^+\left[\overline{D}_0 + \left(\lambda\overline{\nu\Sigma_f} - \overline{\Sigma}_a\right)\overline{D}_2\right]^+ \frac{\partial}{\partial x}\phi_0\left(x_0^+\right), \end{aligned} \tag{4.18}$$

where the current discontinuity factors are defined as:

$$\beta^\pm = \frac{1}{\left[\overline{D}_0 + \left(\lambda\overline{\nu\Sigma_f} - \overline{\Sigma}_a\right)\overline{D}_2\right]^\pm}\int_{-1}^{1}\mu f_1^\pm\left(x_0^\pm,\mu\right)d\mu\,. \tag{4.19}$$

Eqs. (4.15) and (4.19) form the monoenergetic discontinuity factors for Eq. (3.96). They include the clear disadvantage of changing with λ, which requires the discontinuity factors to be periodically updated.

4.1.3 Reflector

In Chapter 3, the lattice functions $f_n(x,\mu,E)$ were calculated with the assumption that the cell of interest is fissile, i.e.

$$\int_0^h \nu\Sigma_f(x,E)\,dx > 0\,. \tag{4.20}$$

In a non-multiplying region, such as a reflector or absorber, this assumption no longer holds. We are therefore left with the question of what ψ should be in a non-multiplying region.

4.1.3.1 Naïve

The naïve answer is to assume the non-multiplying region is a homogeneous medium and use Eqs. (3.114) and (3.116). Under this assumption, Eqs. (4.6), (4.10), (4.15), and (4.19) become

$$\alpha^{\pm}_{reflector,diffusion} = 1\,, \tag{4.21a}$$

$$\beta^{\pm}_{reflector,diffusion} = \frac{1}{\overline{D}_0^{\pm}}\frac{1}{3\Sigma_t} = 1\,, \tag{4.21b}$$

$$\alpha^{\pm}_{reflector,SP_2} = \left[1 + 0\left(\frac{\lambda\overline{\nu\Sigma_f} - \overline{\Sigma}_a}{\overline{D}_0 + \overline{D}_2\left(\overline{\nu\Sigma_f} - \overline{\Sigma}_a\right)}\right)^{\pm} + 0\right] = 1\,, \tag{4.21c}$$

and

$$\begin{aligned}\beta^{\pm}_{reflector,SP_2} &= \frac{1}{\left[\overline{D}_0 + \left(\lambda\overline{\nu\Sigma_f} - \overline{\Sigma}_a\right)\overline{D}_2\right]^{\pm}}\frac{1}{3\Sigma_t} \\ &= \frac{\overline{D}_0}{\left[\overline{D}_0 + \left(\lambda\overline{\nu\Sigma_f} - \overline{\Sigma}_a\right)\overline{D}_2\right]^{\pm}}\,,\end{aligned} \tag{4.21d}$$

respectively.

Eqs. (4.21) are overly simple. They imply that in a non-multiplying region, the diffusion equation captures the complexity of the solution at an interface in its entirety. Moreover, Eq. (4.21d) suggests that the diffusion current is more accurate than the SP_2 current in a reflector.

4.1.3.2 Analytic

While Eqs. (4.21) may be used to obtain *a* solution in the reflector, we desire something with greater accuracy. A second way to derive standard DFs in the reflector is to use an analytic solution of the transport equation in a non-multiplying region with constant cross

sections,

$$\mu\frac{\partial}{\partial x}\psi(x,\mu)+\Sigma_t\psi(x,\mu)=\frac{\Sigma_s}{2}\int_{-1}^{1}\psi(x,\mu')\,d\mu'\,. \tag{4.22}$$

Assuming that the solution ψ is separable in space and angle, we have the ansatz:

$$\psi_{reflector}=a^{+}(\mu)\,e^{\Sigma_t x/\nu_0}+a^{-}(\mu)\,e^{-\Sigma_t x/\nu_0}\,. \tag{4.23}$$

If we consider a reflector on the left side of the problem, we know that $e^{-\Sigma_t x/\nu_0}$ grows large at the left boundary of the problem, when $\psi\to 0$. Therefore, $a^{-}(\mu)\ll 0$ and can be ignored, and Eq. (4.23) becomes

$$\psi_{reflector}=a(\mu)\,e^{\Sigma_t x/\nu_0}\,. \tag{4.24}$$

Substituting Eq. (4.24) into Eq. (4.22), we have

$$\begin{aligned}
\mu\frac{\partial}{\partial x}\Big(a(\mu)\,e^{\Sigma_t x/\nu_0}\Big)+\Sigma_t\left(a(\mu)\,e^{\Sigma_t x/\nu_0}\right)&=\frac{\Sigma_s}{2}\int_{-1}^{1}\Big(a(\mu')\,e^{\Sigma_t x/\nu_0}\Big)d\mu'\\
\mu a(\mu)\,\frac{\Sigma_t}{\nu_0}e^{\Sigma_t x/\nu_0}+a(\mu)\,\Sigma_t e^{\Sigma_t x/\nu_0}&=\frac{\Sigma_s}{2}e^{\Sigma_t x/\nu_0}\int_{-1}^{1}a(\mu')\,d\mu'\\
a(\mu)\Sigma_t\Big(\frac{\mu}{\nu_0}+1\Big)&=\frac{\Sigma_s}{2}\int_{-1}^{1}a(\mu')\,d\mu'\\
a(\mu)&=\frac{1}{\left(\frac{\mu}{\nu_0}+1\right)}\frac{\Sigma_s}{2\Sigma_t}\int_{-1}^{1}a(\mu')\,d\mu'\\
a(\mu)&=\frac{\nu_0}{\mu+\nu_0}\frac{\Sigma_s}{2\Sigma_t}\int_{-1}^{1}a(\mu')\,d\mu'\,.
\end{aligned} \tag{4.25}$$

The constant ν_0 is found by integrating Eq. (4.25) over angle,

$$\begin{aligned}
\int_{-1}^{1} a(\mu)\,d\mu &= \int_{-1}^{1} \frac{\nu_0}{\mu+\nu_0}\frac{\Sigma_s}{2\Sigma_t}\int_{-1}^{1} a(\mu')\,d\mu'\,d\mu \\
\int_{-1}^{1} a(\mu)\,d\mu &= \left(\int_{-1}^{1} \frac{\nu_0}{\mu+\nu_0}d\mu\right)\frac{\Sigma_s}{2\Sigma_t}\int_{-1}^{1} a(\mu')\,d\mu' \\
1 &= \frac{\Sigma_s}{2\Sigma_t}\int_{-1}^{1}\left(\frac{\nu_0}{\mu+\nu_0}\right)d\mu \\
1 &= \frac{\nu_0\Sigma_s}{2\Sigma_t}\ln\left(\frac{\nu_0+1}{\nu_0-1}\right),
\end{aligned} \tag{4.26}$$

and iteratively solving the resulting transcendental equation for ν_0. Combining Eqs. (4.25) and (4.24) yields

$$\begin{aligned}
\psi_{reflector} =& A\frac{\nu_0}{\mu+\nu_0}\frac{\Sigma_s}{2\Sigma_t}e^{\Sigma_t x/\nu_0} \\
=& A\frac{\Sigma_s}{2\Sigma_t}\frac{\nu_0}{\nu_0^2-\mu^2}\Big[\nu_0-\mu\Big]e^{\Sigma_t x/\nu_0} \\
=& \frac{\Sigma_s}{2\Sigma_t}\frac{\nu_0}{\nu_0^2-\mu^2}\left[\nu_0\phi(x)-\frac{\mu\nu_0}{\Sigma_t}\frac{\partial}{\partial x}\phi(x)\right] \\
=& \frac{\Sigma_s}{2\Sigma_t}\frac{\nu_0^2}{\nu_0^2-\mu^2}\left[\phi(x)-\frac{\mu}{\Sigma_t}\frac{\partial}{\partial x}\phi(x)\right] \\
=& f_0(\mu)\,\phi(x)-f_1(\mu)\,\frac{\partial}{\partial x}\phi(x)\,,
\end{aligned} \tag{4.27}$$

where A is an unknown constant,

$$\phi(x) = Ae^{\Sigma_t x/\nu_0}\,, \tag{4.28a}$$

$$f_0(\mu) = \frac{\Sigma_s}{2\Sigma_t}\frac{\nu_0^2}{\nu_0^2-\mu^2}\,, \tag{4.28b}$$

is an even function of μ, and

$$f_1(\mu) = \frac{\Sigma_s}{2\Sigma_t}\frac{\nu_0^2}{\nu_0^2-\mu^2}\frac{\mu}{\Sigma_t} \tag{4.28c}$$

is an odd function of μ.

Our ansatz $\psi_{reflector}$ can also yield a diffusion coefficient for the reflector. The diffusion equation in the reflector is

$$-D\frac{\partial^2}{\partial x^2}\phi(x)+\Sigma_a\phi(x)=0\,. \tag{4.29}$$

Substituting Eq. (4.28a) into Eq. (4.29) and solving for D, we obtain

$$D=\frac{\nu_0^2\Sigma_a}{\Sigma_t^2}\,. \tag{4.30}$$

We perform the same analysis from Section 3.1 to obtain DFs. For diffusion,

$$\begin{aligned}\alpha^{\pm}_{reflector,diffusion}&=\int_{-1}^{1}f_0(\mu)\,d\mu\\&=\frac{\nu_0^2\Sigma_s}{2\Sigma_t}\int_{-1}^{1}\frac{1}{\nu_0^2-\mu^2}d\mu\\&=\frac{\nu_0\Sigma_s}{2\Sigma_t}\ln\left(\frac{\nu_0+1}{\nu_0-1}\right).\end{aligned} \tag{4.31}$$

Using Eq. (4.26), Eq. (4.31) simplifies to

$$\alpha^{\pm}_{reflector,diffusion}=1\,. \tag{4.32}$$

Likewise,

$$\begin{aligned}\beta^{\pm}_{reflector,diffusion}&=\frac{1}{\overline{D}_0^{\pm}}\int_{-1}^{1}\mu f_1(\mu)\,d\mu\\&=\frac{1}{\overline{D}_0^{\pm}}\frac{\nu_0^2\Sigma_s}{2\Sigma_t^2}\int_{-1}^{1}\frac{\mu^2}{\nu_0^2-\mu^2}d\mu\\&=\frac{1}{\overline{D}_0^{\pm}}\frac{\nu_0\Sigma_s}{2\Sigma_t^2}\left[\nu_0\ln\left(\frac{\nu_0+1}{\nu_0-1}\right)-2\right].\end{aligned} \tag{4.33}$$

We use Eqs. (4.26) and (4.30) to simplify Eq. (4.33),

$$\beta^{\pm}_{reflector,diffusion} = \frac{1}{\overline{D}_0^{\pm}} \frac{\nu_0^2(\Sigma_t - \Sigma_s)}{\Sigma_t^2}$$
$$= 1\,. \tag{4.34}$$

The results for SP_2 are the same, although the analytic solution for $\psi_{reflector}$ implies that $\overline{D}_2 = 0$ for the SP_2 current.

4.2 Implementation

In order to evaluate the asymptotic, homogenized, monoenergetic SP_2 theory, several test cases were run. The test cases were designed to:

1. compare standard homogenized diffusion and SP_2 with asymptotic homogenized diffusion and SP_2;

2. evaluate asymptotic homogenized SP_2 flux reconstruction versus asymptotic homogenized diffusion flux reconstruction and standard flux reconstruction;

3. and compare DFs calculated with various moments of angle and analytic reflector DFs.

For each case, the six lattice functions ($f_0(x,\mu,E)$ to $f_5(x,\mu,E)$) and four homogenized parameters required to solve Eqs. (3.75) and (3.96) were calculated with a 1-D, monoenergetic, fine-mesh discrete ordinates (S_{32}) code. The same code was used to obtain reference scalar fluxes for each test problem.

Once the lattice functions and homogenized parameters are calculated for each cell, Eqs. (3.75) and (3.96) can be solved. A central finite-difference approximation with discontinuity factors is used.

While the eigenvalue problem described by Eq. (3.75) can be solved with traditional iterative techniques, like the power method, Eq. (3.96) requires a special solution method. When the standard diffusion equation is discretized, a fixed iteration matrix is obtained. This is not true for SP_2. In a fissile material, the $\partial^2\phi(x)/\partial x^2$ term in Eq. (3.96) includes λ, the global eigenvalue. The discretization of the SP_2 equation, therefore, results in a matrix that changes with λ. This will inherently increase the computational cost, but without affecting the iteration scheme.

An alternate, simpler method for solving Eq. (3.96) uses a change of variables. If we define:

$$\xi(x) = \left(1 - \overline{\Sigma}_t \frac{\overline{D}_2}{\overline{D}_0}\right)\phi(x) + \frac{\overline{D}_2}{\overline{D}_0} Q(x) \,, \tag{4.35}$$

where

$$Q(x) = \left(\lambda \overline{\nu\Sigma}_f + \overline{\Sigma}_s\right)\phi(x) \,, \tag{4.36}$$

then Eq. (3.96) becomes:

$$-\overline{D}_0 \frac{\partial^2 \xi}{\partial x^2} + + \frac{\overline{\Sigma}_t}{1 - \overline{\Sigma}_t \frac{\overline{D}_2}{\overline{D}_0}} \xi(x) = \frac{1}{1 - \overline{\Sigma}_t \frac{\overline{D}_2}{\overline{D}_0}} Q(x) \,. \tag{4.37}$$

Eq. (4.37) can be solved much like Eq. (3.75), but with an intermediate step in which $\xi(x)$ is converted to $\phi(x)$ in order to calculate $Q(x)$ for the next iteration.

For the rest of this chapter, the following standards are followed:

- When eigenvalues (k-eff) are tabulated, they are typically given as differences from the S_N reference. These differences are given in per cent mille:

$$\Delta k_{eff} = \left(k_{eff,S_N} - k_{eff,diff/SP_2}\right) \times 10^5 \,. \tag{4.38}$$

- When fluxes are plotted, they are (unless otherwise noted) plotted as a ratio of the

reconstructed scalar flux to the S_N scalar flux,

$$\frac{\int_{-1}^{1} \psi_{recon}(x,\mu)\, d\mu}{\int_{-1}^{1} \psi_{S_N}(x,\mu)\, d\mu}, \tag{4.39}$$

to give the reader a sense of the relative accuracy of these methods.

4.2.1 Boundary conditions

The transport boundary conditions for (monoenergetic) Eq. (3.1) are:

$$\psi(0,\mu) = \psi_b^+(\mu), \qquad 0 < \mu \leq 1 \tag{4.40a}$$

$$\psi(L,\mu) = \psi_b^-(\mu), \qquad -1 \leq \mu < 0 \tag{4.40b}$$

where $x = 0$ is the left side of the system, $x = L$ is the right side, and $\psi_b^{\pm}(\mu)$ can be any prescribed angular flux on the left (+) or right (−) boundary. Typically, for a vacuum boundary condition, $\psi_b^{\pm}(\mu) = 0$.

To obtain P_N boundary conditions for the left edge of the system, we multiply Eq. (4.40a) by $\mu P_n(\mu)$ for n even and integrate over the incident angles, $\mu = [0,1]$. Using the standard definition for the P_N angular flux,

$$\psi(x,\mu) = \sum_{m=0}^{N} \frac{2m+1}{2} \psi_m(x) P_m(\mu)\,, \tag{4.41}$$

Eq. (4.40a) becomes:

$$\int_0^1 \mu P_n(\mu) \psi_b^+(\mu)\, d\mu = \sum_{m=0}^{N} \frac{2m+1}{2} \left(\int_0^1 \mu P_n(\mu) P_m(\mu)\, d\mu \right) \psi_m(0)\,,$$
$$n = 0, 2, 4, \cdots, N-1\,. \tag{4.42}$$

Performing the same steps on the right edge of the system, Eq. (4.40b), we obtain:

$$\int_0^1 \mu P_n(\mu)\psi_b^-(\mu)\,d\mu = \sum_{m=0}^{N}\frac{2m+1}{2}\left(\int_0^1 \mu P_n(\mu)P_m(\mu)\,d\mu\right)\psi_m(0)\,,$$
$$n = 0,2,4,\cdots,N-1\,. \tag{4.43}$$

For P_2, Eq. (4.41) becomes:

$$\psi(x,\mu) = \frac{1}{2}\psi_0(x) + \frac{3}{2}\psi_1(x)\mu + \frac{5}{2}\psi_2(x)\left(\frac{3\mu^2-1}{2}\right), \tag{4.44}$$

where

$$\psi_1(x) = -\frac{1}{\overline{\Sigma}_t}\frac{\partial}{\partial x}\left(\frac{1}{3}\psi_0 + \frac{4}{15\overline{\Sigma}_t}\left(\overline{\Sigma}_t\psi_0(x) - Q(x)\right)\right), \tag{4.45a}$$

$$\psi_2(x) = \frac{2}{5\overline{\Sigma}_t}\left(\overline{\Sigma}_t\psi_0(x) - Q(x)\right), \tag{4.45b}$$

and

$$Q(x) = \left(\lambda\overline{\nu\Sigma}_f + \overline{\Sigma}_s\right)\psi_0(x)\,. \tag{4.45c}$$

Or, using the standard definitions for $\overline{D}_0$ and $\overline{D}_2$:

$$\psi_1(x) = -\overline{D}_0\frac{\partial}{\partial x}\left(\psi_0 + \frac{\overline{D}_2}{\overline{D}_0}\left(\overline{\Sigma}_t\psi_0(x) - Q(x)\right)\right), \tag{4.46a}$$

$$\psi_2(x) = \frac{\overline{D}_2}{2\overline{D}_0}\left(\overline{\Sigma}_t\psi_0(x) - Q(x)\right), \tag{4.46b}$$

and

$$Q(x) = \left(\lambda\overline{\nu\Sigma}_f + \overline{\Sigma}_s\right)\psi_0(x)\,. \tag{4.46c}$$

Substituting Eqs. (4.44) and (4.46) into Eqs. (4.42) and (4.43) yields:

$$\frac{1}{4}\psi_0(0) + \frac{1}{2}\psi_1(0) + \frac{5}{16}\psi_2(0) = \int_0^1 \mu\psi_b^+(\mu)\,d\mu\,, \tag{4.47}$$

or

$$\frac{1}{4}\psi_0(0)-\frac{1}{2}\overline{D}_0\frac{\partial}{\partial x}\left(\psi_0+\frac{\overline{D}_2}{\overline{D}_0}\left(\overline{\Sigma}_t\psi_0(0)-Q(0)\right)\right) + \frac{5}{32}\frac{\overline{D}_2}{\overline{D}_0}\left(\overline{\Sigma}_t\psi_0(0)-Q(0)\right)=\int_0^1 \mu\psi_b^-(\mu)\,d\mu\,, \tag{4.48}$$

for the left boundary, and

$$\frac{1}{4}\psi_0(L)-\frac{1}{2}\psi_1(L)+\frac{5}{16}\psi_2(L)=\int_{-1}^0 |\mu|\psi_b^+(\mu)\,d\mu\,, \tag{4.49}$$

or

$$\frac{1}{4}\psi_0(L)+\frac{1}{2}\overline{D}_0\frac{\partial}{\partial x}\left(\psi_0+\frac{\overline{D}_2}{\overline{D}_0}\left(\overline{\Sigma}_t\psi_0(L)-Q(L)\right)\right) + \frac{5}{32}\frac{\overline{D}_2}{\overline{D}_0}\left(\overline{\Sigma}_t\psi_0(L)-Q(L)\right)=\int_{-1}^0 |\mu|\psi_b^-(\mu)\,d\mu\,, \tag{4.50}$$

for the right boundary.

4.3 Test Problem Parameters

Three sets of one-group cross sections were used to create five types of problems, described below. The first set of cross sections, from the C5G7 benchmark [30], are used to show how asymptotic SP_2 performs for thermal cross sections with two standard fuel types, uranium oxide and mixed-oxide. The second set, from the Zero-Power Plutonium Reactor [16], explores how accurate asymptotic SP_2 is for fast neutrons, where the mean free paths are longer. With the final set of cross sections, we attempt to emulate a real light water reactor with a mixture of fuel assembly types [15].

4.3.1 C5G7 Thermal Cross Sections

Four sets of macroscopic cross sections were obtained from the C5G7 benchmark [30]: one mixed-oxide fuel (MOX), one uranium-oxide fuel (UOX), and two types of light water moderator. Total, nu-fission (taken as ν times Σ_f), and scattering ($\Sigma_t - \Sigma_a$) cross sections were taken from the thermal (7th) group data provided in the benchmark. For more variation between pin types, different light water cross sections from [15], for water at a 315 C and a pressure of 155 bar with a boron concentration of 1500ppm, were used for MOX fuel pins. The cross sections for all four materials are given in Table 4.1.

Table 4.1 C5G7 Cross Section Data (Thermal)

	MOX	**Light Water (MOX)**	**UOX**	**Light Water (UOX)**
$\Sigma_t\left(\text{cm}^{-1}\right)$	0.688910	2.432572	0.570610	3.305700
$\Sigma_s\left(\text{cm}^{-1}\right)$	0.279560	2.390965	0.287830	3.268461
$\nu\Sigma_f\left(\text{cm}^{-1}\right)$	0.713990	0.0	0.5257105	0.0

Each C5G7 test case was run with 5 (or 6 for the MOX-UOX case), 10, 20, and 40 fuel pins. As the number of fuel pins increases, the problem becomes more like an infinite medium, and we expect all four methods to perform well. It is in the smaller cases (5 or 10 pins) that we anticipate a significant improvement with the asymptotic methods.

Each fuel pin has three regions; the dimensions for a single MOX or UOX fuel pin are given in Table 4.2.

Table 4.2 C5G7 Fuel Pin Dimensions

Pin Type	**Region 1**	**Region 2**	**Region 3**
Thickness	0.21 cm	0.84 cm	0.21 cm
MOX Pin	Light Water (MOX)	MOX	Light Water (MOX)
UOX Pin	Light Water (UOX)	UOX	Light Water (UOX)

Homogenized cross sections are listed in Table 4.3. While the asymptotic diffusion coefficients ($\overline{D}_0$) are only slightly different from the standard diffusion coefficients (< 3% difference), the asymptotic diffusion coefficients ($\overline{D}_2$) are about twice as large as their standard counterparts. It should be noted, however, that in the asymptotic SP_2 equation $\overline{D}_2$ is multiplied by an $O\left(\epsilon^2\right)$ smaller number than $\overline{D}_0$, so this difference may be less impactful than it appears.

Table 4.3 C5G7 Homogenized Cross Sections

XS	MOX	UOX
$\overline{\Sigma}_t$	1.26281 cm^{-1}	1.47107 cm^{-1}
$\overline{\Sigma}_s$	0.97450 cm^{-1}	1.26913 cm^{-1}
$\overline{\nu\Sigma}_f$	0.47899 cm^{-1}	0.35263 cm^{-1}
$\overline{D}_0$	0.25779 cm	0.22011 cm
Std. $\overline{D}_0$	0.26396 cm	0.22659 cm
$\overline{D}_2$	-0.29882 cm^2	-0.28426 cm^2
Std. $\overline{D}_2$	-0.16722 cm^2	-0.12322 cm^2

4.3.2 Zero-Power Plutonium Reactor (ZPPR) Cross Sections

The ZPPR was a plate-fuel reactor at Argonne National Laboratory West (now Idaho National Laboratory), with plates made of uranium-oxide (UOX) and a uranium-plutonium mixture (UPM), separated by sodium coolant. Macroscopic cross sections for the ZPPR were obtained from a paper by Gelbard [16] and are listed in Table 4.4. The reflector consists solely of liquid sodium.

Table 4.4 ZPPR Cross Section Data

	UOX	Sodium	UPM
$\Sigma_t\left(cm^{-1}\right)$	0.1815510	0.0452915	0.2526480
$\Sigma_s\left(cm^{-1}\right)$	0.1178900	0.0267661	0.0860426
$\nu\Sigma_f\left(cm^{-1}\right)$	0.0099800	0.0	0.1850000

A single ZPPR fuel pin consists of 5 sections, with dimensions given in Table 4.5. Like the C5G7 test cases, the ZPPR was run with 5, 10, 20, and 40 fuel pins.

Table 4.5 ZPPR Fuel Pin Dimensions

Material	Dimension (cm)
UOX	0.500
Sodium	0.625
UPM	0.250
Sodium	0.625
UOX	0.500

Homogenized parameters are listed in Table 4.6. Here the difference between the standard diffusion coefficients and the asymptotic diffusion coefficients is less significant. It is also important to note that the homogenized total cross section is small, implying that each pin is optically thin.

Table 4.6 ZPPR Homogenized Cross Sections

XS	ZPPR
$\overline{\Sigma}_t$	0.12022 cm^{-1}
$\overline{\Sigma}_s$	0.06865 cm^{-1}
$\overline{\nu\Sigma}_f$	0.02308 cm^{-1}
$\overline{D}_0$	2.67982 cm
Std. $\overline{D}_0$	2.77269 cm
$\overline{D}_2$	-20.33761 cm^2
Std. $\overline{D}_2$	-18.45080 cm^2

4.3.3 Light Water Reactor (LWR)

The final test case, designed by Han Joo and detailed in [15], aims to be representative of a real LWR. It includes five fuel assembly types and a reflector assembly type. The fuel assemblies contain four fuel types: uranium oxide (UOX), uranium oxide with a lower enrichment (UOX-1), uranium oxide with gadolinium burnable poisons (UOX-Gd), and mixed oxide (MOX). Each fuel assembly has two densities of water, one for the fuel pins (H_2O-Fuel) and one for water holes (H_2O-WH), with a third density of water for the re-

flector (H_2O-Refl). The monoenergetic macroscopic cross sections for the 7 materials are given in Table 4.7.

Table 4.7 LWR Cross Section Data

Material	$\Sigma_t\left(\text{cm}^{-1}\right)$	$\Sigma_s\left(\text{cm}^{-1}\right)$	$\nu\Sigma_f\left(\text{cm}^{-1}\right)$
UOX	3.32734E-1	2.74910E-1	7.97840E-2
UOX-1	3.33356E-1	2.75534E-1	7.96455E-2
UOX-Gd	8.58463E-2	4.32728E-2	1.85589E-3
MOX	2.82548E-1	2.14888E-1	8.64238E-2
H_2O-Refl	7.85602E-2	7.77942E-2	0.0
H_2O-Fuel	1.74713E-1	1.73779E-1	0.0
H_2O-WH	9.01554E-2	8.96296E-2	0.0

The geometry of the LWR case is complex. There are seven pin types, each with three regions of uniform thickness. The fuel pin thicknesses and materials are listed in Table 4.8.

Table 4.8 LWR Pin Data

Pin Type	**Region 1**	**Region 2**	**Region 3**
Thickness	0.425 cm	0.425 cm	0.425 cm
UOX Pin	H_2O-Fuel	UOX	H_2O-Fuel
UOX-1 Pin	H_2O-Fuel	UOX-1	H_2O-Fuel
UOX-Gd Pin	H_2O-Fuel	UOX-Gd	H_2O-Fuel
MOX Pin	H_2O-Fuel	MOX	H_2O-Fuel
H_2O-Refl Pin	H_2O-WH	H_2O-WH	H_2O-WH
H_2O-WH Pin	H_2O-Refl	H_2O-Refl	H_2O-Refl

Table 4.9 details the homogenized cross sections for each assembly type. Again, the asymptotic $\overline{D}_0$ shows little deviation from the standard $\overline{D}_0$, while the asymptotic $\overline{D}_2$ once more shows significant variation (8-15%) from the standard $\overline{D}_2$.

Table 4.9 LWR Homogenized Cross Sections

Assembly	**UOX**	**UOX-1**	**UOX/UOX-Gd**	**MOX**
$\overline{\Sigma}_t\left(\text{cm}^{-1}\right)$	0.21027	0.21045	0.20058	0.19563
$\overline{\Sigma}_s\left(\text{cm}^{-1}\right)$	0.19279	0.19297	0.18368	0.17527
$\overline{\nu\Sigma_f}\left(\text{cm}^{-1}\right)$	0.02328	0.02324	0.02020	0.02522
$\overline{D}_0\,(\text{cm})$	1.58518	1.58382	1.66245	1.70371
Std. $\overline{D}_0\,(\text{cm})$	1.58526	1.58391	1.66185	1.70390
$\overline{D}_2\left(\text{cm}^2\right)$	-6.56708	-6.55525	-7.87304	-7.63486
Std. $\overline{D}_2\left(\text{cm}^2\right)$	-6.03134	-6.02103	-6.62817	-6.96783

The geometry of each assembly is shown in Fig. 4.1. The UOX-Gd assembly is the only assembly with gadolinium fuel pins. Fig. 4.1 also shows the core configuration, which is symmetric except for the single UOX-1 assembly on the right side of the problem.

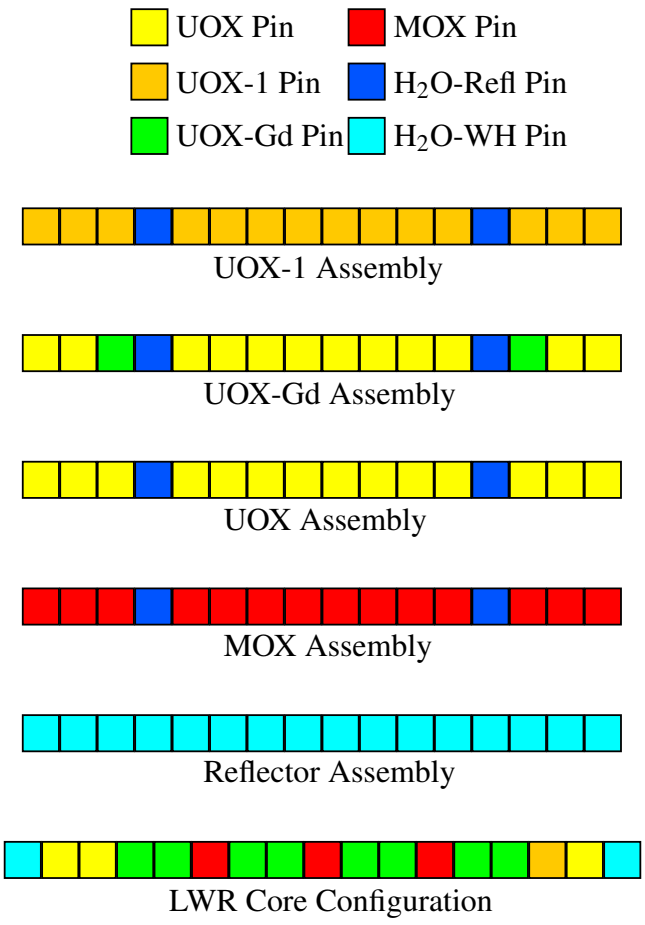

Figure 4.1: LWR Assembly and Core

4.4 Numerical Results

4.4.1 Unreflected Cases

For an initial test, two unreflected (i.e. without reflector regions bounding the problem) cases were run. The first, a pure C5G7 MOX pin problem, is a simple comparison of the methods without any discontinuity factors. The second, a mixed C5G7 MOX-UOX core (MOX on the left, UOX on the right), allows us to evaluate the effectiveness of the various discontinuity factors without the additional complication of a reflector.

4.4.1.1 C5G7 MOX

Our first test is an unreflected C5G7 MOX case. With a single pin type and no reflector, discontinuity factors are not a factor. We are therefore only comparing the four methods: standard homogenized diffusion (HD), standard SP_2 (HSP_2), asymptotic homogenized diffusion (AHD), and asymptotic SP_2 ($AHSP_2$). Eigenvalue results are tabulated in Table 4.10.

Table 4.10 MOX Unreflected k-eff Results

	Ref k_{eff}	**Δk_{eff} (pcm)**			
# of Pins	**S_N**	**AHD**	**$AHSP_2$**	**HD**	**HSP_2**
5	1.442140	-1599.5	-802.6	-1949.3	-1499.8
10	1.588159	-217.9	-121.7	-363.8	-309.1
20	1.640565	-24.7	-16.5	-70.5	-65.8
40	1.655860	-2.8	-2.2	-15.4	-15.1

As we hoped, the asymptotic results show considerable improvement over the standard homogenized results, and the homogenized SP_2 results show significant improvement over the homogenized diffusion results. These improvements are more pronounced in the smaller problem, where flux gradients are more pronounced and the assumptions for classical diffusion break down. Fig. 4.2 shows a ratio of the reconstructed scalar fluxes to the scalar S_N flux for the left half of the problem (because the problem is symmetric the right half is a mirror image of this half) for the 10 pin case.

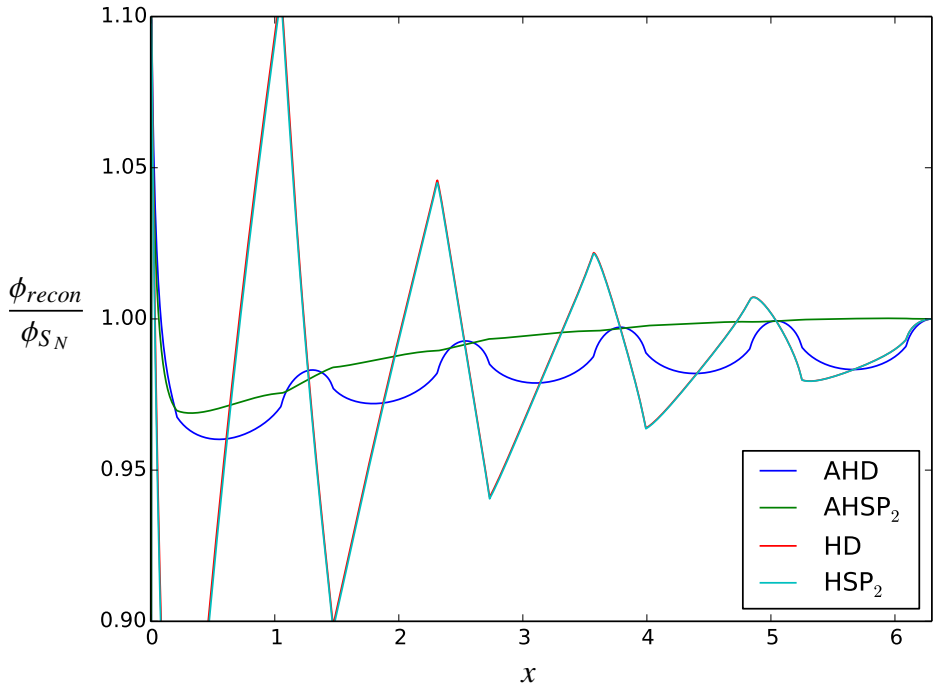

Figure 4.2: Unreflected MOX Flux Ratio - 10 pins

In Fig. 4.2 and all future figures, HD stands for homogenized diffusion, HSP_2 stands for homogenized SP_2, and an A in front of either means it is asymptotic homogenized diffusion/SP_2. Both the standard methods (HD and HSP_2) use only the first term in the flux reconstruction equations in order to match what is currently done in diffusion theory. For this reason, the HD flux curve is hidden *under* the HSP_2 curve. AHD uses Eq. (3.80), while $AHSP_2$ uses Eq. (3.101).

It is clear that the additional terms in Eqs. (3.80) and (3.101) have a "smoothing" effect on the error of the reconstructed flux; each additional term decreases the fluctuation of the error in the pin cells. Furthermore, it appears that for capturing the scalar flux the model used (HD, AHD, HSP_2, $AHSP_2$) is less important than the reconstructed flux equations used. HD and HSP_2, both of which use only the first term in Eq. (3.80), overlap despite a 54.7 pcm difference in the eigenvalue. While the overall trend is the same, the fluctuations in the error are considerably lessened with AHD and almost completely eliminated with

$AHSP_2$. This improvement gives us hope and motivation for future testing with more difficult problems.

4.4.1.2 C5G7 MOX/UOX

Our second test is intended to evaluate the effectiveness of the various discontinuity factors at a fuel-fuel interface. While the homogenized cross sections for the MOX and UOX pins are similar, they are different enough that we expect boundary layer effects at the interface. Eigenvalue results are tabulated in Table 4.11. The total number of pins are tabulated; the number of MOX or UOX pins is exactly one half of the tabulated value. Each run with μ^2 written beside the number of pins refers to a case in which the discontinuity factor for the scalar flux used $g(\mu) = \mu^2$ rather than $g(\mu) = 1$; these runs were only performed with the asymptotic equations.

Table 4.11 MOX-UOX Unreflected k-eff Results

	Ref k_{eff}	**Δk_{eff} (pcm)**			
# of Pins	**S_N**	**AHD**	**$AHSP_2$**	**HD**	**HSP_2**
6	1.508725	-1105.2	-550.0	-1474.3	-1206.3
6 μ^2	1.508725	-1103.9	-550.4	-	-
10	1.617643	-289.2	-138.4	-493.5	-432.9
10 μ^2	1.617643	-286.8	-133.6	-	-
20	1.688828	-82.2	-25.5	-187.7	-170.0
20 μ^2	1.688828	-79.7	-18.1	-	-
40	1.725228	-19.7	-5.2	-71.2	-66.8
40 μ^2	1.725228	-18.9	-2.4	-	-

Again (this will be a common theme in this chapter), the asymptotic results show clear improvement over the standard results. Likewise, SP_2 shows a similar improvement when compared to diffusion. More surprisingly, using $g(\mu) = \mu^2$ shows little improvement over

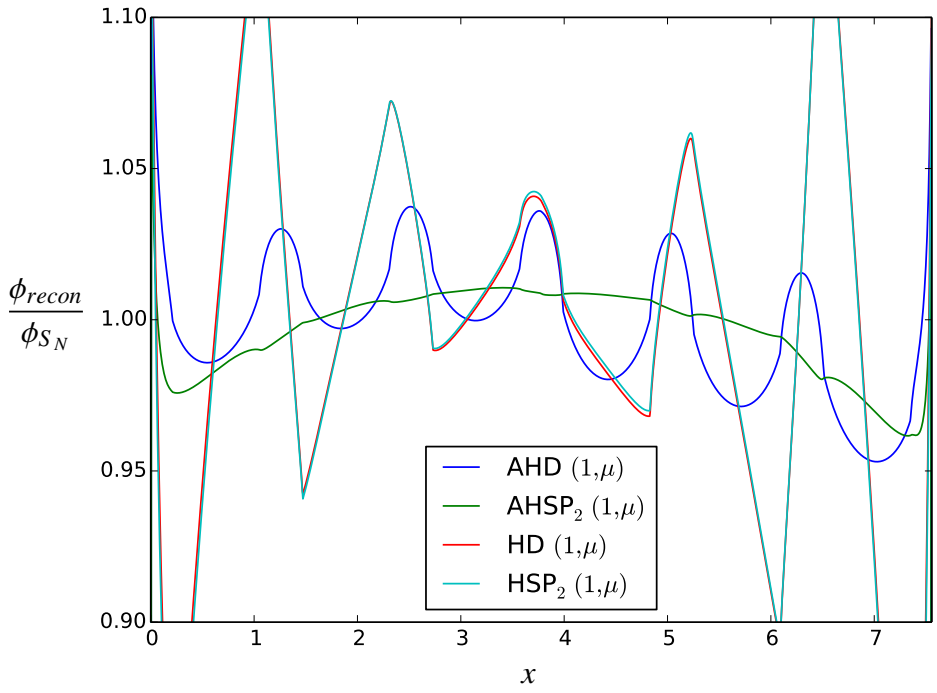

Figure 4.3: Unreflected MOX-UOX Flux Ratio - 6 pins

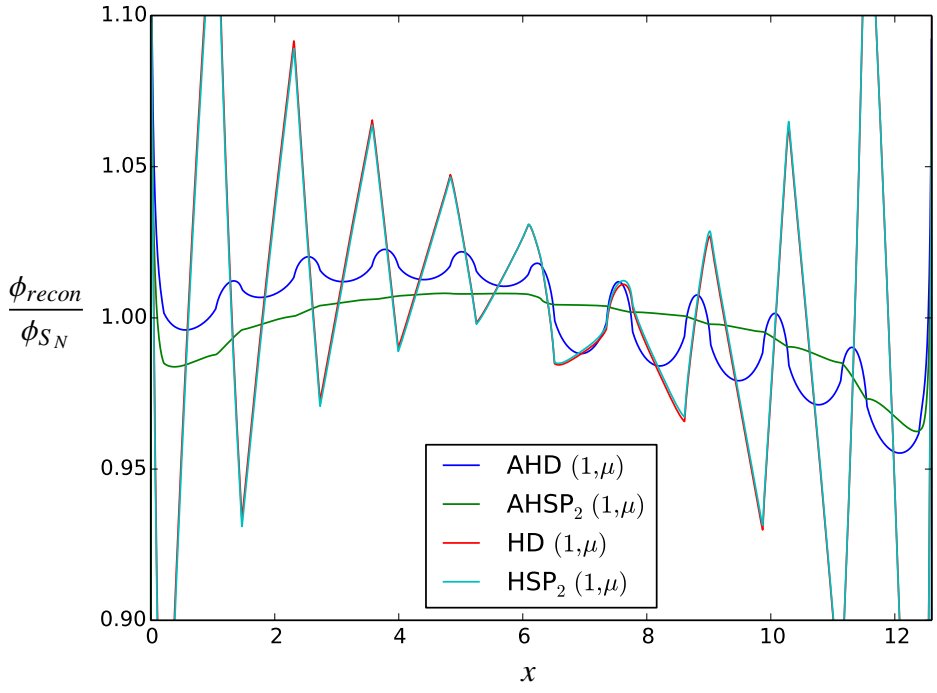

Figure 4.4: Unreflected MOX-UOX Flux Ratio - 10 pins

$g(\mu) = 1$. It only makes an appreciable difference when the number of pins is large, and the the results are already accurate.

Figs. 4.3 and 4.4 give reconstructed scalar flux comparisons between the standard and asymptotic methods. Each diffusion or SP_2 solution is normalized by the total flux in the core. Again, $AHSP_2$ yields results that are the smoothest and closest to unity, followed by AHD and the standard methods, with HD and HSP_2 mostly overlapping. It is also important to notice that the error is much greater in the six-pin case than in the ten-pin case. The flux gradients are sharper in the smaller problem, and even though $AHSP_2$ gives better results, it is still not capable of fully capturing these effects.

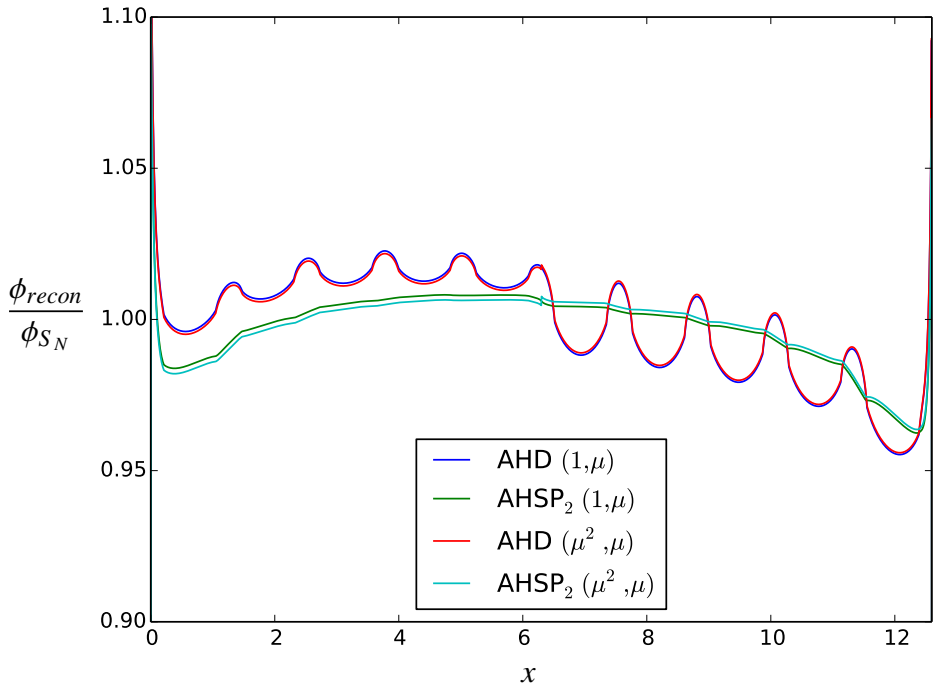

Figure 4.5: Unreflected MOX-UOX Flux Ratio (1 vs μ^2) - 10 pins

Fig. 4.5 compares the fluxes for $g(\mu) = 1$ versus $g(\mu) = \mu^2$. Here we can see slight improvement for $g(\mu) = \mu^2$, which matches with the improvement in the eigenvalue. However, we can also see that the scalar flux is *discontinuous* at the middle of the problem. This is a natural side-effect of preserving an integral of μ^2 rather than 1.

4.4.2 Reflected Cases

In each of the following cases, the core is surrounded on both sides by several centimeters of the same moderator used in each pin. The C5G7 MOX, C5G7 UOX, and ZPPR cases allow us to investigate the various reflector discontinuity factors.

4.4.2.1 C5G7 MOX

For the C5G7 MOX case, also explored without a reflector, a range of reflector discontinuity factors are tried. Table 4.12 lists the cases and their eigenvalue results, and Pcur refers to a case that used the partial currents to obtain discontinuity factors, where

$$\int_0^1 \psi^+(x,\mu)\,d\mu = \int_0^1 \psi^-(x,\mu)\,d\mu\,, \tag{4.51a}$$

and

$$\int_{-1}^0 \psi^+(x,\mu)\,d\mu = \int_{-1}^0 \psi^-(x,\mu)\,d\mu\,, \tag{4.51b}$$

are used instead of Eq. (4.1).

Table 4.12 MOX Reflected k-eff Results

			Ref k_{eff}	**Δk**	**(pcm)**		
# of Pins	**g(μ)**	**Analytic?**	**S_N**	**AHD**	**$AHSP_2$**	**HD**	**HSP_2**
5	$(1,\mu)$	No	1.567390	-235.6	80.6	-452.7	-302.3
5	(μ^2,μ)	No	1.567390	-280.7	162.5	-498.7	-301.5
5	$(1,\mu)$	Yes	1.567390	-238.8	35.1	-	-
5	(μ^2,μ)	Yes	1.567390	-283.9	31.2	-	-
5	Pcur	Yes	1.567390	-218.2	75.0	-	-
10	$(1,\mu)$	No	1.621938	-39.0	19.9	-132.0	-98.6
10	(μ^2,μ)	No	1.621938	-54.0	40.4	-147.4	-98.3
10	$(1,\mu)$	Yes	1.621938	-40.0	4.1	-	-
10	(μ^2,μ)	Yes	1.621938	-55.1	-5.3	-	-
10	Pcur	Yes	1.621938	-33.1	13.7	-	-
20	$(1,\mu)$	No	1.647175	-4.7	4.1	-38.5	-32.4
20	(μ^2,μ)	No	1.647175	-8.4	8.4	-42.3	-32.3
40	$(1,\mu)$	No	1.656913	-0.4	0.7	-11.1	-10.1
40	(μ^2,μ)	No	1.656913	-1.1	1.5	-11.8	-10.1

Standard diffusion and SP_2 were only run for the non-analytic cases. In general, the analytic representation of the returns a more accurate k_{eff} with $g(\mu) = (1, \mu)$ providing the best solution, followed by the partial current solution.

Fig. 4.6 shows the flux ratio for the 10-pin case, while Fig 4.7 zooms in on the core-reflector interface for the same case. Here the extra A refers to "Analytic" solutions. There are several important things to notice. The first is that $AHSP_2$ appears to perform the best in the reflector. However, it is also the worst in the core near the core-reflector interface. Clearly, the eigenvalue is influenced more by accuracy in the core. However, in direct contrast, the $AAHSP_2$ solution with $g(\mu) = \left(\mu^2, \mu\right)$ is more accurate than the $g(\mu) = (1, \mu)$ case in the core, but less accurate in the reflector; however, their eigenvalue results imply the opposite.

Again, the discontinuities at the interface are for cases without $g(\mu) = 1$.

4.4.2.2 C5G7 UOX

Eigenvalue results for the reflected C5G7 UOX case are given in Table 4.13. The trends are the same as with the MOX case, except that the partial current AHD performs slightly better than the $g(\mu) = (1, \mu)$ case.

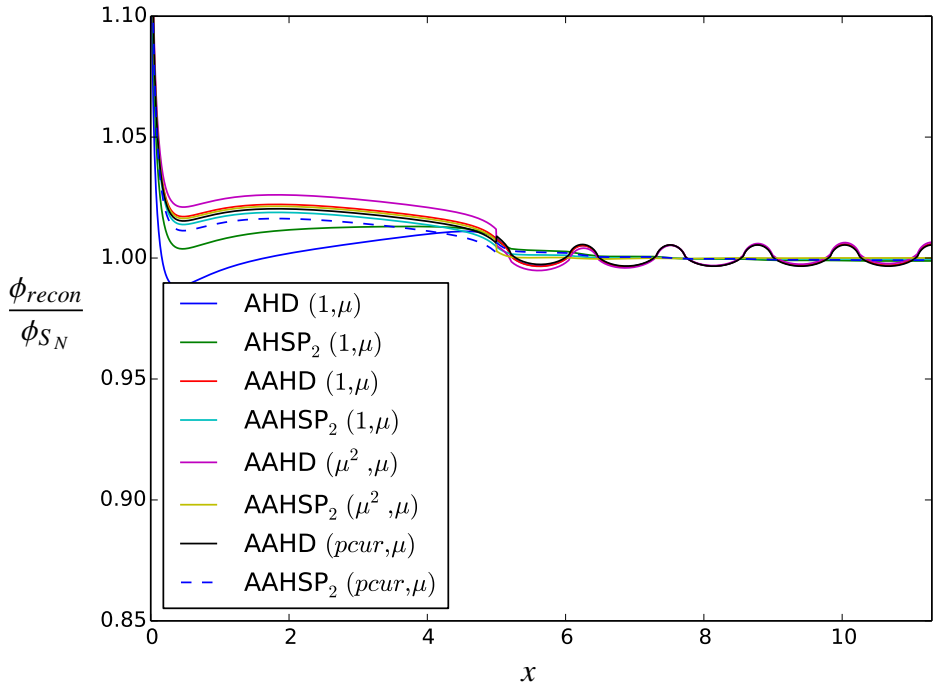

Figure 4.6: Reflected MOX Flux Ratio - 10 pins

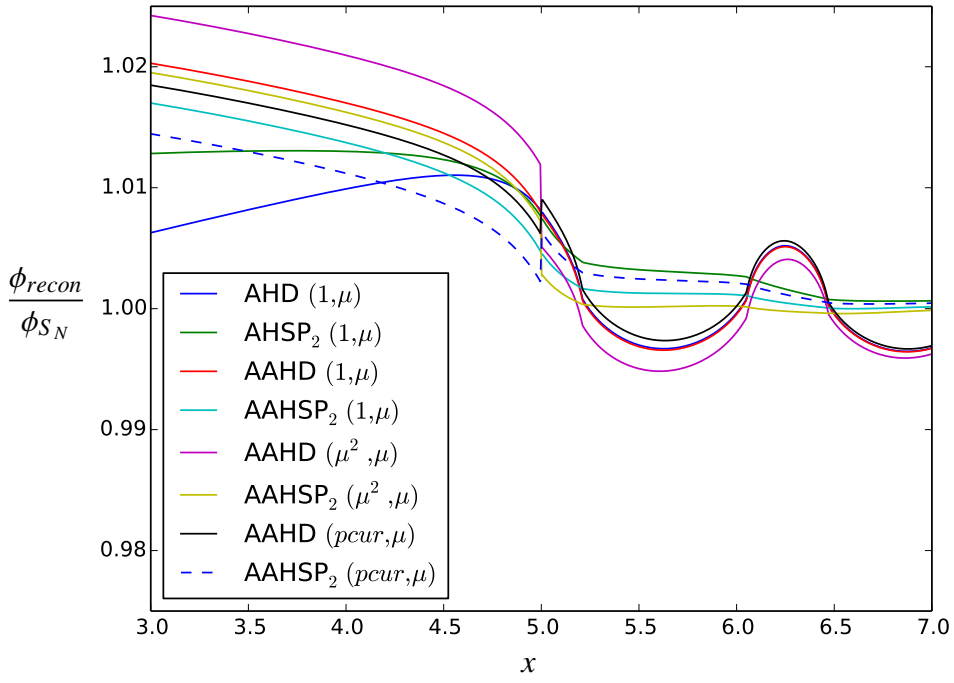

Figure 4.7: Reflected MOX Flux Ratio - 10 pins (Zoomed)

Table 4.13 UOX Reflected k-eff Results

			Ref k_{eff}	**Δk**	**(pcm)**		
# of Pins	**g(μ)**	**Analytic?**	**S_N**	**AHD**	**$AHSP_2$**	**HD**	**HSP_2**
5	$(1,\mu)$	No	1.631711	-274.4	79.5	-596.0	-468.4
5	(μ^2,μ)	No	1.631711	-316.3	138.5	-	-
5	$(1,\mu)$	Yes	1.631711	-276.1	13.1	-	-
5	(μ^2,μ)	Yes	1.631711	-317.9	32.1	-	-
5	Pcur	Yes	1.631711	-265.1	68.3	-	-
10	$(1,\mu)$	No	1.697512	-45.7	19.4	-186.3	-157.3
10	(μ^2,μ)	No	1.697512	-60.1	34.4	-	-
10	$(1,\mu)$	Yes	1.697512	-46.2	6.4	-	-
10	(μ^2,μ)	Yes	1.697512	-60.6	-3.7	-	-
10	Pcur	Yes	1.697512	-42.4	12.2	-	-
20	$(1,\mu)$	No	1.728467	-5.5	4.0	-57.4	-52.0
20	(μ^2,μ)	No	1.728467	-9.1	7.1	-	-
40	$(1,\mu)$	No	1.740598	-0.5	0.7	-17.0	-16.1
40	(μ^2,μ)	No	1.740598	-1.2	1.3	-	-

The flux plots for UOX were almost identical to those from the MOX cases, and are hence not shown. Instead, Fig. 4.8 shows the difference between standard and asymptotic flux reconstruction for a reflected problem. The trends are similar to what was seen with the unreflected case. However, there are two important things to note. First, the SP_2 solution is almost horizontal in the reflector, implying that it has the correct shape. Second, the SP_2 solution has a bump at the core-reflector interface that causes it to be off by a constant. This implies that there is still some issue with our discontinuity factors.

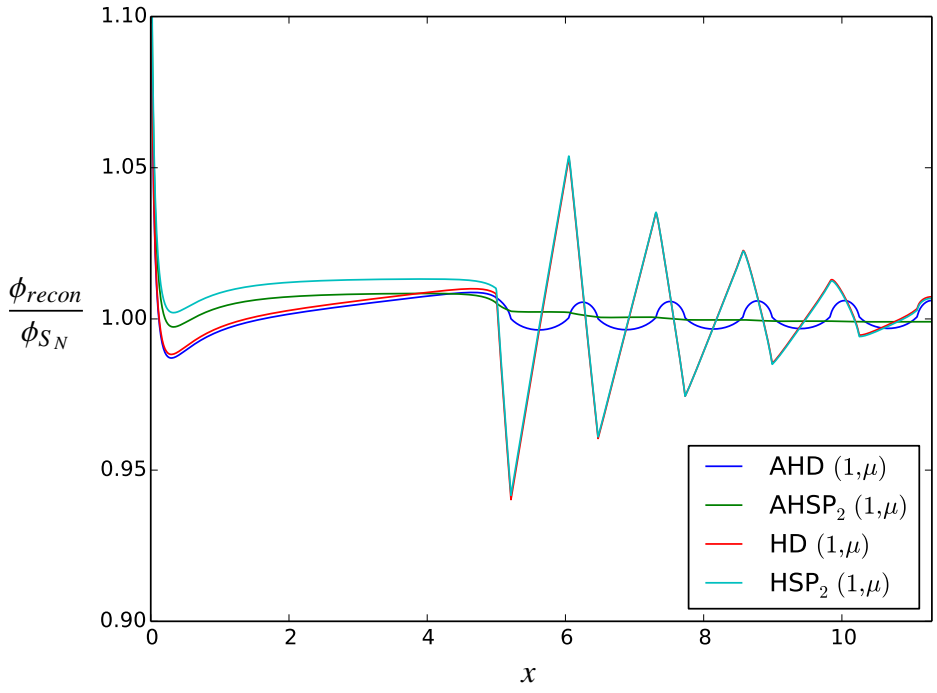

Figure 4.8: Reflected UOX Flux Ratio Standard vs. Asymptotic - 10 pins

4.4.2.3 ZPPR

The ZPPR presents a unique challenge, due to the optical thinness of each pin, as well as the reflector. Table 4.14 lists the eigenvalues for each case. It takes 25 pins before the eigenvalues become reasonably accurate, though the analytic reflector expression yields a few good results in the 11 pin case. However, as the flux plots show, an accurate eigenvalue does not ensure an accurate reconstructed flux.

In Figs. 4.9 and 4.10 (for the 11 and 25 pin cases, respectively), we see the error increase rapidly as soon as the solution reaches the reflector. Furthermore, any DF that allows a discontinuous scalar flux has a very large jump at the fuel-reflector interface. This implies that there is an extreme disconnect between the fuel and reflector that must be compensated for with large adjustments. From these figures, it is difficult to determine which method performed the "best". Furthermore, in many cases the diffusion solution is more accurate

Table 4.14 ZPPR Reflected k-eff Results

			Ref k_{eff}	**Δk**	**(pcm)**		
# of Pins	**g(μ)**	**Analytic?**	**S_N**	**AHD**	**$AHSP_2$**	**HD**	**HSP_2**
5	$(1,\mu)$	No	0.259660	-2608.7	-2012.3	-2989.3	1297.9
5	(μ^2,μ)	No	0.259660	-2792.5	-4649.4	-	-
5	$(1,\mu)$	Yes	0.259660	-2959.3	643.3	-	-
5	(μ^2,μ)	Yes	0.259660	-3141.2	2286.2	-	-
5	Pcur	Yes	0.259660	-1090.3	2940.2	-	-
11	$(1,\mu)$	No	0.349135	-966.1	718.1	-1247.7	368.2
11	(μ^2,μ)	No	0.349135	-1066.75	1845.4	-	-
11	$(1,\mu)$	Yes	0.349135	-1158.1	-161.3	-	-
11	(μ^2,μ)	Yes	0.349135	-1257.9	163.5	-	-
11	Pcur	Yes	0.349135	-138.1	916.6	-	-
25	$(1,\mu)$	No	0.412677	-169.9	151.1	-285.9	32.4
25	(μ^2,μ)	No	0.412677	-194.8	418.4	-	-
25	$(1,\mu)$	Yes	0.412677	-217.3	-98.5	-	-
25	(μ^2,μ)	Yes	0.412677	-241.7	-90.5	-	-
25	Pcur	Yes	0.412677	40.2	162.5	-	-
40	$(1,\mu)$	No	0.430925	-48.4	50.3	-105.3	-6.1
40	(μ^2,μ)	No	0.430925	-56.8	142.9	-	-
40	$(1,\mu)$	Yes	0.430925	-64.4	-38.4	-	-
40	(μ^2,μ)	Yes	0.430925	-72.7	-41.6	-	-
40	Pcur	Yes	0.430925	24.1	50.7	-	-

than the SP_2 solution, an unusual occurrence.

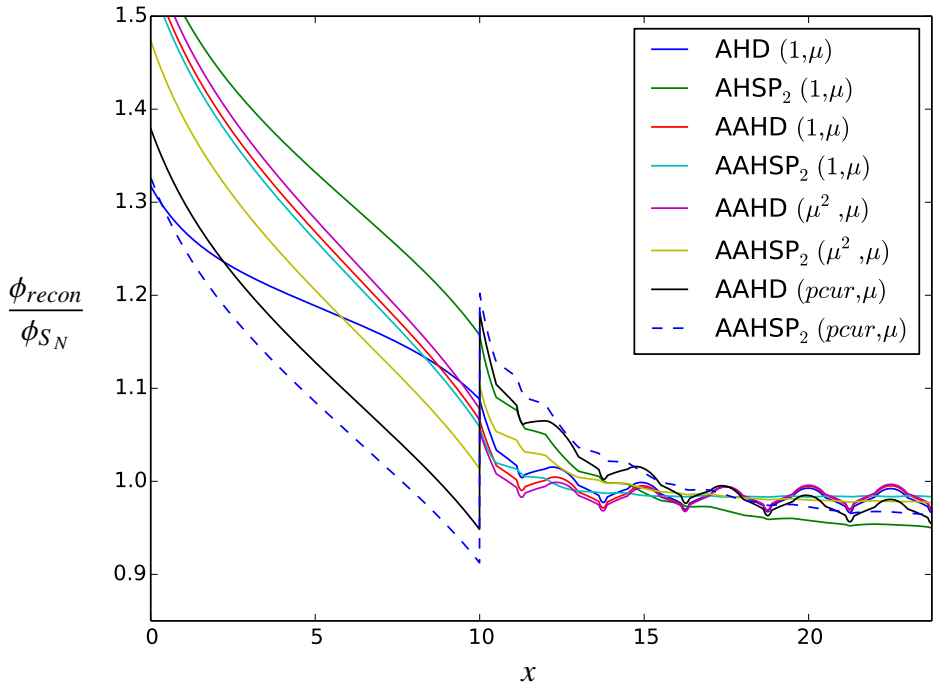

Figure 4.9: Reflected ZPPR Flux Ratio - 11 pins

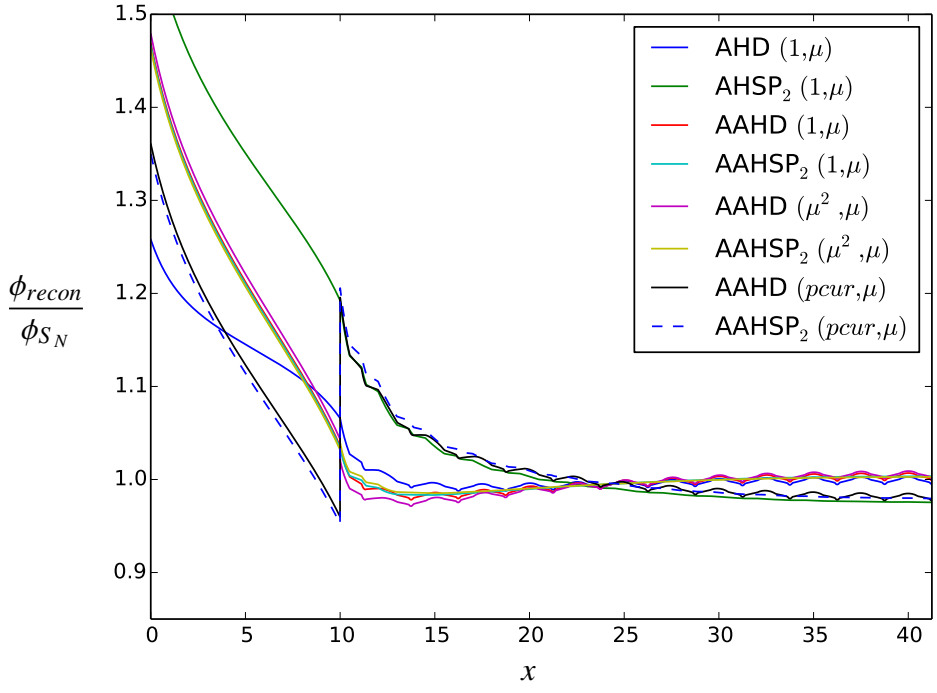

Figure 4.10: Reflected ZPPR Flux Ratio - 25 pins

4.4.2.4 LWR

The LWR presents a unique reflected case. It does not have a variable number of pins, it homogenizes over an entire assembly rather than a single pin, and it contains greater variety between cells. Due to the size and complexity of the problem, an analytic expression for the flux in the reflector was *not* used. Instead, we explored the impact of $g(\mu)$.

Table 4.15 lists the eigenvalue results for each calculation. The problem is optically thick, and so the errors are small. Again, we find that $AHSP_2$ is better than AHD. More surprisingly, we see that $g\left(\mu^2,\mu\right)$ yields the best result for $AHSP_2$.

Table 4.15 LWR Reflected k-eff Results

Method	$g(?,?)$	$k_{eff}/\Delta k_{eff}$ (pcm)
S_N	–	1.212207
Standard Homog Diffusion	$(1,\mu)$	-32.0
Standard Homog SP_2	$(1,\mu)$	-12.9
Asymptotic Homog Diffusion	$(1,\mu)$	-31.5
Asymptotic Homog SP_2	$(1,\mu)$	-10.4
Asymptotic Homog Diffusion	$\left(\mu^2,\mu\right)$	-32.9
Asymptotic Homog SP_2	$\left(\mu^2,\mu\right)$	3.1

Fig. 4.11 shows the flux ratios for the four asymptotic cases. This case shows the effectiveness of $g(\mu) = \left(\mu^2,\mu\right)$ in full, along with the discontinuities it creates. Looking at Fig. 4.11, it is clear why $AHSP_2$ captured the core eigenvalue better than any other method. Furthermore, we see how the additional terms with the $AHSP_2$ flux reconstruction improve the scalar flux towards the outer edges of the problem, where the flux gradients are steeper.

4.5 Summary

Using five test cases, with variations in size and whether the core was reflected or not, we have shown the accuracy of the newly derived asymptotic SP_2 method and its accompanying flux reconstruction formula. In most cases, asymptotic homogenized SP_2 is more accurate than asymptotic diffusion, standard SP_2 , and standard diffusion. Only in prob-

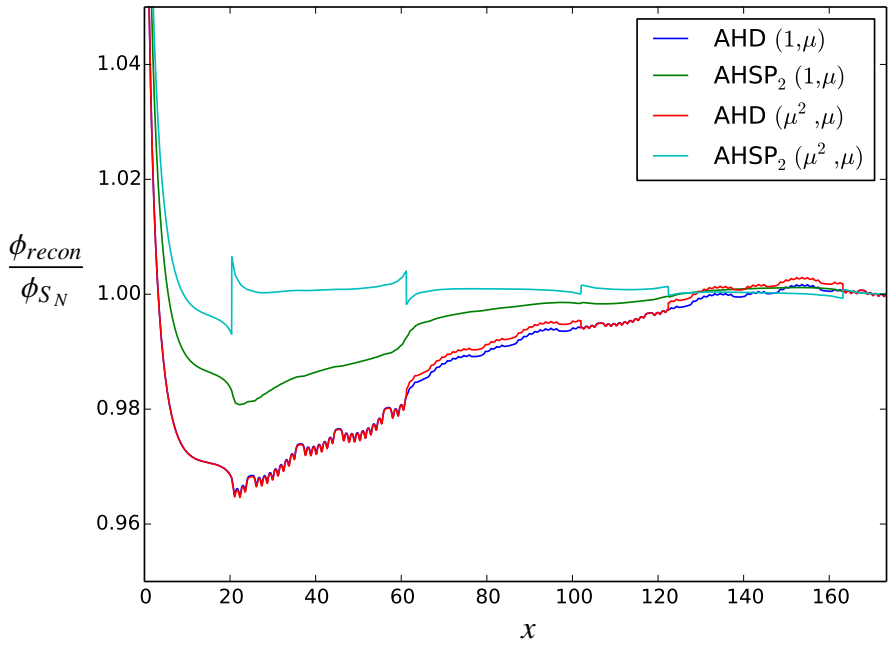

Figure 4.11: LWR Flux Ratios (1 vs. μ^2)

lems that are optically thin with large discontinuity factors does asymptotic diffusion yield slightly better results.

When choosing which angular moments to make continuous at an interface, the best choice appears to vary from problem to problem, making it impossible to choose one for a general scenario. In addition, discontinuity factors and diffusion coefficients for the reflector that are generated from an analytic expression for the angular flux generally produce better solutions in the fuel than a naïve diffusion expression. Finally, the asymptotic SP_2 reconstructed flux formula captures the spatial oscillations in the scalar flux much more accurately than the asymptotic diffusion solution (i.e. the $AHSP_2$ errors are much smoother and closer to zero).

CHAPTER 5

Derivation of a Scaling Factor for the Homogenized, Multigroup Transport Equation

"Standard" homogenized multigroup cross sections are defined to preserve the multigroup infinite lattice eigenfunction and eigenvalue. These cross sections can be altered through multiplication by an arbitrary scaling factor while still preserving the infinite lattice eigenfunction and eigenvalue. In this chapter, we show that the multiplicative scaling factor can be chosen so that the "scaled" multigroup transport equations (with the properly scaled multigroup cross sections) satisfy an extra element of transport physics. In addition to preserving the infinite lattice eigenfunction and eigenvalue, these equations also preserve the asymptotic diffusion or SP_2 limit of the continuous energy Boltzmann equation.

Because the "scaled" multigroup equations preserve additional space-dependent transport physics, it is logical to hypothesize that the solution of these equations will be more accurate than solutions of the standard multigroup equations. That is, the "scaled" multigroup solution should agree more closely with the continuous energy transport solution. In Chapter 6, we confirm this hypothesis through numerical simulations.

5.1 The Homogenized Multigroup Transport Equation

To derive the 1-D, homogenized, multigroup transport equation, we begin with the 1-D, lattice-geometry, continuous-energy transport equation introduced in Chapter 3:

$$\begin{aligned}\mu\frac{\partial\psi}{\partial x}(x,\mu,E)+\Sigma_t(x,E)\psi(x,\mu,E)&\\ =\int_0^\infty\int_{-1}^1\Sigma_s(x,\mu'\to\mu,E'\to E)\psi(x,\mu',E')\,d\mu'dE'&\\ +\lambda\frac{\chi(x,E)}{2}\int_0^\infty\int_{-1}^1\nu\Sigma_f(x,E')\psi(x,\mu',E')\,d\mu'dE',&\end{aligned}\tag{5.1}$$

where

$$\lambda=\frac{1}{\mathrm{k}}=1-\rho=\text{ eigenvalue},$$

and

$$\psi(x,\mu,E)=\text{ eigenfunction}.$$

In the case of an infinite periodic lattice with symmetric cells, we denote the solution to Eq. (5.1) as $f_0(x,\mu,E)$, with $\lambda=\lambda_0$, as in Eq. (3.15):

$$\begin{aligned}\mu\frac{\partial f_0}{\partial x}(x,\mu,E)+\Sigma_t(x,E)f_0(x,\mu,E)&\\ =\int_0^\infty\int_{-1}^1\Sigma_s(x,\mu'\to\mu,E'\to E)f_0(x,\mu',E')\,d\mu'dE'&\\ +\lambda_0\frac{\chi(x,E)}{2}\int_0^\infty\int_{-1}^1\nu\Sigma_f(x,E')f_0(x,\mu',E')\,d\mu'dE'.&\end{aligned}\tag{5.2}$$

We then define an energy-grid of G bins, with boundaries ranging from $E_G=E_{\min}$ to $E_0=E_{\max}$. Any energy integral may now be written as a summation of integrals over the

G energy groups, e.g.:

$$\int_0^\infty \nu\Sigma_f(x,E)\psi(x,\mu,E)\,dE = \sum_{g=1}^{G}\int_{E_g}^{E_{g-1}} \nu\Sigma_f(x,E)\psi(x,\mu,E)\,dE\,. \tag{5.3}$$

If we integrate Eq. (5.2) over a spatial cell i ($x = [x_{i-1/2}, x_{i+1/2}]$), an energy bin g ($E = [E_g, E_{g-1}]$), and all angles ($\mu = [-1,1]$) we have:

$$\begin{aligned}
&\int_{-1}^{1}\mu\Big(\int_{E_g}^{E_{g-1}} f_0(x_{i+1/2},\mu,E)\,dE - \int_{E_g}^{E_{g-1}} f_0(x_{i-1/2},\mu,E)\,dE\Big)d\mu \\
&\qquad + \int_{x_{i-1/2}}^{x_{i+1/2}}\int_{E_g}^{E_{g-1}} \Sigma_t(x,E)\,F_0(x,E)\,dE dx \\
&= \int_{x_{i-1/2}}^{x_{i+1/2}}\int_{E_g}^{E_{g-1}}\int_0^\infty \Sigma_{s,0}(x,E'\to E)\,F_0(x,E')\,dE' dE dx \\
&\qquad + \lambda_0\int_{x_{i-1/2}}^{x_{i+1/2}}\int_{E_g}^{E_{g-1}} \chi(x,E)\int_0^\infty \nu\Sigma_f(x,E')\,F_0(x,E')\,dE' dE dx\,,
\end{aligned} \tag{5.4}$$

where

$$F_0(x,E) = \int_{-1}^{1} f_0(x,\mu,E)\,d\mu\,, \tag{5.5}$$

and

$$\begin{aligned}
\Sigma_{s,0}(x,E'\to E) &= \int_{-1}^{1}\Sigma_s(x,\mu'\to\mu,E'\to E)\,d\mu \\
&= \int_{-1}^{1}\sum_{n=0}^{\infty}\frac{2n+1}{2}P_n(\mu)\,P_n(\mu')\,\Sigma_{s,n}(x,E'\to E)\,d\mu \\
&= P_0(\mu')\,\Sigma_{s,0}(x,E'\to E)\,.
\end{aligned} \tag{5.6}$$

In Eq. (5.6), we have assumed a Legendre polynomial expansion of the differential scattering cross section.

The streaming term can be eliminated by noting that each cell is symmetric:

$$f_0(x_{i+1/2},\mu,E) = f_0(x_{i-1/2},\mu,E)\,. \tag{5.7}$$

With this simplification, we rewrite Eq. (5.4) in homogenized, multigroup form:

$$\overline{\Sigma}_{t,i,g}\overline{F}_{0,i,g} = \sum_{g=1}^{G}\overline{\Sigma}_{s,0,i,g'\to g}\overline{F}_{0,i,g'} + \lambda_0\overline{\chi}_{i,g}\sum_{g=1}^{G}\overline{\nu\Sigma}_{f,i,g'}\overline{F}_{0,i,g'}\,, \tag{5.8}$$

where

$$\overline{F}_{0,i,g} = \int_{x_{i-1/2}}^{x_{i+1/2}}\int_{E_g}^{E_{g-1}} F_0(x,E)\,dEdx\,, \tag{5.9a}$$

$$\overline{\Sigma}_{t,i,g} = \frac{\displaystyle\int_{x_{i-1/2}}^{x_{i+1/2}}\int_{E_g}^{E_{g-1}} \Sigma_t(x,E)\,F_0(x,E)\,dEdx}{\displaystyle\int_{x_{i-1/2}}^{x_{i+1/2}}\int_{E_g}^{E_{g-1}} F_0(x,E)\,dEdx}\,, \tag{5.9b}$$

$$\overline{\Sigma}_{s,0,i,g'\to g} = \frac{\displaystyle\int_{x_{i-1/2}}^{x_{i+1/2}}\int_{E_g}^{E_{g-1}}\int_{E_{g'}}^{E_{g'-1}} \Sigma_{s,0}(x,E'\to E)\,F_0(x,E')\,dE'dEdx}{\displaystyle\int_{x_{i-1/2}}^{x_{i+1/2}}\int_{E_{g'}}^{E_{g'-1}} F_0(x,E')\,dE'dx}\,, \tag{5.9c}$$

$$\overline{\nu\Sigma}_{f,i,g'} = \frac{\displaystyle\int_{x_{i-1/2}}^{x_{i+1/2}}\int_{E_g}^{E_{g-1}} \nu\Sigma_f(x,E)\,F_0(x,E)\,dEdx}{\displaystyle\int_{x_{i-1/2}}^{x_{i+1/2}}\int_{E_g}^{E_{g-1}} F_0(x,E)\,dEdx}\,, \tag{5.9d}$$

and

$$\overline{\chi}_{i,g} = \frac{\displaystyle\int_{x_{i-1/2}}^{x_{i+1/2}}\int_{E_g}^{E_{g-1}} \chi(x,E)\int_0^{\infty}\nu\Sigma_f(x,E')\,F_0(x,E')\,dE'dEdx}{\displaystyle\int_{x_{i-1/2}}^{x_{i+1/2}}\int_0^{\infty}\nu\Sigma_f(x,E')\,F_0(x,E')\,dE'dx}\,. \tag{5.9e}$$

Eqs. (5.4) and (5.9) are exact; however, an approximation is introduced when we generalize Eqs. (5.9) to the finite-medium, homogenized multigroup transport equation:

$$\begin{aligned}\mu\frac{\partial\overline{\psi}_{i,g}}{\partial x}(x,\mu) + \overline{\Sigma}_{t,i,g}\overline{\psi}_{i,g}(x,\mu) &= \sum_{g=1}^{G}\overline{\Sigma}_{s,0,i,g'\to g}\int_{-1}^{1}\overline{\psi}_{i,g'}(x,\mu')\,d\mu' \\ &\quad + \lambda\frac{\overline{\chi}_{i,g}}{2}\sum_{g=1}^{G}\overline{\nu\Sigma}_{f,i,g'}\int_{-1}^{1}\overline{\psi}_{i,g'}(x,\mu')\,d\mu'\,.\end{aligned} \tag{5.10}$$

Using the standard multigroup cross sections defined in Eqs. (5.9), we see that Eq. (5.8) preserves the homogenized infinite-lattice solution $\overline{F}_{0,g}$ and λ_0. This statement is still true if we multiply Eq. (5.8) by a constant, ρ_G:

$$(\rho_G\overline{\Sigma}_{t,i,g})\overline{F}_{0,i,g} = \sum_{g=1}^{G}(\rho_G\overline{\Sigma}_{s,0,i,g'\to g})\overline{F}_{0,i,g'} + \lambda\overline{\chi}_{i,g}\sum_{g=1}^{G}(\rho_G\overline{\nu\Sigma}_{f,i,g'})\overline{F}_{0,i,g'}\,,$$

or

$$\widehat{\Sigma}_{t,i,g}\overline{F}_{0,i,g} = \sum_{g=1}^{G}\widehat{\Sigma}_{s,i,g'\to g}\overline{F}_{0,i,g'} + \lambda\overline{\chi}_{i,g}\sum_{g=1}^{G}\widehat{\nu\Sigma}_{f,i,g'}\overline{F}_{0,i,g'}\,,$$

where

$$\boxed{\widehat{\Sigma}_g = \rho_G\overline{\Sigma}_g\,.} \tag{5.11}$$

In the remainder of this section, we use the cross sections defined in Eq. (5.11) with the following understandings:

1. If we set $\rho_G = 1$, we obtain the standard homogenized multigroup approximation.
2. For any G, ρ_G can be chosen to improve the accuracy of the multigroup transport solution without affecting the infinite-lattice eigenvalue or eigenfunction.
3. As $G \to \infty$, $\rho_G \to 1$.

With these thoughts in mind, we propose the following multigroup, finite lattice-homogenized-medium transport equation with the scaled cross sections from Eq. (5.11) to approximate Eq. (5.1):

$$\boxed{\begin{aligned}\mu\frac{\partial\overline{\psi}_{i,g}}{\partial x}(x,\mu) + \widehat{\Sigma}_{t,i,g}\overline{\psi}_{i,g}(x,\mu) &= \sum_{g=1}^{G}\widehat{\Sigma}_{s,0,i,g'\to g}\int_{-1}^{1}\overline{\psi}_{i,g'}(x,\mu')\,d\mu' \\ &\quad + \lambda\frac{\overline{\chi}_{i,g}}{2}\sum_{g=1}^{G}\widehat{\nu\Sigma}_{f,i,g'}\int_{-1}^{1}\overline{\psi}_{i,g'}(x,\mu')\,d\mu'\,, \\ &\qquad x \in [x_{i-1/2}, x_{i+1/2}]\,,\end{aligned}} \tag{5.12}$$

or

$$\boxed{\begin{aligned}\frac{\mu}{\rho_G}\frac{\partial\overline{\psi}_{i,g}}{\partial x}(x,\mu)+\overline{\Sigma}_{t,i,g}\overline{\psi}_{i,g}(x,\mu)=\sum_{g=1}^{G}\overline{\Sigma}_{s,0,i,g'\to g}\int_{-1}^{1}\overline{\psi}_{i,g'}(x,\mu')\,d\mu'\\ +\lambda\frac{\overline{\chi}_{i,g}}{2}\sum_{g=1}^{G}\overline{\nu\Sigma}_{f,i,g'}\int_{-1}^{1}\overline{\psi}_{i,g'}(x,\mu')\,d\mu'\,,\\ x\in[x_{i-1/2},x_{i+1/2}]\,.\end{aligned}} \tag{5.13}$$

In the following sections, we use the result of an asymptotic analysis to define ρ_G in a way that improves the accuracy of Eq. (5.13).

5.2 Asymptotic Analysis

As in Chapter 3, we consider an optically thick system, in which $\lambda \approx \lambda_0$. This can be done by fixing $\widehat{\Sigma}(E)$ and letting $x = O(1/\epsilon)$ for $\epsilon \ll 1$, or defining a slow spatial variable:

$$z = \epsilon x\,. \tag{5.14}$$

Because the lattice has already been homogenized, there is no periodic variable y. Introducing Eq. (5.14) into Eq. (5.13), and defining

$$\Psi_{i,g}(z,\mu) = \overline{\psi}_{i,g}(x,\mu) \tag{5.15a}$$

and

$$\lambda = \lambda_0 + \epsilon^2\lambda_2\,, \tag{5.15b}$$

we obtain:

$$\begin{aligned}\epsilon\frac{\mu}{\rho_G}\frac{\partial\Psi_{i,g}}{\partial z}(z,\mu)+\overline{\Sigma}_{t,i,g}\Psi_{i,g}(z,\mu)=\sum_{g=1}^{G}\overline{\Sigma}_{s,0,i,g'\to g}\int_{-1}^{1}\Psi_{i,g'}(z,\mu')\,d\mu'\\ +(\lambda_0+\epsilon^2\lambda_2)\frac{\overline{\chi}_{i,g}}{2}\sum_{g=1}^{G}\overline{\nu\Sigma}_{f,i,g'}\int_{-1}^{1}\Psi_{i,g'}(z,\mu')\,d\mu'\,.\end{aligned} \tag{5.16}$$

There is no $\epsilon\lambda_1$ in Eq. (5.16) because, as in Chapter 3, $\lambda_1 = 0$. Setting $\epsilon = 0$ produces the correct infinite-medium transport equation.

The following asymptotic analysis is similar to the one performed in Chapter 3. The only differences are:

1. Eq. (5.16) has cross sections that are independent of y.
2. Eq. (5.16) is multigroup, rather than continuous energy.
3. Eq. (5.16) contains an unspecified constant, ρ_G.

To solve Eq. (5.16), we assume that $\Psi_{i,g}$ can be expanded in powers of ϵ:

$$\Psi_{i,g}(z,\mu) = \sum_{l=0}^{\infty} \epsilon^l \Psi_{i,g}^{(l)}(z,\mu) \,. \tag{5.17}$$

Introducing Eq. (5.17) into Eq. (5.16) and equating the coefficients of ϵ, we obtain the following system of equations:

ϵ^0:

$$L\Psi_{i,g}^{(0)}(z,\mu) = 0\,; \tag{5.18a}$$

ϵ^1:

$$L\Psi_{i,g}^{(1)}(z,\mu) = -\frac{\mu}{\rho_G}\frac{\partial}{\partial z}\Psi_{i,g}^{(0)}(z,\mu)\,; \tag{5.18b}$$

ϵ^n for $n \geq 2$:

$$L\Psi_{i,g}^{(n)}(z,\mu) = -\frac{\mu}{\rho_G}\frac{\partial}{\partial z}\Psi_{i,g}^{(n-1)}(z,\mu) + \lambda_2 \frac{\overline{\chi}_{i,g}}{2} \sum_{g'=1}^{G} \overline{\nu\Sigma}_{f,i,g'} \int_{-1}^{1} \Psi_{i,g'}^{(n-2)}(z,\mu')\, d\mu' \,. \tag{5.18c}$$

Here L is the homogenized, infinite-medium multigroup transport operator, with the infinite-

medium eigenvalue λ_0:

$$L\Psi_{i,g}(z,\mu) \equiv \overline{\Sigma}_{t,i,g}\Psi_{i,g}(z,\mu) - \sum_{g'=1}^{G}\overline{\Sigma}_{s,0,i,g'\to g}\int_{-1}^{1}\Psi_{i,g'}(z,\mu')\,d\mu' - \lambda_0\frac{\overline{\chi}_{i,g}}{2}\sum_{g'=1}^{G}\overline{\nu\Sigma}_{f,i,g'}\int_{-1}^{1}\Psi_{i,g'}(z,\mu')\,d\mu' . \tag{5.19}$$

By design, Eq. (5.18a) has the general solution:

$$\Psi^{(0)}_{i,g}(z,\mu) = \frac{1}{2}\overline{F}_{0,i,g}\Phi^{(0)}(z) , \tag{5.20}$$

where $\Phi^{(0)}(z)$ is unspecified.

From the properties of L and the Fredholm alternative theorem (FAT) [29], we know that an equation of the form:

$$Lf_g(\mu) = Q_g(\mu) , \tag{5.21}$$

has a solution if and only if:

$$\sum_{g=1}^{G}\overline{F}^{*}_{0,g}\int_{-1}^{1}Q_g(\mu)\,d\mu = 0 . \tag{5.22}$$

This is called the *solvability condition* for Eq. (5.21).

Introducing Eq. (5.20) into Eq. (5.18b) and applying Eq. (5.22), we obtain the solvability condition for $\Psi^{(1)}_{i,g}$:

$$\begin{aligned} 0 &= \sum_{g=1}^{G}\int_{-1}^{1}\overline{F}^{*}_{0,g}\Big[-\mu\frac{\partial}{\partial z}\frac{1}{2}\overline{F}_{0,i,g}\Phi^{(0)}(z)\Big]d\mu \\ &= \sum_{g=1}^{G}\overline{F}^{*}_{0,g}[0]d\mu \\ &= 0 , \end{aligned} \tag{5.23}$$

which is automatically satisfied. Eq. (5.18b) therefore has a homogeneous solution (the solution to $L\Psi^{(1)}_{i,g} = 0$) and a particular solution. Combining the two, we obtain:

$$\begin{aligned}\Psi^{(1)}_{i,g}(z,\mu) &= \Psi^{(1)}_{g,\text{homog}}(z,\mu) + \Psi^{(1)}_{g,\text{part}}(z,\mu) \\ &= \frac{1}{2}\overline{F}_{0,g}(\mu)\Phi^{(1)}(z) - \frac{1}{\rho_G}L^{-1}\left[\frac{\mu}{2}\overline{F}_{0,g}\right]\frac{\partial}{\partial z}\Phi^{(0)}(z) \\ &= \frac{1}{2}\overline{F}_{0,g}(\mu)\Phi^{(1)}(z) - \frac{1}{\rho_G}\overline{f}_{1,g}(\mu)\frac{\partial}{\partial z}\Phi^{(0)}(z)\,,\end{aligned} \tag{5.24}$$

where $\Phi^{(1)}(z)$ is another unspecified function and

$$\overline{f}_{1,g}(\mu) = L^{-1}\left[\frac{\mu}{2}\overline{F}_{0,g}\right]. \tag{5.25}$$

We next consider Eq. (5.18c) for $n = 2$. The solvability condition is:

$$\begin{aligned}0 &= \sum_{g=1}^{G} F^*_{0,g}\int_{-1}^{1}\Big[-\frac{\mu}{\rho_G}\frac{\partial}{\partial z}\Psi^{(1)}_{i,g}(z,\mu) + \lambda_2\frac{\chi_g}{2}\sum_{g'=1}^{G}\nu\Sigma_{f,g'}\int_{-1}^{1}\Psi^{(0)}_{i,g'}(z,\mu')\,d\mu'\Big]d\mu \\ &= \sum_{g=1}^{G} F^*_{0,g}\int_{-1}^{1}\Big[-\frac{\mu}{\rho_G}\frac{\partial}{\partial z}\left(\frac{1}{2}\overline{F}_{0,g}\Phi^{(1)}(z) - \frac{1}{\rho_G}\overline{f}_{1,g}(\mu)\frac{\partial}{\partial z}\Phi^{(0)}(z)\right) \\ &\qquad\qquad + \lambda_2\frac{\chi_g}{2}\sum_{g'=1}^{G}\nu\Sigma_{f,g'}\overline{F}_{0,g'}\Phi^{(0)}(z)\Big]d\mu \\ &= \frac{1}{\rho_G^2}\left(\sum_{g=1}^{G} F^*_{0,g}\int_{-1}^{1}\mu f_{1,g}(\mu)\,d\mu\right)\frac{\partial^2\Phi^{(0)}}{\partial z^2} \\ &\qquad + \lambda_2\left(\sum_{g=1}^{G} F^*_{0,g}\chi_g\right)\left(\sum_{g'=1}^{G}\nu\Sigma_{f,g'}F_{0,g'}\right)\Phi^{(0)}(z)\,.\end{aligned} \tag{5.26}$$

The adjoint operator adjoint operator L^* is defined, such that:

$$L^*F^*_{0,g} = 0\,, \tag{5.27}$$

$$F^*_{0,g} = \text{infinite medium multigroup adjoint spectrum}\,,$$

and

$$\sum_{g=1}^{G} F_{0,g}^{*} F_{0,g} = 1 \,. \tag{5.28}$$

We also define the operators P_0 and P:

$$P_0 \eta_g(\mu) = \sum_{g=1}^{G} F_{0,g}^{*} \int_{-1}^{1} \eta_g(\mu') \, d\mu' \,, \tag{5.29}$$

and

$$\begin{aligned} P\eta_g(\mu) =& F_{0,g} \sum_{g=1}^{G} F_{0,g}^{*} \int_{-1}^{1} \eta_g(\mu') \, d\mu' \\ =& f_{0,g}(\mu) \, P_0 \eta_g(\mu) \,, \end{aligned} \tag{5.30}$$

where

$$P^2 = P \,. \tag{5.31}$$

We can therefore rewrite Eq. (5.26) as:

$$\begin{aligned} 0 = \frac{1}{\rho_G^2} P\Big(\mu f_{1,g}(\mu)\Big) \frac{\partial^2 \Phi^{(0)}}{\partial z^2} \\ + \lambda_2 P \left(\frac{\chi_g}{2} \sum_{g'=1}^{G} \nu \Sigma_{f,g'} F_{0,g'} \right) \Phi^{(0)}(z) \,, \end{aligned} \tag{5.32}$$

and, by subtracting Eq. (5.32) from Eq. (5.18c) for $n = 2$, we have:

$$\begin{aligned}
L\Psi^{(2)}_{i,g}(z,\mu) &= -(I-P)\frac{\mu}{\rho_G}\frac{\partial}{\partial z}\Psi^{(1)}_{i,g}(z,\mu) \\
&\quad + \lambda_2 (I-P)\frac{\chi_g}{2}\sum_{g'=1}^{G}\nu\Sigma_{f,g'}\int_{-1}^{1}\Psi^{(0)}_{g'}(z,\mu')\,d\mu' \\
&= -(I-P)\frac{\mu}{\rho_G}\frac{\partial}{\partial z}\left[\frac{1}{2}F_{0,g}\Phi^{(1)}(z) - \frac{1}{\rho_G}f_{1,g}(\mu)\frac{\partial}{\partial z}\Phi^{(0)}(z)\right] \\
&\quad + \lambda_2 (I-P)\frac{\chi_g}{2}\sum_{g'=1}^{G}\nu\Sigma_{f,g'}F_{0,g'}\Phi(z)\,d\mu' \\
&= -\frac{\mu}{2\rho_G}F_{0,g}\frac{\partial\Phi^{(1)}}{\partial z} + (I-P)\left[\frac{\mu}{\rho_G^2}f_{1,g}(\mu)\right]\frac{\partial^2\Phi^{(0)}}{\partial z^2} \\
&\quad + \lambda_2 (I-P)\frac{\chi_g}{2}\left(\sum_{g'=1}^{G}\nu\Sigma_{f,g'}\int_{-1}^{1}F_{0,g'}\right)\Phi^{(0)}(z)\,.
\end{aligned} \tag{5.33}$$

Eq. (5.33) now automatically satisfies the solvability condition, and by the FAT, its solution can be written:

$$\begin{aligned}
\Psi^{(2)}_{i,g}(z,\mu) =& \frac{1}{2}F_{0,g}\Phi^{(2)}(z) - \frac{1}{\rho_G}L^{-1}\Big[\frac{\mu}{2}F_{0,g}\Big]\frac{\partial\Phi^{(1)}}{\partial z} + \frac{1}{\rho_G^2}L^{-1}\Big[(I-P)\mu f_{1,g}(\mu)\Big]\frac{\partial^2\Phi^{(0)}}{\partial z^2} \\
&+ \lambda_2 L^{-1}\left[(I-P)\frac{\chi_g}{2}\left(\sum_{g'=1}^{G}\nu\Sigma_{f,g'}F_{0,g'}\right)\right]\Phi^{(0)}(z)\,,
\end{aligned} \tag{5.34}$$

or

$$\begin{aligned}
\Psi^{(2)}_{i,g}(z,\mu) =& \frac{1}{2}F_{0,g}\Phi^{(2)}(z) - \frac{1}{\rho_G}f_{1,g}(\mu)\frac{\partial\Phi^{(1)}}{\partial z} + \frac{1}{\rho_G^2}f_{2,g}(\mu)\frac{\partial^2\Phi^{(0)}}{\partial z^2} \\
&+ \lambda_2 f_{3,g}(\mu)\Phi^{(0)}(z)\,.
\end{aligned} \tag{5.35}$$

Here

$$f_{2,g}(\mu) = L^{-1}\Big[(I-P)\mu f_{1,g}(\mu)\Big] \tag{5.36}$$

and

$$f_{3,g}(\mu) = L^{-1}\left[(I-P)\frac{\chi_g}{2}\left(\sum_{g'=1}^{G}\nu\Sigma_{f,g'}F_{0,g'}\right)\right] \tag{5.37}$$

are new multigroup lattice functions.

Next, we consider Eq. (5.18c) for $n = 3$. The solvability condition is:

$$\begin{aligned}
0 &= \sum_{g=1}^{G} F^*_{0,g}\int_{-1}^{1}\Big[-\frac{\mu}{\rho_G}\frac{\partial}{\partial z}\Psi^{(2)}_{i,g}(z,\mu) + \lambda_2\frac{\chi_g}{2}\sum_{g'=1}^{G}\nu\Sigma_{f,g'}\int_{-1}^{1}\Psi^{(1)}_{i,g'}(z,\mu')\,d\mu'\Big]d\mu \\
&= \sum_{g=1}^{G} F^*_{0,g}\int_{-1}^{1}\Big[-\frac{\mu}{\rho_G}\frac{\partial}{\partial z}\Big(\frac{1}{2}F_{0,g}\Phi^{(2)}(z) - \frac{1}{\rho_G}f_{1,g}(\mu)\frac{\partial\Phi^{(1)}}{\partial z} \\
&\qquad\qquad + \frac{1}{\rho_G^2}f_{2,g}(\mu)\frac{\partial^2\Phi^{(0)}}{\partial z^2} + \lambda_2 f_{3,g}(\mu)\Phi^{(0)}(z)\Big) \\
&\qquad + \lambda_2\frac{\chi_g}{2}\sum_{g'=1}^{G}\nu\Sigma_{f,g'}\int_{-1}^{1}\Big(\overline{F}_{0,g}\Phi^{(1)}(z) - \frac{1}{\rho_G}\overline{f}_{1,g}(\mu')\frac{\partial}{\partial z}\Phi^{(0)}(z)\Big)d\mu'\Big]d\mu \\
&= \frac{1}{\rho_G^2}\left(\sum_{g=1}^{G}F^*_{0,g}\int_{-1}^{1}\mu f_{1,g}(\mu)\,d\mu\right)\frac{\partial^2\Phi^{(1)}}{\partial z^2} \\
&\qquad + \lambda_2\left(\sum_{g=1}^{G}F^*_{0,g}\chi_g\right)\left(\sum_{g'=1}^{G}\nu\Sigma_{f,g'}F_{0,g'}\right)\Phi^{(1)}(z)\,,
\end{aligned} \tag{5.38}$$

or, multiplying through by $f_{0,g}$:

$$\begin{aligned}
0 &= \frac{1}{\rho_G^2}P\Big(\mu f_{1,g}(\mu)\Big)\frac{\partial^2\Phi^{(1)}}{\partial z^2} \\
&\qquad + \lambda_2 P\left(\frac{\chi_g}{2}\sum_{g'=1}^{G}\nu\Sigma_{f,g'}F_{0,g'}\right)\Phi^{(1)}(z)\,.
\end{aligned} \tag{5.39}$$

As with $\Psi^{(2)}_{i,g}$, we subtract Eq. (5.39) from Eq. (5.18c) for $n = 3$, yielding:

$$\begin{aligned}
L\Psi^{(3)}_{i,g}(z,\mu) &= -(I-P)\frac{\mu}{\rho_G}\frac{\partial}{\partial z}\Psi^{(2)}_{i,g}(z,\mu) \\
&\quad + \lambda_2 (I-P)\frac{\chi_g}{2}\sum_{g'=1}^{G}\nu\Sigma_{f,g'}\int_{-1}^{1}\Psi^{(1)}_{g'}(z,\mu')\,d\mu' \\
&= -(I-P)\frac{\mu}{\rho_G}\frac{\partial}{\partial z}\Big[\frac{1}{2}F_{0,g}\Phi^{(2)}(z) - \frac{1}{\rho_G}f_{1,g}(\mu)\frac{\partial\Phi^{(1)}}{\partial z} + \frac{1}{\rho_G^2}f_{2,g}(\mu)\frac{\partial^2\Phi^{(0)}}{\partial z^2} \\
&\quad + \lambda_2 f_{3,g}(\mu)\Phi^{(0)}(z)\Big] + \lambda_2(I-P)\frac{\chi_g}{2}\sum_{g'=1}^{G}\nu\Sigma_{f,g'} \\
&\quad \times \int_{-1}^{1}\Big[\frac{1}{2}F_{0,g}\Phi^{(1)}(z) - \frac{1}{\rho_G}f_{1,g}(\mu')\frac{\partial}{\partial z}\Phi^{(0)}(z)\Big]d\mu' \qquad (5.40)\\
&= -\frac{1}{\rho_G}\frac{\mu}{2}F_{0,g}\frac{\partial\Phi^{(2)}}{\partial z} + \frac{1}{\rho_G^2}(I-P)[\mu f_{1,g}(\mu)]\frac{\partial^2\Phi^{(1)}}{\partial z^2} \\
&\quad - \frac{1}{\rho_G^3}\mu f_{2,g}(\mu)\frac{\partial^3\Phi^{(0)}}{\partial z^3} - \lambda_2\frac{1}{\rho_G}\mu f_{3,g}(\mu)\frac{\partial\Phi^{(0)}}{\partial z} \\
&\quad + \lambda_2(I-P)\Big[\frac{\chi_g}{2}\sum_{g'=1}^{G}\nu\Sigma_{f,g'}F_{0,g'}\Big]\Phi^{(1)}(z)
\end{aligned}$$

Eq. (5.40) now automatically satisfies the solvability condition, and the solution for $\Psi^{3}_{i,g}(z,\mu)$ is:

$$\begin{aligned}
\Psi^{(3)}_{i,g}(z,\mu) =& \frac{1}{2}F_{0,g}\Phi^{(3)}(z) - \frac{1}{\rho_G}f_{1,g}(\mu)\frac{\partial\Phi^{(2)}}{\partial z} + \frac{1}{\rho_G^2}f_{2,g}(\mu)\frac{\partial^2\Phi^{(1)}}{\partial z^2} \\
&- \frac{1}{\rho_G^3}f_{4,g}(\mu)\frac{\partial^3\Phi^{(0)}}{\partial z^3} - \lambda_2\frac{1}{\rho_G}f_{5,g}(\mu)\frac{\partial\Phi^{(0)}}{\partial z} + \lambda_2 f_{3,g}(\mu)\Phi^{(1)}(z)\,, \qquad (5.41)
\end{aligned}$$

where

$$f_{4,g}(\mu) = L^{-1}\Big[\mu f_{2,g}(\mu)\Big], \qquad (5.42)$$

and

$$f_{5,g}(\mu) = L^{-1}\Big[\mu f_{3,g}(\mu)\Big], \qquad (5.43)$$

are new multigroup lattice functions.

Finally, we consider Eq. (5.18c) for $n = 4$. The solvability condition is:

$$
\begin{aligned}
0 &= \sum_{g=1}^{G} F^*_{0,g} \int_{-1}^{1} \Big[-\frac{\mu}{\rho_G}\frac{\partial}{\partial z}\Psi^{(3)}_{i,g}(z,\mu) + \lambda_2 \frac{\chi_g}{2} \sum_{g'=1}^{G} \nu\Sigma_{f,g'} \int_{-1}^{1} \Psi^{(2)}_{i,g'}(z,\mu')\,d\mu' \Big] d\mu \\
&= \sum_{g=1}^{G} F^*_{0,g} \int_{-1}^{1} \Big[-\frac{\mu}{\rho_G}\frac{\partial}{\partial z}\Big(\frac{1}{2} F_{0,g}\Phi^{(3)}(z) - \frac{1}{\rho_G} f_{1,g}(\mu)\frac{\partial \Phi^{(2)}}{\partial z} \\
&\qquad\qquad + \frac{1}{\rho_G^2} f_{2,g}(\mu)\frac{\partial^2 \Phi^{(1)}}{\partial z^2} - \frac{1}{\rho_G^3} f_{4,g}(\mu)\frac{\partial^3 \Phi^{(0)}}{\partial z^3} \\
&\qquad\qquad - \lambda_2 \frac{1}{\rho_G} f_{5,g}(\mu)\frac{\partial \Phi^{(0)}}{\partial z} + \lambda_2 f_{3,g}(\mu)\Phi^{(1)}(z) \Big) \\
&\quad + \lambda_2 \frac{\chi_g}{2} \sum_{g'=1}^{G} \nu\Sigma_{f,g'} \int_{-1}^{1} \Big(\frac{1}{2} F_{0,g}\Phi^{(2)}(z) - \frac{1}{\rho_G} f_{1,g}(\mu')\frac{\partial \Phi^{(1)}}{\partial z} \\
&\qquad\qquad + \frac{1}{\rho_G^2} f_{2,g}(\mu')\frac{\partial^2 \Phi^{(0)}}{\partial z^2} + \lambda_2 f_{3,g}(\mu')\Phi^{(0)}(z) \Big) d\mu' \Big] d\mu \\
&= \sum_{g=1}^{G} F^*_{0,g} \int_{-1}^{1} \Big[-\frac{\mu}{\rho_G}\frac{\partial}{\partial z}\Big(0 - \frac{1}{\rho_G} f_{1,g}(\mu)\frac{\partial \Phi^{(2)}}{\partial z} \\
&\qquad\qquad + 0 - \frac{1}{\rho_G^3} f_{4,g}(\mu)\frac{\partial^3 \Phi^{(0)}}{\partial z^3} \\
&\qquad\qquad - \lambda_2 \frac{1}{\rho_G} f_{5,g}(\mu)\frac{\partial \Phi^{(0)}}{\partial z} + 0 \Big) \\
&\quad + \lambda_2 \frac{\chi_g}{2} \sum_{g'=1}^{G} \nu\Sigma_{f,g'} \int_{-1}^{1} \Big(F_{0,g}\Phi^{(2)}(z) - 0 \\
&\qquad\qquad + \frac{1}{\rho_G^2} f_{2,g}(\mu')\frac{\partial^2 \Phi^{(0)}}{\partial z^2} + \lambda_2 f_{3,g}(\mu')\Phi^{(0)}(z) \Big) d\mu' \Big] d\mu\,,
\end{aligned}
\tag{5.44}
$$

or, more clearly,

$$
\begin{aligned}
0 = &\frac{1}{\rho_G^2}\left(\sum_{g=1}^{G} F_{0,g}^{*} \int_{-1}^{1} \mu f_{1,g}(\mu)\, d\mu\right)\frac{\partial^2 \Phi^{(2)}}{\partial z^2} \\
&+ \frac{1}{\rho_G^4}\left(\sum_{g=1}^{G} F_{0,g}^{*} \int_{-1}^{1} \mu f_{4,g}(\mu)\, d\mu\right)\frac{\partial^4 \Phi^{(0)}}{\partial z^4} \\
&+ \lambda_2 \frac{1}{\rho_G^2}\left(\sum_{g=1}^{G} F_{0,g}^{*} \int_{-1}^{1} f_{5,g}(\mu)\, d\mu\right)\frac{\partial^2 \Phi^{(0)}}{\partial z^2} \\
&+ \lambda_2 \left(\sum_{g=1}^{G} F_{0,g}^{*} \chi_g\right)\left(\sum_{g'=1}^{G} \nu\Sigma_{f,g'} F_{0,g'}\right)\Phi^{(2)}(z)\,, \\
&+ \lambda_2 \frac{1}{\rho_G^2}\left(\sum_{g=1}^{G} F_{0,g}^{*} \chi_g\right)\left(\sum_{g'=1}^{G} \nu\Sigma_{f,g'} \int_{-1}^{1} f_{2,g'}(\mu')\, d\mu'\right)\frac{\partial^2 \Phi^{(0)}}{\partial z^2}(z)\,, \\
&+ \lambda_2^2 \left(\sum_{g=1}^{G} F_{0,g}^{*} \chi_g\right)\left(\sum_{g'=1}^{G} \nu\Sigma_{f,g'} \int_{-1}^{1} f_{3,g'}(\mu')\, d\mu'\right)\Phi^{(0)}(z)\,.
\end{aligned}
\tag{5.45}
$$

The procedure outlined above can be repeated to obtain a solution for $\Psi_{i,g}^{(4)}$. However, we are only interested in the solvability condition for $\Psi_{i,g}^{(4)}$ and $\Psi_{i,g}^{(5)}$. For brevity, we state that the solvability condition for $\Psi_{i,g}^{(5)}$ is identical to Eq. (**??**), but with $\Phi^{(1)}$ and $\Phi^{(3)}$ in place of $\Phi^{(0)}$ and $\Phi^{(2)}$, respectively.

Derivations of one group asymptotic diffusion and SP_2 equations are performed in the same manner as Sections 3.2 and 3.3, with linear combinations of solvability conditions. If we define:

$$
\phi^{(0)}(x) = \Phi^{(0)}(z) + \epsilon\Phi^{(1)}(z)\,, \tag{5.46}
$$

then we obtain a monoenergetic diffusion equation:

$$
-D_0 \frac{\partial^2 \phi^{(0)}}{\partial x^2} + \overline{\Sigma}_a \phi^{(0)}(x) = \lambda \overline{\nu\Sigma}_f \phi^{(0)}(x)\,, \tag{5.47}
$$

where

$$\overline{\Sigma}_a = \frac{\sum_{g=1}^{G} F_{0,g}\left(\Sigma_{t,g} - \sum_{g'=0}^{G} \Sigma_{s,0,g\to g'}\right)}{\sum_{g=1}^{G} F_{0,g}}, \tag{5.48a}$$

$$\overline{\nu\Sigma}_f = \frac{\sum_{g=1}^{G} F_{0,g}\overline{\nu\Sigma}_{f,g}}{\sum_{g=1}^{G} F_{0,g}}, \tag{5.48b}$$

and

$$D_0 = \frac{\sum_{g=1}^{G} F^*_{0,g}\int_{-1}^{1} \mu f_{1,g}(\mu)\, d\mu}{\rho_G^2\left(\sum_{g=1}^{G} F^*_{0,g}\chi_g\right)\left(\sum_{g=1}^{G} F_{0,g}\right)}. \tag{5.49}$$

Likewise, if we define:

$$\phi(x) = (\Phi^{(0)}(z) + \epsilon\Phi^{(1)}(z)) + \epsilon^2(\Phi^{(2)}(z) + \epsilon\Phi^{(3)}(z)), \tag{5.50}$$

we obtain a monoenergetic SP_2 equation:

$$-\left[D_0 + D_2\left(\lambda\overline{\nu\Sigma}_f - \overline{\Sigma}_a\right)\right]\frac{\partial^2\phi}{\partial x^2} + \overline{\Sigma}_a\phi(x) = \lambda\overline{\nu\Sigma}_f\phi(x), \tag{5.51}$$

where D_0 is defined in Eq. (5.49), and

$$D_2 = \frac{1}{\rho_G^2}\Bigg[-\frac{\sum_{g=1}^{G} F_{0,g}^* \int_{-1}^{1} \mu f_{5,g}(\mu)\, d\mu}{\sum_{g=1}^{G} F_{0,g}^* \int_{-1}^{1} \mu f_{1,g}(\mu)\, d\mu} + \frac{\sum_{g=1}^{G} F_{0,g}^* \int_{-1}^{1} \mu f_{4,g}(\mu)\, d\mu}{\left(\sum_{g=1}^{G} F_{0,g}^* \overline{\chi}_g\right)\left(\sum_{g=1}^{G} F_{0,g} \overline{\nu\Sigma}_{f,g}\right)} + \frac{\sum_{g=1}^{G} F_{3,g} \overline{\nu\Sigma}_f}{\sum_{g=1}^{G} F_{0,g} \overline{\nu\Sigma}_{f,g}} - \frac{\sum_{g=1}^{G} F_{0,g}^* \int_{-1}^{1} \mu f_{1,g}(\mu)\, d\mu}{\left(\sum_{g=1}^{G} F_{0,g}^* \overline{\chi}_g\right)\left(\sum_{g=1}^{G} F_{0,g} \overline{\nu\Sigma}_{f,g}\right)} \times \frac{\left(\sum_{g=1}^{G} F_{0,g}^* \overline{\chi}_g\right)\left(\sum_{g=1}^{G} F_{2,g} \overline{\nu\Sigma}_{f,g}\right)}{\left(\sum_{g=1}^{G} F_{0,g}^* \overline{\chi}_g\right)\left(\sum_{g=1}^{G} F_{0,g} \overline{\nu\Sigma}_{f,g}\right)} \Bigg]. \tag{5.52}$$

5.3 Solving for ρ_G

The final step in our analysis is to determine ρ_G, the scaling factor for the multigroup cross sections. This can be carried out in one of two ways, by either (i) preserving the asymptotic diffusion limit of the continuous energy transport equation, or (ii) preserving the asymptotic SP_2 limit of the continuous energy transport equation. Both cases are presented here, with numerical results compared in Chapter 6.

5.3.1 Asymptotic Diffusion Limit

One of the constraints mentioned earlier was that as $G \to \infty$, $\rho_G \to 1$. Taking this limit, Eq. (5.49) becomes:

$$D = \frac{\left(\int_0^\infty F_0^*(E) \int_{-1}^{1} \mu f_1(\mu, E)\, d\mu dE\right)}{\left(\int_0^\infty F_0^*(E)\chi(E)\, dE\right)\left(\int_0^\infty F_0(E)\, dE\right)}. \tag{5.53}$$

We define ρ_G such that the multigroup and continuous energy transport equations have the same asymptotic limit, or, equivalently, that Eqs. (5.49) and (5.53) are equal:

$$\frac{\left(\sum_{g=1}^{G} F_{0,g}^{*} \int_{-1}^{1} \mu f_{1,g}(\mu)\, d\mu\right)}{\rho_G^2 \left(\sum_{g=1}^{G} F_{0,g}^{*} \chi_g\right)\left(\sum_{g'=1}^{G} F_{0,g'}\right)} = \frac{\left(\int_0^\infty F_0^*(E) \int_{-1}^{1} \mu f_1(\mu, E)\, d\mu dE\right)}{\left(\int_0^\infty F_0^*(E)\chi(E)\, dE\right)\left(\int_0^\infty F_0(E)\, dE\right)}. \tag{5.54}$$

This equation yields the following asymptotic diffusion definition of the multigroup scaling factor ρ_G:

$$\boxed{\rho_G = \left[\left(\frac{\sum_{g=1}^{G} F_{0,g}^{*} \int_{-1}^{1} \mu f_{1,g}(\mu)\, d\mu}{\int_0^\infty F_0^*(E) \int_{-1}^{1} \mu f_1(\mu, E)\, d\mu dE}\right) \times \left(\frac{\int_0^\infty F_0^*(E)\chi(E)\, dE}{\sum_{g=1}^{G} F_{0,g}^{*} \chi_g}\right)\right]^{1/2}}. \tag{5.55}$$

5.3.2 Asymptotic SP_2 Limit

For SP_2 , we cannot consider a single diffusion coefficient. Instead, we consider the constant in front of the spatial derivative of ϕ:

$$D_0 + D_2\left(\lambda\overline{\nu\Sigma}_f - \overline{\Sigma}_a\right). \tag{5.56}$$

As in Section 5.3.1, we take the limit as $G \to \infty$, $\rho_G \to 1$, to obtain:

$$\frac{1}{\rho_G^2}\left[D_{0,G} + D_{2,G}\left(\lambda\overline{\nu\Sigma}_f - \overline{\Sigma}_a\right)\right] = \overline{D}_0 + \overline{D}_2\left(\lambda\overline{\nu\Sigma}_f - \overline{\Sigma}_a\right), \tag{5.57}$$

where $D_{0,G}$ and $D_{2,G}$ are defined as in Eqs. (5.49) and (5.52) (G is the number of energy groups),

$$\overline{D}_0 = \frac{\left(\int_0^\infty F_0^*(E) \int_{-1}^{1} \mu f_1(\mu, E)\, d\mu dE\right)}{\left(\int_0^\infty F_0^*(E)\chi(E)\, dE\right)\left(\int_0^\infty F_0(E)\, dE\right)}, \tag{5.58}$$

and

$$\begin{aligned}\overline{D}_2 = &-\frac{\int_0^\infty F_0^*(E)\int_{-1}^1 \mu f_5(\mu,E)\,d\mu dE}{\int_0^\infty F_0^*(E)\int_{-1}^1 \mu f_1(\mu,E)\,d\mu dE} + \frac{\int_0^\infty \nu\Sigma_f(E)\int_{-1}^1 f_3(\mu,E)\,d\mu dE}{\int_0^\infty \nu\Sigma_f(E)F_0(E)\,dE} \\ &+ \frac{\int_0^\infty F_0^*(E)\int_{-1}^1 \mu f_4(\mu,E)\,d\mu dE}{\left(\int_0^\infty \chi(E)F_0^*(E)\,dE\right)\left(\int_0^\infty \nu\Sigma_f(E)F_0(E)\,dE\right)} \\ &- \frac{\int_0^\infty F_0^*(E)\int_{-1}^1 \mu f_1(\mu,E)\,d\mu dE}{\left(\int_0^\infty \chi(E)F_0^*(E)\,dE\right)\left(\int_0^\infty \nu\Sigma_f(E)F_0(E)\,dE\right)} \\ &\times \frac{\int_0^\infty \nu\Sigma_f(E)\int_{-1}^1 f_2(\mu,E)\,d\mu dE}{\int_0^\infty \nu\Sigma_f(E)F_0(E)\,dE}.\end{aligned} \tag{5.59}$$

This equation yields the following asymptotic SP_2 equation for the multigroup scaling factor ρ_G:

$$\boxed{\rho_G = \left[\frac{D_{0,G} + D_{2,G}\left(\lambda\overline{\nu\Sigma}_f - \overline{\Sigma}_a\right)}{\overline{D}_0 + \overline{D}_2\left(\lambda\overline{\nu\Sigma}_f - \overline{\Sigma}_a\right)}\right]^{1/2}}. \tag{5.60}$$

Eq. (5.60) has one obvious disadvantage; it requires knowledge of the unknown eigenvalue λ. This can be mitigated by lagging the calculation of ρ_G, and updating it only periodically, or with large changes in λ. However, as we shall see in Chapter 6, this increased computational cost may not be worth the accompanying increase in accuracy.

5.4 Discussion

By our definitions of $\overline{D}_0$, $\overline{D}_2$, $\overline{D}_{0,g}$, and $\overline{D}_{2,g}$, it is clear that Eqs. (5.55) and (5.60) will approach unity as $G \to \infty$. By applying the scaling factors, we are preserving the asymptotic

limit of the *homogenized* continuous energy transport equation. Alternatively, ρ_G could be defined to preserve the asymptotic limit of the lattice continuous energy transport equation, a topic for future work.

In the following chapter, the scaling factors defined in Eqs. (5.55) and (5.60) are numerically tested for a set of test problems.

CHAPTER 6

Derivation of a Scaling Factor for the Homogenized, Multigroup Transport Equation – Numerical Results

In this chapter, we numerically evaluate the scaling factors ρ_G defined in Chapter 5 using a 1-D, multigroup S_N code. Because continuous energy solutions for f_0 and f_0^* were unavailable, we used two "fine" group structures for our "continuous energy" libraries, and performed energy group collapses on these libraries.

Two sets of cross section libraries were used. The first, a 56-group library, was obtained from the MPACT code [31] with a homogeneous mixture of UO_2 and light water. The second, a seven-group library, comes from the C5G7 reactor benchmark [30]. The 56 group library demonstrates the efficacy of the scaling factors for homogeneous media with fine group structures, and is meant to mimic the ultra-fine group 0- and 1-D calculations performed at an early stage in cross section generation. The C5G7 library establishes the accuracy of the scaling factors for problems with a relatively coarse energy group structure and heterogeneous geometry.

The 56-group numerical results show that the scaling factor significantly reduces the eigenvalue and flux errors for a homogeneous medium. In most cases, SP_2 scaling factor proves to be slightly more accurate than the diffusion scaling factor. Results from seven group simulations also show an improvement in accuracy when the scaling factor is

used; however, the diffusion-based scaling factor outperforms the SP_2-based scaling factor for these problems. Because the SP_2 scaling factor is more expensive to calculate, the diffusion-based ρ_G formulation is recommended for most practical calculations.

6.1 56-Group Library

The 56-group library was obtained using the MPACT code [31] with a homogeneous mixture of UO_2 fuel and light water (borated) moderator. Number densities for the fine group library were obtained from the VERA benchmark [32] for 3.1% enriched fuel and 0.743 g/cc light water moderator with 1300 ppm boron, and were then volume weighted to obtain the number densities presented in Table 6.1.

Table 6.1 Test Problem Number Densities

Fuel	U-234	U-235	U-236	U-238	O-Fuel
N $\frac{\text{atoms}}{\text{barn-cm}}$	2.03134E-06	2.38415-04	1.09511-03	7.35517E-03	1.51934-02
Moderator	O-16	H-1	B-10	B-11	
N $\frac{\text{atoms}}{\text{barn-cm}}$	1.65741E-02	3.31481E-02	7.15235E-06	2.87892E-05	

Forward and adjoint scalar fluxes were obtained for an infinite homogeneous medium, and were used to collapse the cross sections in energy. Forward and adjoint homogeneous infinite medium scalar fluxes were again calculated using the few-group cross sections, and, combined with the fine group fluxes, were substituted in to Eqs. (5.55) and (5.60) to calculate ρ_G.

6.1.1 Results

The few and fine group cross sections obtained from the infinite homogeneous medium calculation were used in a series of homogeneous medium simulations for finite systems of varying widths L. All results were generated using a 1-D, isotropic scattering S_N code with vacuum boundary conditions. The 56 group results were used as a reference solution, with

the eigenvalue error reported in percent mille (pcm):

$$\Delta k_{eff} = \left(k_{eff,56G} - k_{eff,\text{Few Group}}\right) \times 10^5 (\text{pcm}) \,. \tag{6.1}$$

Fig. 6.1 and Tables 6.2-6.4 show the eigenvalue error with standard, diffusion-scaled and SP_2-scaled few group cross sections for 2, 4, 16, and 24 energy groups, as functions of the system width L. As the number of energy groups increases, we approach the continuous energy problem, and the eigenvalue error decreases. Likewise, as L increases, the problem becomes more like the infinite homogeneous medium problem that the cross sections are meant to designed, and the error decreases.

When the scaled cross sections are used, we see a decrease in the eigenvalue error of up to two orders of magnitude. This error reduction becomes even more significant as the problem width increases. Since the scaling factor is chosen to preserve a diffusion approximation of Eq. (5.1), it performs less consistently as the problem size decreases.

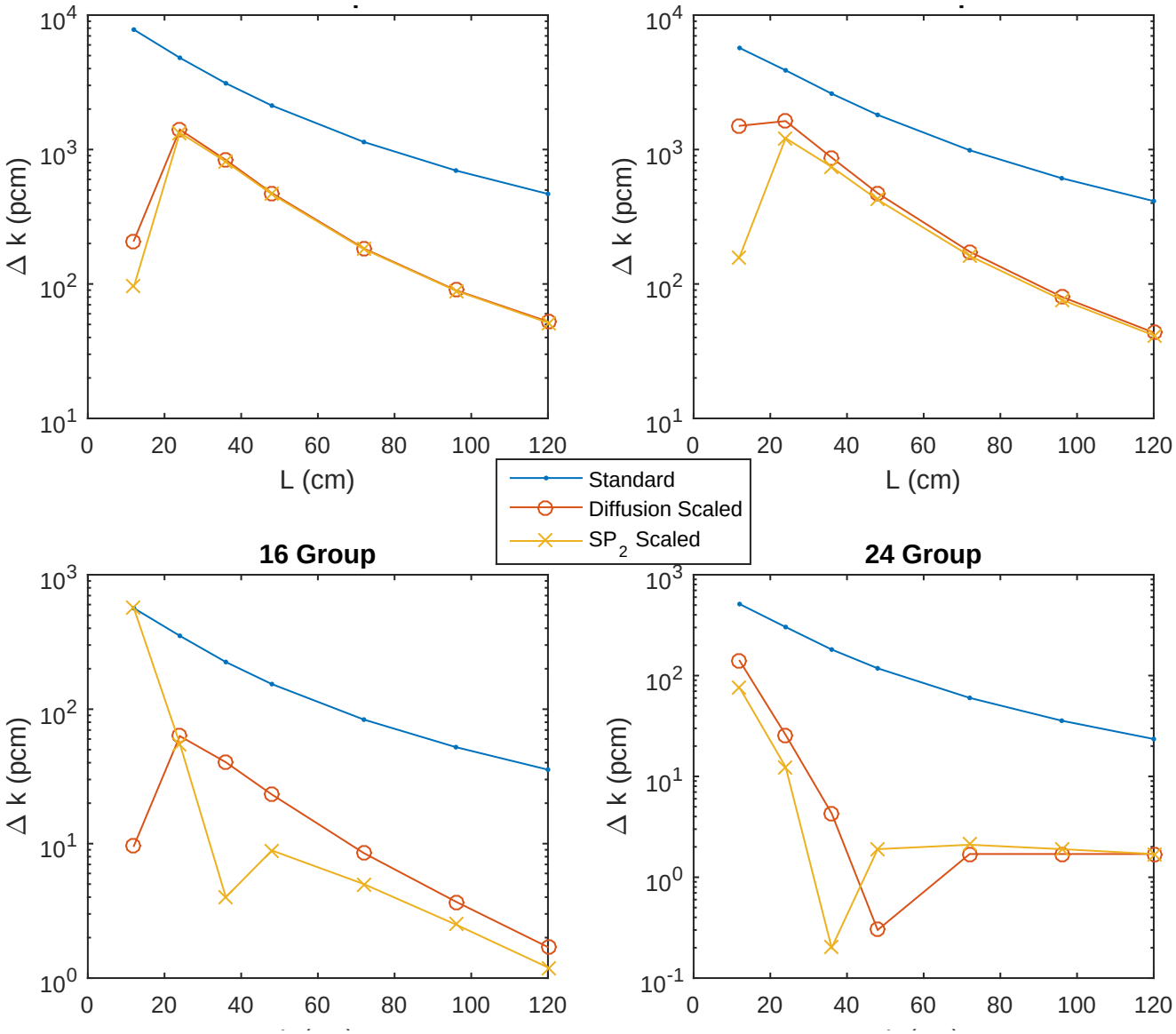

Figure 6.1: Eigenvalue Error (Δk) in pcm

Table 6.2 Unscaled Results

Length (cm)	56 Group (Reference) k-eff	24 Group Δk (pcm)	16 Group Δk (pcm)	4 Group Δk (pcm)	2 Group Δk (pcm)
12	0.426928	-512.1	-564.4	-5694.3	-7799.6
24	0.746386	-303.1	-351.4	-3882.4	-4812.5
36	0.870090	-181.3	-224.3	-2604.3	-3109.2
48	0.926879	-118.1	-153.7	-1810.1	-2122.7
72	0.974806	-60.1	-83.7	-987.6	-1137.8
96	0.993721	-	-52.2	-611.7	-697.8
120	1.003003	-23.0	-35.0	-413.0	-467.0

Table 6.3 Diffusion Scaled Results

Length (cm) or ρ	56 Group (Reference) k-eff	24 Group Δk (pcm)	16 Group Δk (pcm)	4 Group Δk (pcm)	2 Group Δk (pcm)
ρ_G	–	0.99256	0.98892	0.86060	0.84002
12	0.426928	-140.3	-9.6	1501.1	209.6
24	0.746386	-25.8	63.1	1628.5	1408.0
36	0.870090	-4.3	40.3	871.3	835.6
48	0.926879	0.3	23.2	473.5	474.0
72	0.974806	1.7	8.5	173.	183.7
96	0.993721	1.7	3.7	80.3	89.8
120	1.003003	1.7	1.7	43.5	52.5

Table 6.4 SP_2 Scaled Results

Length (cm) or ρ	56 Group (Reference) k-eff	24 Group Δk (pcm)	16 Group Δk (pcm)	4 Group Δk (pcm)	2 Group Δk (pcm)
ρ_G	–	0.99258	0.98895	0.086061	0.84004
12	0.426928	-75.6	-564.4	-159.4	-95.5
24	0.746386	-12.4	-55.4	1214.3	1330.6
36	0.870090	-0.2	4.0	742.3	811.4
48	0.926879	1.9	8.9	423.2	464.5
72	0.974806	2.1	5.0	161.7	181.4
96	0.993721	1.9	2.5	76.2	89.0
120	1.003003	1.7	1.2	41.5	51.5

Fig. 6.1 and Tables 6.2-6.4 only show that the scaling factor improves the eigenvalue. To more locally characterize the scaling factor's effect, we consider the spatially-dependent fission source,

$$F_G(x) = \sum_{g=1}^{G} \nu\Sigma_{f,g}\phi_g(x) \, . \tag{6.2}$$

In Eq. (6.2), the flux has been normalized such that the total fission source (integrated over the spatial domain) equals unity.

Figs. 6.2 and 6.3 show, for 2 / 4 groups and 16 / 24 groups respectively, the absolute error $\varepsilon = F_{56G}(x) - F_{MG}$ for $L = 36$ cm. An error of zero indicates that the multigroup results exactly reproduce the 56 fine group solution.

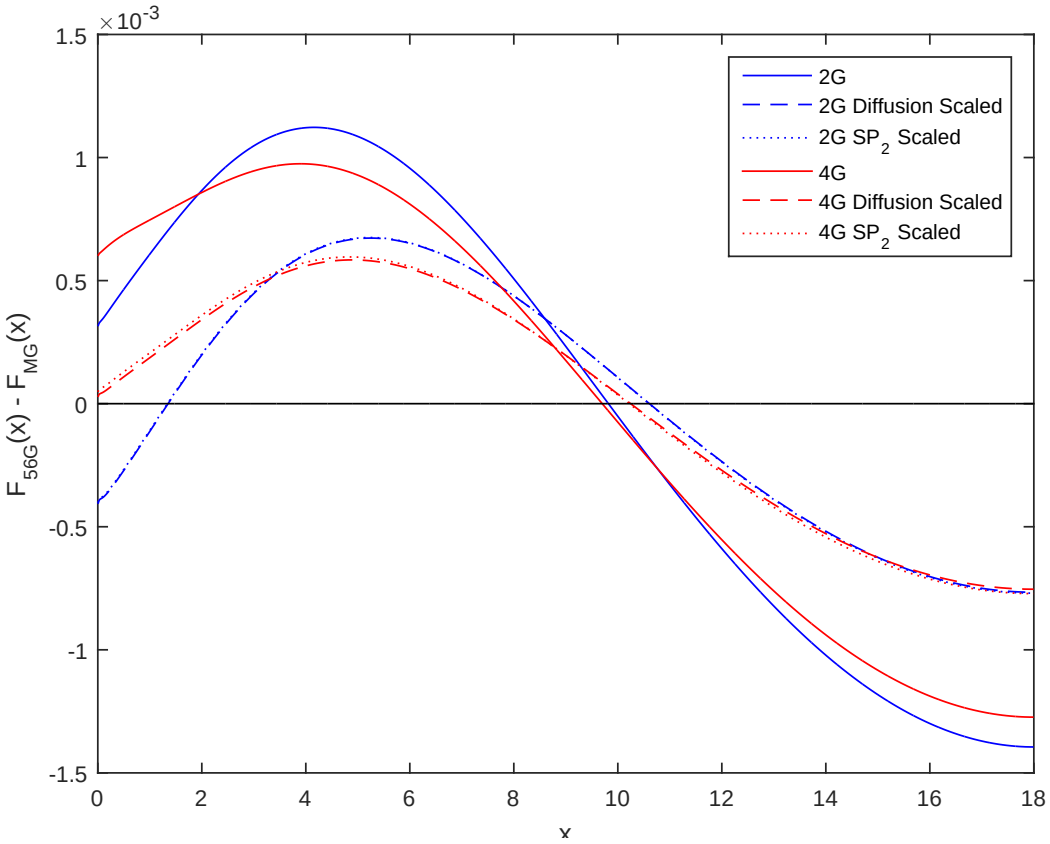

Figure 6.2: Fission source error for 2 and 4 groups

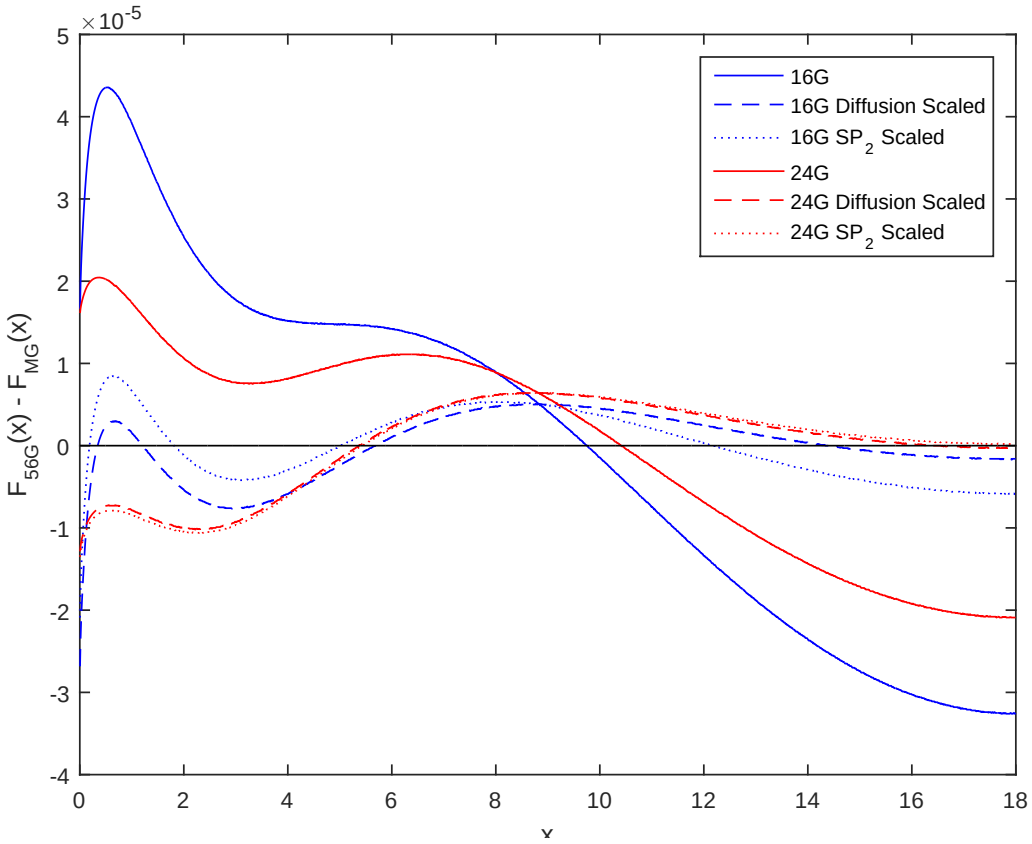

Figure 6.3: Fission source error for 16 and 24 groups

In Fig. 6.2, we see that the maximum errors for the unscaled fission rates for 2 and 4 groups are approximately twice the maximum errors for the scaled fission rates. In Fig. 6.3, for 16 and 24 groups, this improvement is even greater. Furthermore, we see that for 2 and 4 groups, the diffusion and SP_2 scaling factors lead to almost identical fission sources (the curves lie almost on top of each other). It is only for 16 groups that the two curves do not overlap.

The improvement in accuracy that results from using the SP_2-based ρ_G instead of the diffusion-based ρ_G is modest and inconsistent, even for small problems. Since the SP_2 ρ_G requires periodic updates as λ is updated, it also takes longer (both in run time and convergence, as one also must wait for ρ_G to converge). These drawbacks, combined with the results from the next section, lead us to recommend the diffusion-based scaling factor over

the SP_2-based scaling factor for practical calculations.

6.2 C5G7 Library

The seven-group C5G7 cross sections were taken directly from the benchmark document [30]. In the C5G7 benchmark problem definition, cladding is already homogenized with the fuel. To represent the 2-D pin geometry from the benchmark in 1-D, area fractions were preserved. Thus, the 2-D fuel pin was converted to an effective 1-D "fuel pin." The geometry conversion is summarized in Table 6.5. While the dimensions and areas are not identical, the *ratio* of the fuel area to moderator area is similar.

Table 6.5 C5G7 Problem Geometry

Dimensions	Fuel Dimension	Fuel Area	Moderator Length	Moderator Area
Original	0.54 cm (radius)	0.916088 cm^2	1.26 cm	0.671512 cm^2
Converted	1.01 cm (length)	1.01 cm^2	0.74 cm	0.74 cm^2

The same geometry was used for each fuel pin, guide tube, and fission chamber. Four fuel types are present, as defined in the benchmark; a UO_2 pin, and three MOX pins with 4.3%, 7.0% and 8.7% MOX.

6.2.1 Homogeneous Pin

A strategy identical to that of Section 6.1 was initially pursued, in which each pin was individually homogenized and tested as a homogeneous medium of variable size with vacuum boundary conditions. In each case, the reference solution was generated using seven groups and an array of heterogeneous 1-D pins. The reference case is compared to homogeneous cases with seven energy groups, two energy groups, two energy groups with the diffusion-based scaling factor in Eq. (5.55), and two energy groups with the SP_2-based scaling factor in Eq. (5.60).

The eigenvalue errors (in pcm) for the four fuel pin types, with problem sizes ranging from 5 to 40 homogenized fuel pins, are presented in Tables 6.6-6.9.

Table 6.6 Homogenized UO_2 Pin

# Pins	10	20	40	80
Reference	0.661406	1.038419	1.22705	1.291361
7G	-339	-144.1	-45.1	-13.2
2G	-12664.4	-5546.7	-602.5	1359.1
2G Diffusion	-2070.3	118.3	127.8	32.6
2G SP_2	1020.7	742.1	195.3	37.9

Table 6.7 Homogenized MOX 4.3% Pin

# Pins	10	20	40	80
Reference	0.602261	0.911137	1.064162	1.116335
7G	-175.7	-58.7	-15.8	-4.4
2G	-5569.7	-2458.6	-899.7	-275
2G Diffusion	-1618.1	162	115.2	25.3
2G SP_2	744.9	635.7	166.4	29.3

Table 6.8 Homogenized MOX 7.0% Pin

# Pins	10	20	40	80
Reference	0.634581	0.942415	1.093713	1.145177
7G	-104.8	-23.4	-3.9	-0.7
2G	-5285.9	-2318.3	-854.7	-261.4
2G Diffusion	-1408.6	224.9	124.8	27.9
2G SP_2	772.5	658.1	171.5	31.5

Table 6.9 Homogenized MOX 8.7% Pin

# Pins	10	20	40	80
Reference	0.65204	0.959192	1.10947	1.160509
7G	-71.7	-8.2	0.6	0.3
2G	-5109.6	-2243	-834.8	-259.2
2G Diffusion	-1052.7	405.6	183	41.2
2G SP_2	802.9	667.5	169.1	27.4

As anticipated, we see that for all four fuel pin types, the seven-group homogenized cross sections outperform all of the two-group result, and that the scaling factor improves the two-group solution. Unexpectedly, we note that the diffusion scaling factor outperforms the SP_2 scaling factor for most of the cases presented here. Only when the problem is very small (10 fuel pins), or occasionally for the 8.7% MOX fuel pin, does the SP_2 scaling factor result in a smaller eigenvalue error than the diffusion scaling factor.

6.2.2 Heterogeneous Assembly

To further explore the effect of *spatial* homogenization on the scaling factor, a "slice" of the C5G7 core was simulated. This was taken as a single row cutting through both a UO_2 and MOX assembly. The geometry is presented in Fig. 6.4.

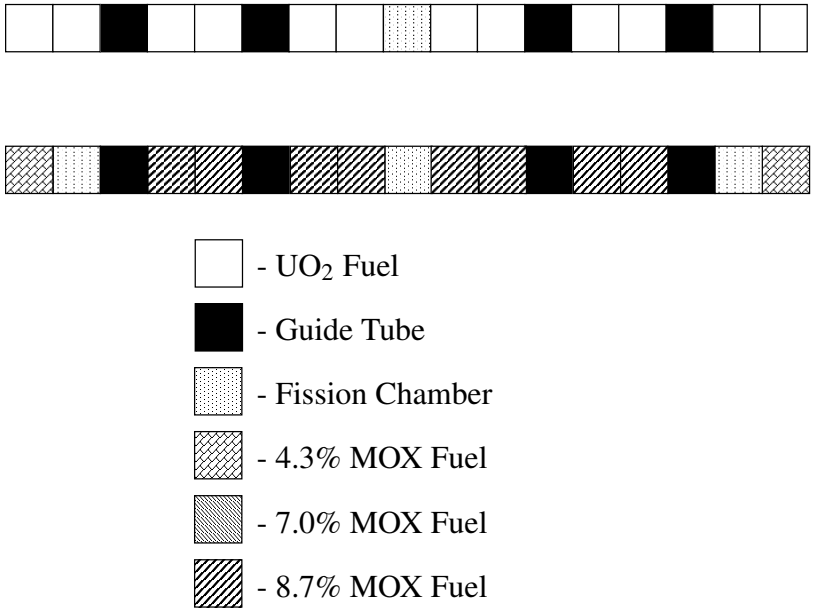

Figure 6.4: Assembly Slice Geometry

Each assembly slice was homogenized separately to both seven and two groups, and the two homogenized assembly rows were modeled next to each other. In addition to eigenvalues, core absorption and leakage (from the left side of the problem) were calculated. All three values are shown in Table 6.10. With the exception of the reference case, eigenvalue errors are reported in pcm, and absorption and leakage errors are given as relative percent errors.

Table 6.10 Two Assembly

	k	Absorption	Leakage
Reference	1.19872	0.809933	-0.0243002
7G	-31	0.098279734	-2.378992765
2G	-361	0.022717929	9.585517815
2G Diffusion	156	-0.034817695	5.520530695
2G SP_2	180	-0.035928898	5.322178418

As before, we see an improvement in eigenvalue accuracy when the scaling factor is included. However, due to the relatively small size of the problem, the improvement is less significant. We also note that the SP_2 scaling factor yields a less accurate eigenvalue than the diffusion scaling factor. In each case, the total absorption was calculated with minimal error. However, the scaling factor clearly helps the two-group solution more accurately capture the leakage from the core.

6.3 Summary

In this chapter, the scaling factor formulations derived in Chapter 5 were numerically tested using two multigroup cross section libraries. When the "continuous energy" library was coarse, the SP_2-based scaling factor, defined in Eq. (5.60), wass *less* accurate than the diffusion-based scaling factor, defined in Eq. (5.55). This was generally not the case for the fine-group cross section library. However, even with 56 energy groups, the SP_2-based scaling factor yielded inconsistent results.

The diffusion-based scaling factor emerges as a clear favorite when one considers the additional computational burden in calculating the SP_2-based ρ_G, which in practice leads to longer run times per iteration and slower convergence.

CHAPTER 7

Asymptotic Analysis of the Hypothesized 1-D Homogenized, Multigroup SP_2 Equation

In this chapter, an asymptotic analysis is applied to a hypothesized system of 1-D, multigroup, homogenized SP_2 equations. We again define the dimensionless ratio $\epsilon = 1/N \ll 1$, where N is the number of *homogenized* pins or assemblies in the system. The solution to the hypothesized equation is expanded in powers of ϵ^2. As in Chapter 3, these equations are solved sequentially, from ϵ^0 to ϵ^4. The solvability conditions for ϵ^2 and ϵ^4 are used to generate a 1-D, monoenergetic SP_2 equation. We define the multigroup diffusion coefficients in our hypothesized SP_2 equation by equating this monoenergetic SP_2 equation with the one derived from the continuous energy lattice-transport equation in Chapter 3. There are an infinite number of ways to define the multigroup diffusion coefficients, and we choose a few logical definitions to test in Chapter 8. Each definition is chosen such that the hypothesized multigroup SP_2 equation has the same asymptotic limit as the continuous energy transport equation.

7.1 The Hypothesized Multigroup SP_2 Equation

We begin by hypothesizing the 1-D, homogenized, multigroup simplified P_2 eigenvalue equation:

$$-\frac{d^2}{dx^2}\left[\overline{D}_{0,g}\phi_g(x)+\overline{D}_{2,g}\left(\overline{\Sigma}_{t,g}\phi_g(x)-\sum_{g'=1}^{G}\overline{\Sigma}_{s,g'\to g}\phi_{g'}(x)-\lambda\overline{\chi}_g\sum_{g'=1}^{G}\overline{\nu\Sigma}_{f,g'}\phi_{g'}(x)\right)\right]$$
$$+\overline{\Sigma}_{t,g}\phi_g(x)=\sum_{g'=1}^{G}\overline{\Sigma}_{s,g'\to g}\phi_{g'}(x)+\lambda\overline{\chi}_g\sum_{g'=1}^{G}\overline{\nu\Sigma}_{f,g'}\phi_{g'}(x)\,, \tag{7.1}$$

where

$$\lambda=\frac{1}{\mathrm{k}}=1-\rho=\text{eigenvalue}\,,$$

and

$$\phi_g(x)=\text{multigroup eigenfunction, for } E=[E_g,E_{g-1}]\,.$$

The multigroup cross sections, as in Eqs. (5.9), are homogenized with the scalar flux of the lattice solution, $F_0(x,E)$:

$$\overline{\Sigma}_{t,g}=\frac{\displaystyle\int_0^h\int_{E_g}^{E_{g-1}}\Sigma_t(x,E)\,F_0(x,E)\,dEdx}{\displaystyle\int_0^h\int_{E_g}^{E_{g-1}}F_0(x,E)\,dEdx}\,, \tag{7.2a}$$

$$\overline{\Sigma}_{s,g'\to g}=\frac{\displaystyle\int_0^h\int_{E_g}^{E_{g-1}}\int_{E_{g'}}^{E_{g'-1}}\Sigma_{s,0}(x,E'\to E)\,F_0(x,E')\,dE'dEdx}{\displaystyle\int_0^h\int_{E_{g'}}^{E_{g'-1}}F_0(x,E')\,dE'dx}\,, \tag{7.2b}$$

$$\overline{\nu\Sigma}_{f,g} = \frac{\int_0^h \int_{E_g}^{E_{g-1}} \nu\Sigma_f(x,E) F_0(x,E) dE dx}{\int_0^h \int_{E_g}^{E_{g-1}} F_0(x,E) dE dx}, \tag{7.2c}$$

and

$$\overline{\chi}_g = \frac{\int_0^h \left(\int_{E_g}^{E_{g-1}} \chi(x,E) dE \right) \left(\int_0^\infty \nu\Sigma_f(x,E') F_0(x,E') dE' \right) dx}{\int_0^h \int_0^\infty \nu\Sigma_f(x,E') F_0(x,E') dE' dx}. \tag{7.2d}$$

Here h is the width of a single cell in the lattice, and $[E_g, E_{g-1}]$ are the energy bounds of group g. $\overline{D}_{0,g}$ and $\overline{D}_{2,g}$ are unknown group constants, to-be-determined.

While Eqs. (7.1) are hypothesized, if we set $\overline{D}_{0,g} = \overline{D}_{2,g} = 0$ and use the homogenized cross sections defined in Eqs. (7.2), then Eqs. (7.1) are satisfied by the exact infinite-medium eigenfunction and eigenvalue. Furthermore, if we set $\overline{D}_{2,g} = 0$ in Eqs. (7.1), we arrive at the result previously obtained by Trahan [15], with

$$\begin{aligned} \overline{D}_{0,g} = & \frac{\sum_{g''=1}^G \overline{F}^*_{0,g''} \overline{\chi}_{g''} \sum_{g'=1}^G \overline{\nu\Sigma}_{f,g'} \overline{F}_{0,g'}}{\int_0^h \left(\int_0^\infty F_0^*(x,E) \chi(x,E) dE \right) \left(\int_0^\infty \nu\Sigma_f(x,E) F_0(x,E) \right) dx} \\ & \times \frac{2 \int_0^h \int_{E_g}^{E_{g-1}} \int_{-1}^1 \mu f_0^*(x,\mu,E) f_1(x,\mu,E) d\mu dE dx}{\overline{F}^*_{0,g} \overline{F}_{0,g}}. \end{aligned} \tag{7.3}$$

This definition of $\overline{D}_{0,g}$ is not unique; other definitions exist that satisfy the asymptotic condition derived by Trahan. Nonetheless, Eq. (7.3) is more intuitive than other asymptotically-consistent definitions, and consistently yields more accurate numerical results than conventional homogenized diffusion coefficients [15].

In this thesis we use the same definition for $\overline{D}_{0,g}$ [Eq. (7.3)] as Trahan. In doing so, the only undetermined constants remaining in Eq. (7.1) are $\overline{D}_{2,g}$. In order to determine a condition that $\overline{D}_{2,g}$ should satisfy, we employ an asymptotic analysis. We then propose several definitions of $\overline{D}_{2,g}$ that satisfy this condition. These definitions are numerically

tested and compared in Chapter 8.

7.2 Asymptotic Analysis

We perform the same asymptotic scaling of the spatial variable as in Chapters 3 and 5:

$$\phi_g(x) = \Phi_g(z)\,, \tag{7.4a}$$

where

$$z = \epsilon x\,, \tag{7.4b}$$

and

$$\frac{\partial}{\partial x}\phi_g(x) = \epsilon \frac{\partial}{\partial z}\Phi_g(z)\,. \tag{7.4c}$$

Because Eq. (7.1) is homogenized, the fast variable y does not appear.

With this scaling, we expand Φ_g and λ in ϵ:

$$\Phi_g(z) = \Phi_{0,g}(z) + \epsilon^2 \Phi_{2,g}(z) + \epsilon^4 \Phi_{4,g}(z) + \cdots\,, \tag{7.5a}$$

$$\lambda = \lambda_0 + \epsilon^2 \lambda_2\,. \tag{7.5b}$$

Introducing Eqs. (7.4) and (7.5)) into Eq. (7.1), we obtain:

$$
\begin{aligned}
-\epsilon^2 \frac{d^2}{dz^2}\Bigg[& \overline{D}_{0,g}\Big[\Phi_{0,g}(z)+\epsilon^2\Phi_{2,g}(z)+\epsilon^4\Phi_{4,g}(z)+\cdots\Big] \\
& +\overline{D}_{2,g}\Bigg(\overline{\Sigma}_{t,g}\Big[\Phi_{0,g}(z)+\epsilon^2\Phi_{2,g}(z)+\epsilon^4\Phi_{4,g}(z)+\cdots\Big] \\
& \quad -\sum_{g'=1}^{G}\overline{\Sigma}_{s,g'\to g}\Big[\Phi_{0,g'}(z)+\epsilon^2\Phi_{2,g'}(z)+\epsilon^4\Phi_{4,g'}(z)+\cdots\Big] \\
& \quad -\Big(\lambda_0+\epsilon^2\lambda_2\Big)\overline{\chi}_g\sum_{g'=1}^{G}\overline{\nu\Sigma}_{f,g'}\Big[\Phi_{0,g'}(z)+\epsilon^2\Phi_{2,g'}(z)+\epsilon^4\Phi_{4,g'}(z)+\cdots\Big]\Bigg)\Bigg] \\
& +\overline{\Sigma}_{t,g}\Big[\Phi_{0,g}(z)+\epsilon^2\Phi_{2,g}(z)+\epsilon^4\Phi_{4,g}(z)+\cdots\Big] \\
& \quad -\sum_{g'=1}^{G}\overline{\Sigma}_{s,g'\to g}\Big[\Phi_{0,g'}(z)+\epsilon^2\Phi_{2,g'}(z)+\epsilon^4\Phi_{4,g'}(z)+\cdots\Big] \\
& \quad -\Big(\lambda_0+\epsilon^2\lambda_2\Big)\overline{\chi}_g\sum_{g'=1}^{G}\overline{\nu\Sigma}_{f,g'}\Big[\Phi_{0,g'}(z)+\epsilon^2\Phi_{2,g'}(z)+\epsilon^4\Phi_{4,g'}(z)+\cdots\Big].
\end{aligned}
\tag{7.6}
$$

We now equate the coefficients of the powers of ϵ:

ϵ^0:

$$
L_g\Phi_{0,g}(z)=0\,; \tag{7.7a}
$$

ϵ^2:

$$
\begin{aligned}
L_g\Phi_{2,g}(z) = {} & \lambda_2\overline{\chi}_g\sum_{g'=1}^{G}\overline{\nu\Sigma}_{f,g'}\Phi_{0,g'}(z)+\overline{D}_{0,g}\frac{d^2}{dz^2}\Phi_{0,g}(z) \\
& +\frac{d^2}{dz^2}\Bigg[\overline{D}_{2,g}\Bigg(\overline{\Sigma}_{t,g}\Phi_{0,g}(z)-\sum_{g'=1}^{G}\overline{\Sigma}_{s,g'\to g}\Phi_{0,g'}(z) \\
& \qquad -\lambda_0\overline{\chi}_g\sum_{g'=1}^{G}\overline{\nu\Sigma}_{f,g'}\Phi_{0,g'}(z)\Bigg)\Bigg];
\end{aligned}
\tag{7.7b}
$$

ϵ^n for $n \geq 4$:

$$
\begin{aligned}
L_g \Phi_{n,g}(z) = \lambda_2 \overline{\chi}_g \sum_{g'=1}^{G} \overline{\nu\Sigma}_{f,g'} \Phi_{n-2,g'}(z) + \overline{D}_{0,g} \frac{d^2}{dz^2} \Phi_{n-2,g}(z) \\
+ \frac{d^2}{dz^2} \Bigg[\overline{D}_{2,g} \Bigg(\overline{\Sigma}_{t,g} \Phi_{n-2,g}(z) - \sum_{g'=1}^{G} \overline{\Sigma}_{s,g'\to g} \Phi_{n-2,g'}(z) \\
- \lambda_0 \overline{\chi}_g \sum_{g'=1}^{G} \overline{\nu\Sigma}_{f,g'} \Phi_{n-2,g'}(z) \Bigg) \Bigg] \qquad (7.7c) \\
- \lambda_2 \frac{d^2}{dz^2} \Bigg[\overline{D}_{2,g} \overline{\chi}_g \sum_{g'=1}^{G} \overline{\nu\Sigma}_{f,g'} \Phi_{n-4,g'}(z) \Bigg] .
\end{aligned}
$$

Here L_g is the homogenized, infinite-lattice SP_2 operator (which, coincidentally, is identical to the homogenized, infinite-lattice diffusion operator):

$$
L_g \Phi_g(z) \equiv \overline{\Sigma}_{t,g} \Phi_g(z) - \sum_{g'=1}^{G} \overline{\Sigma}_{s,g'\to g} \Phi_{g'}(z) - \lambda_0 \overline{\chi}_g \sum_{g'=1}^{G} \overline{\nu\Sigma}_{f,g'} \Phi_{g'}(z) . \qquad (7.8)
$$

We now solve Eqs. (7.7) sequentially, beginning with Eq. (7.7a). Noting that Eq. (7.7a) is simply the neutron balance equation for an infinite homogenized lattice, it is clear that the solution to this equation will be the cell-integrated multigroup lattice function multiplied by an arbitrary function of z:

$$
\Phi_{0,g}(z) = \overline{F}_{0,g} A_0(z) , \qquad (7.9)
$$

where

$$
\overline{F}_{0,g} = \int_0^h \int_{E_g}^{E_{g-1}} F_0(y,E)\, dE dy , \qquad (7.10)
$$

and

$$
L_g \overline{F}_{0,g} = 0 . \qquad (7.11)
$$

We now define the adjoint of Eq. (7.8):

$$L_g^*\Phi_g^*(z) \equiv \overline{\Sigma}_{t,g}\Phi_g^*(z) - \sum_{g'=1}^{G}\overline{\Sigma}_{s,g\to g'}\Phi_{g'}^*(z) - \lambda_0\overline{\nu\Sigma}_g\sum_{g'=1}^{G}\overline{\chi}_{g'}\Phi_{g'}^*(z)\,, \tag{7.12}$$

and its eigenfunction $\overline{F}_{0,g}^*$:

$$L_g^*\overline{F}_{0,g}^* = 0\,. \tag{7.13}$$

Unlike $\overline{F}_{0,g}$, $\overline{F}_{0,g}^*$ has no direct relation to $F_0^*(y,E)$, i.e.:

$$\overline{F}_{0,g}^* \neq \int_0^h \int_{E_g}^{E_{g-1}} F_0^*(y,E)\,dEdy\,. \tag{7.14}$$

For Eq. (7.7b) to have a solution, its solvability condition must be met. The solvability condition for the multigroup SP_2 equation is obtained by multiplying both sides of Eq. (7.7b) by $\overline{F}_{0,g}^*$ and summing over all energy groups:

$$\begin{aligned}\sum_{g=1}^{G}\overline{F}_{0,g}^* L_g\Phi_{2,g}(z) = \sum_{g=1}^{G}\overline{F}_{0,g}^*\Bigg\{&\lambda_2\overline{\chi}_g\sum_{g'=1}^{G}\overline{\nu\Sigma}_{f,g'}\Phi_{0,g'}(z) + \overline{D}_{0,g}\frac{d^2}{dz^2}\Phi_{0,g}(z) \\ &+ \frac{d^2}{dz^2}\Bigg[\overline{D}_{2,g}\Bigg(\overline{\Sigma}_{t,g}\Phi_{0,g}(z) - \sum_{g'=1}^{G}\overline{\Sigma}_{s,g'\to g}\Phi_{0,g'}(z) - \lambda_0\overline{\chi}_g\sum_{g'=1}^{G}\overline{\nu\Sigma}_{f,g'}\Phi_{0,g'}(z)\Bigg)\Bigg]\Bigg\},\end{aligned} \tag{7.15}$$

By the definition of L_g, L_g^*, and $\overline{F}_{0,g}^*$, the left side of Eq. (7.15) is zero, implying the right side must also be zero:

$$0 = \sum_{g=1}^{G}\overline{F}_{0,g}^*\Bigg(\lambda_2\overline{\chi}_g\sum_{g'=1}^{G}\overline{\nu\Sigma}_{f,g'}\Phi_{0,g'}(z)\Bigg) + \sum_{g=1}^{G}\overline{F}_{0,g}^*\Bigg(\overline{D}_{0,g}\frac{d^2}{dz^2}\Phi_{0,g}(z)\Bigg) \tag{7.16}$$

$$\begin{aligned}+\sum_{g=1}^{G}\overline{F}_{0,g}^*\Bigg(\frac{d^2}{dz^2}\Bigg[\overline{D}_{2,g}\Bigg(\overline{\Sigma}_{t,g}\Phi_{0,g}(z) - \sum_{g'=1}^{G}\overline{\Sigma}_{s,g'\to g}\Phi_{0,g'}(z) \\ - \lambda_0\overline{\chi}_g\sum_{g'=1}^{G}\overline{\nu\Sigma}_{f,g'}\Phi_{0,g'}(z)\Bigg)\Bigg]\Bigg).\end{aligned} \tag{7.17}$$

Eq. (7.16) is the solvability condition for $\Phi_{2,g}$. Substituting into this Eq. (7.9), we obtain:

$$
\begin{aligned}
0 = \lambda_2 &\left(\sum_{g=1}^{G} \overline{F}^{*}_{0,g}\overline{\chi}_g\right)\left(\sum_{g'=1}^{G} \overline{\nu\Sigma}_{f,g'}\overline{F}_{0,g}\right)A_0(z) + \left(\sum_{g=1}^{G} \overline{F}^{*}_{0,g}\overline{D}_{0,g}\overline{F}_{0,g}\right)\frac{d^2}{dz^2}A_0(z) \\
&+ \sum_{g=1}^{G} \overline{F}^{*}_{0,g}\left(\overline{D}_{2,g}\left(\overline{\Sigma}_{t,g}\overline{F}_{0,g} - \sum_{g'=1}^{G}\overline{\Sigma}_{s,g'\to g}\overline{F}_{0,g'}\right.\right. \\
&\qquad \left.\left. - \lambda_0\overline{\chi}_g\sum_{g'=1}^{G}\overline{\nu\Sigma}_{f,g'}\overline{F}_{0,g'}\right)\right)\left(\frac{d^2}{dz^2}A_0(z)\right) \\
= \lambda_2 &\left(\sum_{g=1}^{G} \overline{F}^{*}_{0,g}\overline{\chi}_g\right)\left(\sum_{g'=1}^{G} \overline{\nu\Sigma}_{f,g'}\overline{F}_{0,g}\right)A_0(z) + \left(\sum_{g=1}^{G} \overline{F}^{*}_{0,g}\overline{D}_{0,g}\overline{F}_{0,g}\right)\frac{d^2}{dz^2}A_0(z) \\
&+ \sum_{g=1}^{G} \overline{F}^{*}_{0,g}\left(\overline{D}_{2,g}L_g\overline{F}_{0,g}\right)\left(\frac{d^2}{dz^2}A_0(z)\right) \\
= \lambda_2 &\left(\sum_{g=1}^{G} \overline{F}^{*}_{0,g}\overline{\chi}_g\right)\left(\sum_{g'=1}^{G} \overline{\nu\Sigma}_{f,g'}\overline{F}_{0,g}\right)A_0(z) + \left(\sum_{g=1}^{G} \overline{F}^{*}_{0,g}\overline{D}_{0,g}\overline{F}_{0,g}\right)\frac{d^2}{dz^2}A_0(z) \\
&+ \sum_{g=1}^{G} \overline{F}^{*}_{0,g}\left(\overline{D}_{2,g}(0)\right)\left(\frac{d^2}{dz^2}A_0(z)\right) \\
= \lambda_2 &\left(\sum_{g=1}^{G} \overline{F}^{*}_{0,g}\overline{\chi}_g\right)\left(\sum_{g'=1}^{G} \overline{\nu\Sigma}_{f,g'}\overline{F}_{0,g}\right)A_0(z) + \left(\sum_{g=1}^{G} \overline{F}^{*}_{0,g}\overline{D}_{0,g}\overline{F}_{0,g}\right)\frac{d^2}{dz^2}A_0(z)\,.
\end{aligned}
\tag{7.18}
$$

Once rearranged, (Eq. (7.18) is similar to the 1-D diffusion equation obtained from the continuous energy analysis, and identical to the result obtained in [25].

If we define the operator P:

$$
Ph_g = \overline{F}_{0,g}\sum_{g=1}^{G}\overline{F}^{*}_{0,g}h_g\,, \tag{7.19}
$$

and require:

$$
\sum_{g=1}^{G}\overline{F}_{0,g}\overline{F}^{*}_{0,g} = 1\,, \tag{7.20}
$$

then P is a projection operator, and we can subtract the product of $\overline{F}_{0,g}$ and Eq. (7.18) from Eq. (7.7b). The resulting expression automatically satisfies the solvability condition, and

can be inverted to obtain a solution for $\Phi_{2,g}$:

$$\begin{aligned}\Phi_{2,g}(z) &= \overline{F}_{0,g}A_2(z) + \lambda_2 L_g^{-1}\left[\left((I-P)\overline{\chi}_g\right)\left(\sum_{g'=1}^{G}\overline{\nu\Sigma}_{f,g'}\overline{F}_{0,g'}\right)\right]A_0(z) \\ &\quad + L_g^{-1}\left[(I-P)\overline{D}_{0,g}\overline{F}_{0,g}\right]\frac{d^2A_0}{dz^2} \\ &= \overline{F}_{0,g}A_2(z) + \lambda_2\overline{F}_{1,g}A_0(z) + \overline{F}_{2,g}\frac{d^2A_0}{dz^2}.\end{aligned} \tag{7.21}$$

Here,

$$\overline{F}_{1,g} = L_g^{-1}\left[\left((I-P)\overline{\chi}_g\right)\left(\sum_{g'=1}^{G}\overline{\nu\Sigma}_{f,g'}\overline{F}_{0,g'}\right)\right], \tag{7.22a}$$

and

$$\overline{F}_{2,g} = L_g^{-1}\left[(I-P)\overline{D}_{0,g}\overline{F}_{0,g}\right]. \tag{7.22b}$$

The solvability condition for Eq. (7.7c) ($n = 4$) is:

$$\begin{aligned}0 &= \lambda_2\left(\sum_{g=1}^{G}\overline{F}^*_{0,g}\overline{\chi}_g\right)\left(\sum_{g'=1}^{G}\overline{\nu\Sigma}_{f,g'}\Phi_{2,g'}(z)\right) + \left(\sum_{g=1}^{G}\overline{F}^*_{0,g}\overline{D}_{0,g}\frac{d^2\Phi_{2,g}}{dz^2}\right) \\ &\quad + \frac{d^2}{dz^2}\left(\sum_{g=1}^{G}\overline{F}^*_{0,g}\overline{D}_{2,g}\left[L_g\Phi_{2,g}(z)\right]\right) \\ &\quad - \lambda_2\frac{d^2}{dz^2}\left(\sum_{g=1}^{G}\overline{F}^*_{0,g}\overline{D}_{2,g}\overline{\chi}_g\right)\left(\sum_{g'=1}^{G}\overline{\nu\Sigma}_{f,g'}\Phi_{0,g'}(z)\right) \\ &= \lambda_2\left(\sum_{g=1}^{G}\overline{F}^*_{0,g}\overline{\chi}_g\right)\left(\sum_{g'=1}^{G}\overline{\nu\Sigma}_{f,g'}\Phi_{2,g'}(z)\right) + \left(\sum_{g=1}^{G}\overline{F}^*_{0,g}\overline{D}_{0,g}\frac{d^2\Phi_{2,g}}{dz^2}\right) \\ &\quad + \frac{d^2}{dz^2}\left(\sum_{g=1}^{G}\overline{F}^*_{0,g}\overline{D}_{2,g}\left[\lambda_2\overline{\chi}_g\sum_{g'=1}^{G}\overline{\nu\Sigma}_{f,g'}\Phi_{0,g'}(z) + \overline{D}_{0,g}\frac{d^2}{dz^2}\Phi_{0,g}(z)\right]\right) \\ &\quad - \lambda_2\frac{d^2}{dz^2}\left(\sum_{g=1}^{G}\overline{F}^*_{0,g}\overline{D}_{2,g}\overline{\chi}_g\right)\left(\sum_{g'=1}^{G}\overline{\nu\Sigma}_{f,g'}\Phi_{0,g'}(z)\right),\end{aligned} \tag{7.23}$$

or, after rearranging,

$$
\begin{aligned}
0 = {} & \lambda_2 \Bigg(\sum_{g=1}^{G} \overline{F}^{*}_{0,g} \overline{\chi}_g \Bigg) \Bigg(\sum_{g'=1}^{G} \overline{\nu\Sigma}_{f,g'} \overline{F}_{0,g} \Bigg) A_2(z) \\
& + \lambda_2^2 \Bigg(\sum_{g=1}^{G} \overline{F}^{*}_{0,g} \overline{\chi}_g \Bigg) \Bigg(\sum_{g'=1}^{G} \overline{\nu\Sigma}_{f,g'} \overline{F}_{1,g} \Bigg) A_0(z) \\
& + \lambda_2 \Bigg(\sum_{g=1}^{G} \overline{F}^{*}_{0,g} \overline{\chi}_g \Bigg) \Bigg(\sum_{g'=1}^{G} \overline{\nu\Sigma}_{f,g'} \overline{F}_{2,g} \Bigg) \frac{d^2 A_0}{dz^2} \\
& + \Bigg(\sum_{g=1}^{G} \overline{F}^{*}_{0,g} \overline{D}_{0,g} \overline{F}_{0,g} \Bigg) \frac{d^2 A_2}{dz^2} + \lambda_2 \Bigg(\sum_{g=1}^{G} \overline{F}^{*}_{0,g} \overline{D}_{0,g} \overline{F}_{1,g} \Bigg) \frac{d^2 A_0}{dz^2} \\
& + \Bigg(\sum_{g=1}^{G} \overline{F}^{*}_{0,g} \overline{D}_{0,g} \overline{F}_{2,g} \Bigg) \frac{d^4 A_0}{dz^4} + \Bigg(\sum_{g=1}^{G} \overline{F}^{*}_{0,g} \overline{D}_{2,g} \Big[\overline{D}_{0,g} \overline{F}_{0,g} \Big] \Bigg) \frac{d^4 A_0}{dz^4} \\
& + \lambda_2 \Bigg(\sum_{g=1}^{G} \overline{F}^{*}_{0,g} \overline{D}_{2,g} \Big[\overline{\chi}_g \sum_{g'=1}^{G} \overline{\nu\Sigma}_{f,g'} \overline{F}_{0,g} \Big] \Bigg) \frac{d^2 A_0}{dz^2} \\
& - \lambda_2 \Bigg(\sum_{g=1}^{G} \overline{F}^{*}_{0,g} \overline{D}_{2,g} \overline{\chi}_g \Bigg) \Bigg(\sum_{g'=1}^{G} \overline{\nu\Sigma}_{f,g'} \overline{F}_{0,g'}(z) \Bigg) \frac{d^2 A_0}{dz^2} .
\end{aligned}
\tag{7.24}
$$

We then use Eq. (7.18) to eliminate $\frac{d^4A_0}{dz^4}$ and λ_2^2 from Eq. (7.24), which yields:

$$
\begin{aligned}
0 = {} & \lambda_2\Bigg(\sum_{g=1}^{G}\overline{F}^{*}_{0,g}\overline{\chi}_g\Bigg)\Bigg(\sum_{g'=1}^{G}\overline{\nu\Sigma}_{f,g'}\overline{F}_{0,g'}\Bigg)A_2(z) \\
& - \lambda_2\Bigg(\sum_{g=1}^{G}\overline{F}^{*}_{0,g}\overline{D}_{0,g}\overline{F}_{0,g}\Bigg)\frac{\Bigg(\sum_{g'=1}^{G}\overline{\nu\Sigma}_{f,g'}\overline{F}_{1,g'}\Bigg)}{\Bigg(\sum_{g''=1}^{G}\overline{\nu\Sigma}_{f,g''}\overline{F}_{0,g''}\Bigg)}\frac{d^2A_0}{dz^2} \\
& + \lambda_2\Bigg(\sum_{g=1}^{G}\overline{F}^{*}_{0,g}\overline{\chi}_g\Bigg)\Bigg(\sum_{g'=1}^{G}\overline{\nu\Sigma}_{f,g'}\overline{F}_{2,g'}\Bigg)\frac{d^2A_0}{dz^2} \\
& + \Bigg(\sum_{g=1}^{G}\overline{F}^{*}_{0,g}\overline{D}_{0,g}\overline{F}_{0,g}\Bigg)\frac{d^2A_2}{dz^2} + \lambda_2\Bigg(\sum_{g=1}^{G}\overline{F}^{*}_{0,g}\overline{D}_{0,g}\overline{F}_{1,g}\Bigg)\frac{d^2A_0}{dz^2} \\
& - \lambda_2\Bigg(\sum_{g=1}^{G}\overline{F}^{*}_{0,g}\overline{\chi}_g\Bigg)\Bigg(\sum_{g'=1}^{G}\overline{\nu\Sigma}_{f,g'}\overline{F}_{0,g'}\Bigg)\frac{\Bigg(\sum_{g''=1}^{G}\overline{F}^{*}_{0,g''}\overline{D}_{0,g''}\overline{F}_{2,g''}\Bigg)}{\Bigg(\sum_{g'''=1}^{G}\overline{F}^{*}_{0,g'''}\overline{D}_{0,g'''}\overline{F}_{0,g'''}\Bigg)}\frac{d^2A_0}{dz^2} \\
& - \lambda_2\Bigg(\sum_{g=1}^{G}\overline{F}^{*}_{0,g}\overline{\chi}_g\Bigg)\Bigg(\sum_{g'=1}^{G}\overline{\nu\Sigma}_{f,g'}\overline{F}_{0,g'}\Bigg)\frac{\Bigg(\sum_{g''=1}^{G}\overline{F}^{*}_{0,g''}\overline{D}_{2,g''}\Big[\overline{D}_{0,g''}\overline{F}_{0,g''}\Big]\Bigg)}{\Bigg(\sum_{g'''=1}^{G}\overline{F}^{*}_{0,g'''}\overline{D}_{0,g'''}\overline{F}_{0,g'''}\Bigg)}\frac{d^2A_0}{dz^2} \\
& + \lambda_2\Bigg(\sum_{g=1}^{G}\overline{F}^{*}_{0,g}\overline{D}_{2,g}\Big[\overline{\chi}_g\sum_{g'=1}^{G}\overline{\nu\Sigma}_{f,g'}\overline{F}_{0,g'}\Big]\Bigg)\frac{d^2A_0}{dz^2} \\
& - \lambda_2\Bigg(\sum_{g=1}^{G}\overline{F}^{*}_{0,g}\overline{D}_{2,g}\overline{\chi}_g\Bigg)\Bigg(\sum_{g'=1}^{G}\overline{\nu\Sigma}_{f,g'}\overline{F}_{0,g'}\Bigg)\frac{d^2A_0}{dz^2},
\end{aligned}
\tag{7.25}
$$

or

$$
\begin{aligned}
0 = \lambda_2 &\left(\sum_{g=1}^{G} \overline{F}^*_{0,g} \overline{\chi}_g \right) \left(\sum_{g'=1}^{G} \overline{\nu\Sigma}_{f,g'} \overline{F}_{0,g'} \right) A_2(z) \\
&+ \frac{d^2}{dz^2} \left\{ \left(\sum_{g=1}^{G} \overline{F}^*_{0,g} \overline{D}_{0,g} \overline{F}_{0,g} \right) A_2 \right. \\
&+ \lambda_2 \left[- \left(\sum_{g=1}^{G} \overline{F}^*_{0,g} \overline{D}_{0,g} \overline{F}_{0,g} \right) \frac{\left(\sum_{g'=1}^{G} \overline{\nu\Sigma}_{f,g'} \overline{F}_{1,g'} \right)}{\left(\sum_{g''=1}^{G} \overline{\nu\Sigma}_{f,g''} \overline{F}_{0,g''} \right)} \right. \\
&+ \left(\sum_{g=1}^{G} \overline{F}^*_{0,g} \overline{\chi}_g \right) \left(\sum_{g'=1}^{G} \overline{\nu\Sigma}_{f,g'} \overline{F}_{2,g'} \right) \\
&+ \left(\sum_{g=1}^{G} \overline{F}^*_{0,g} \overline{D}_{0,g} \overline{F}_{1,g} \right) \\
&- \left(\sum_{g=1}^{G} \overline{F}^*_{0,g} \overline{\chi}_g \right) \left(\sum_{g'=1}^{G} \overline{\nu\Sigma}_{f,g'} \overline{F}_{0,g'} \right) \frac{\left(\sum_{g''=1}^{G} \overline{F}^*_{0,g''} \overline{D}_{0,g''} \overline{F}_{2,g''} \right)}{\left(\sum_{g'''=1}^{G} \overline{F}^*_{0,g'''} \overline{D}_{0,g'''} \overline{F}_{0,g'''} \right)} \\
&- \left(\sum_{g=1}^{G} \overline{F}^*_{0,g} \overline{\chi}_g \right) \left(\sum_{g'=1}^{G} \overline{\nu\Sigma}_{f,g'} \overline{F}_{0,g'} \right) \frac{\left(\sum_{g''=1}^{G} \overline{F}^*_{0,g''} \overline{D}_{2,g''} \left[\overline{D}_{0,g''} \overline{F}_{0,g''} \right] \right)}{\left(\sum_{g'''=1}^{G} \overline{F}^*_{0,g'''} \overline{D}_{0,g'''} \overline{F}_{0,g'''} \right)} \\
&+ \left(\sum_{g=1}^{G} \overline{F}^*_{0,g} \overline{D}_{2,g} \left[\overline{\chi}_g \sum_{g'=1}^{G} \overline{\nu\Sigma}_{f,g'} \overline{F}_{0,g'} \right] \right) \\
&\left. \left. - \left(\sum_{g=1}^{G} \overline{F}^*_{0,g} \overline{D}_{2,g} \overline{\chi}_g \right) \left(\sum_{g'=1}^{G} \overline{\nu\Sigma}_{f,g'} \overline{F}_{0,g'} \right) \right] A_0(z) \right\}.
\end{aligned}
\tag{7.26}
$$

Rearranging, we have:

$$
\begin{aligned}
0 = \lambda_2 &\left(\sum_{g=1}^{G} \overline{F}^{*}_{0,g}\overline{\chi}_g\right)\left(\sum_{g'=1}^{G} \overline{\nu\Sigma}_{f,g'}\overline{F}_{0,g'}\right)A_2(z) \\
&+ \frac{d^2}{dz^2}\Bigg\{\left(\sum_{g=1}^{G} \overline{F}^{*}_{0,g}\overline{D}_{0,g}\overline{F}_{0,g}\right)A_2(z) + \lambda_2 \sum_{g=1}^{G} \overline{F}^{*}_{0,g}\Bigg[\overline{D}_{0,g}\overline{F}_{1,g} \\
&+ \overline{\chi}_g\left(\sum_{g'=1}^{G} \overline{\nu\Sigma}_{f,g'}\overline{F}_{2,g'}\right) \\
&- \overline{D}_{0,g}\overline{F}_{0,g}\frac{\left(\sum_{g'=1}^{G} \overline{\nu\Sigma}_{f,g'}\overline{F}_{1,g'}\right)}{\left(\sum_{g''=1}^{G} \overline{\nu\Sigma}_{f,g''}\overline{F}_{0,g''}\right)} \\
&- \overline{D}_{0,g}\overline{F}_{2,g}\frac{\left(\sum_{g'=1}^{G} \overline{F}^{*}_{0,g'}\overline{\chi}_{g'}\right)\left(\sum_{g''=1}^{G} \overline{\nu\Sigma}_{f,g''}\overline{F}_{0,g''}\right)}{\left(\sum_{g'''=1}^{G} \overline{F}^{*}_{0,g'''}\overline{D}_{0,g'''}\overline{F}_{0,g'''}\right)} \\
&+ \overline{D}_{2,g}\overline{\chi}_g\left(\sum_{g'=1}^{G} \overline{\nu\Sigma}_{f,g'}\overline{F}_{0,g'}\right) \\
&- \overline{D}_{2,g}\left[\overline{D}_{0,g}\overline{F}_{0,g}\right]\frac{\left(\sum_{g'=1}^{G} \overline{F}^{*}_{0,g'}\overline{\chi}_{g'}\right)\left(\sum_{g''=1}^{G} \overline{\nu\Sigma}_{f,g''}\overline{F}_{0,g''}\right)}{\left(\sum_{g'''=1}^{G} \overline{F}^{*}_{0,g'''}\overline{D}_{0,g'''}\overline{F}_{0,g'''}\right)} \\
&- \overline{D}_{2,g}\overline{\chi}_g\left(\sum_{g'=1}^{G} \overline{\nu\Sigma}_{f,g'}\overline{F}_{0,g'}\right)\Bigg]A_0(z)\Bigg\}.
\end{aligned}
\tag{7.27}
$$

We now multiply Eq. (7.27) by ϵ^2, add the result to Eq. (7.18) (introducing additional ϵ^4 terms as needed), and divide through by:

$$
\left(\sum_{g=1}^{G} \overline{F}^{*}_{0,g}\overline{\chi}_g\right)\left(\sum_{g'=1}^{G} \overline{\nu\Sigma}_{f,g'}\overline{F}_{0,g'}\right)
$$

we obtain:

$$
\begin{aligned}
0 = \lambda_2 \Phi(z) + \Bigg\{ & \frac{\left(\sum_{g=1}^{G} \overline{F}^{*}_{0,g} \overline{D}_{0,g} \overline{F}_{0,g}\right)}{\left(\sum_{g'=1}^{G} \overline{F}^{*}_{0,g'} \overline{\chi}_{g'}\right)\left(\sum_{g''=1}^{G} \overline{\nu\Sigma}_{f,g''} \overline{F}_{0,g''}\right)} \\
& + \lambda_2 \sum_{g=1}^{G} \overline{F}^{*}_{0,g} \Bigg[\frac{\overline{D}_{0,g} \overline{F}_{1,g}}{\left(\sum_{g'=1}^{G} \overline{F}^{*}_{0,g'} \overline{\chi}_{g'}\right)\left(\sum_{g''=1}^{G} \overline{\nu\Sigma}_{f,g''} \overline{F}_{0,g''}\right)} \\
& + \overline{\chi}_g \frac{\left(\sum_{g'=1}^{G} \overline{\nu\Sigma}_{f,g'} \overline{F}_{2,g'}\right)}{\left(\sum_{g''=1}^{G} \overline{F}^{*}_{0,g''} \overline{\chi}_{g''}\right)\left(\sum_{g'''=1}^{G} \overline{\nu\Sigma}_{f,g'''} \overline{F}_{0,g'''}\right)} \\
& - \overline{D}_{0,g} \overline{F}_{0,g} \frac{\left(\sum_{g'=1}^{G} \overline{\nu\Sigma}_{f,g'} \overline{F}_{1,g'}\right)}{\left(\sum_{g''=1}^{G} \overline{F}^{*}_{0,g''} \overline{\chi}_{g''}\right)\left(\sum_{g'''=1}^{G} \overline{\nu\Sigma}_{f,g'''} \overline{F}_{0,g'''}\right)^2} \\
& - \frac{\overline{D}_{0,g} \overline{F}_{2,g}}{\left(\sum_{g'=1}^{G} \overline{F}^{*}_{0,g'} \overline{D}_{0,g'} \overline{F}_{0,g'}\right)} + \frac{\overline{D}_{2,g} \overline{\chi}_g}{\left(\sum_{g'=1}^{G} \overline{F}^{*}_{0,g'} \overline{\chi}_{g'}\right)} \\
& - \frac{\overline{D}_{2,g}\left[\overline{D}_{0,g} \overline{F}_{0,g}\right]}{\left(\sum_{g'=1}^{G} \overline{F}^{*}_{0,g'} \overline{D}_{0,g'} \overline{F}_{0,g'}\right)} - \frac{\overline{D}_{2,g} \overline{\chi}_g}{\left(\sum_{g'=1}^{G} \overline{F}^{*}_{0,g'} \overline{\chi}_{g'}\right)} \Bigg] \Bigg\} \frac{d^2}{dz^2} \Phi(z) \,,
\end{aligned}
\tag{7.28}
$$

where

$$
\Phi(z) = A_0(z) + \epsilon^2 A_2(z) \,. \tag{7.29}
$$

The expression in Eq. (7.28) closely resembles the monoenergetic asymptotic SP_2 equa-

tion obtained from the continuous-energy analysis (shown again below):

$$
\begin{aligned}
0 = \Bigg\{ & \frac{\int_0^h \int_0^\infty \int_{-1}^1 \mu f_0^*(y,\mu,E)\, f_1(y,\mu,E)\, d\mu dE dy}{\int_0^h \int_0^\infty F_0^*(y,E)\, \frac{1}{2}\chi(y,E) \int_0^\infty \nu\Sigma_f(y,E')\, F_0(y,E')\, dE' dE dy} \\
& + \lambda_2 \Bigg[- \frac{\int_0^h \int_0^\infty \int_{-1}^1 \mu f_0^*(y,\mu,E)\, f_6(y,\mu,E)\, d\mu dE dy}{\int_0^h \int_0^\infty \int_{-1}^1 \mu f_0^*(y,\mu,E)\, f_1(y,\mu,E)\, d\mu dE dy} \\
& \quad + \frac{\int_0^h \int_0^\infty \int_{-1}^1 \mu f_0^*(y,\mu,E)\, f_5(y,\mu,E)\, d\mu dE dy}{\int_0^h \int_0^\infty F_0^*(y,E)\, \frac{1}{2}\chi(y,E) \int_0^\infty \nu\Sigma_f(y,E')\, F_0(y,E')\, dE' dE dy} \\
& \quad + \frac{\int_0^h \int_0^\infty F_0^*(y,\mu,E)\, \frac{1}{2}\chi(y,E) \int_0^\infty \nu\Sigma_f(y,E')\, F_3(y,E')\, dE' dE dy}{\int_0^h \int_0^\infty F_0^*(y,E)\, \frac{1}{2}\chi(y,E) \int_0^\infty \nu\Sigma_f(y,E')\, F_0(y,E')\, dE' dE dy} \\
& \quad - \frac{\int_0^h \int_0^\infty F_0^*(y,\mu,E)\, \frac{1}{2}\chi(y,E) \int_0^\infty \nu\Sigma_f(y,E')\, F_2(y,E')\, dE' dE dy}{\int_0^h \int_0^\infty F_0^*(y,E)\, \frac{1}{2}\chi(y,E) \int_0^\infty \nu\Sigma_f(y,E')\, F_0(y,E')\, dE' dE dy} \times \\
& \quad \frac{\int_0^h \int_0^\infty \int_{-1}^1 \mu f_0^*(y,\mu,E)\, f_1(y,\mu,E)\, d\mu dE dy}{\int_0^h \int_0^\infty F_0^*(y,E)\, \frac{1}{2}\chi(y,E) \int_0^\infty \nu\Sigma_f(y,E')\, F_0(y,E')\, dE' dE dy} \Bigg] \Bigg\} \frac{\partial^2}{\partial z^2}\Phi(z) \\
& + \lambda_2 \Phi(z) \, .
\end{aligned}
\tag{7.30}
$$

If we equate Eqs. (7.28) and (7.30), we obtain a condition for $\overline{D}_{2,g}$:

$$
\begin{aligned}
&\sum_{g=1}^{G} \overline{F}^{*}_{0,g} \Bigg[\frac{\overline{D}_{0,g}\overline{F}_{1,g}}{\left(\sum_{g'=1}^{G} \overline{F}^{*}_{0,g'}\overline{\chi}_{g'}\right)\left(\sum_{g''=1}^{G} \overline{\nu\Sigma}_{f,g''}\overline{F}_{0,g''}\right)} \\
&+ \overline{\chi}_{g} \frac{\left(\sum_{g'=1}^{G} \overline{\nu\Sigma}_{f,g'}\overline{F}_{2,g'}\right)}{\left(\sum_{g''=1}^{G} \overline{F}^{*}_{0,g''}\overline{\chi}_{g''}\right)\left(\sum_{g'''=1}^{G} \overline{\nu\Sigma}_{f,g'''}\overline{F}_{0,g'''}\right)} \\
&- \overline{D}_{0,g}\overline{F}_{0,g} \frac{\left(\sum_{g'=1}^{G} \overline{\nu\Sigma}_{f,g'}\overline{F}_{1,g'}\right)}{\left(\sum_{g''=1}^{G} \overline{F}^{*}_{0,g''}\overline{\chi}_{g''}\right)\left(\sum_{g'''=1}^{G} \overline{\nu\Sigma}_{f,g'''}\overline{F}_{0,g'''}\right)^{2}} \\
&- \frac{\overline{D}_{0,g}\overline{F}_{2,g}}{\left(\sum_{g'=1}^{G} \overline{F}^{*}_{0,g'}\overline{D}_{0,g'}\overline{F}_{0,g'}\right)} + \frac{\overline{D}_{2,g}\overline{\chi}_{g}}{\left(\sum_{g'=1}^{G} \overline{F}^{*}_{0,g'}\overline{\chi}_{g'}\right)} \\
&- \frac{\overline{D}_{2,g}\left[\overline{D}_{0,g}\overline{F}_{0,g}\right]}{\left(\sum_{g'=1}^{G} \overline{F}^{*}_{0,g'}\overline{D}_{0,g'}\overline{F}_{0,g'}\right)} - \frac{\overline{D}_{2,g}\overline{\chi}_{g}}{\left(\sum_{g'=1}^{G} \overline{F}^{*}_{0,g'}\overline{\chi}_{g'}\right)} \Bigg]
\end{aligned}
\tag{7.31}
$$

$$
\begin{aligned}
&= \int_0^h \int_0^\infty \int_{-1}^1 \Bigg[- \frac{\mu f_0^*(y,\mu,E)\, f_6(y,\mu,E)}{\int_0^h \int_0^\infty \int_{-1}^1 \mu' f_0^*(y',\mu',E')\, f_1(y',\mu',E')\, d\mu' dE' dy'} \\
&+ \frac{\mu f_0^*(y,\mu,E)\, f_5(y,\mu,E)}{\int_0^h \int_0^\infty F_0^*(y',E')\, \frac{1}{2}\chi(y',E') \int_0^\infty \nu\Sigma_f(y',E'')\, F_0(y',E'')\, dE'' dE' dy'} \\
&+ \frac{F_0^*(y,E)\, \frac{1}{2}\chi(y,E) \int_0^\infty \nu\Sigma_f(y,E')\, F_3(y,E')\, dE'}{\int_0^h \int_0^\infty F_0^*(y',E'')\, \frac{1}{2}\chi(y',E'') \int_0^\infty \nu\Sigma_f(y',E''')\, F_0(y',E''')\, dE''' dE'' dy'} \\
&- \frac{F_0^*(y,E)\, \frac{1}{2}\chi(y,E) \int_0^\infty \nu\Sigma_f(y,E')\, F_2(y,E')\, dE'}{\int_0^h \int_0^\infty F_0^*(y',E'')\, \frac{1}{2}\chi(y',E'') \int_0^\infty \nu\Sigma_f(y',E''')\, F_0(y',E''')\, dE''' dE'' dy'} \\
&\times \frac{\int_0^h \int_0^\infty \int_{-1}^1 \mu' f_0^*(y',\mu',E')\, f_1(y',\mu',E')\, d\mu' dE' dy'}{\int_0^h \int_0^\infty F_0^*(y'',E'')\, \frac{1}{2}\chi(y'',E'') \int_0^\infty \nu\Sigma_f(y'',E''')\, F_0(y'',E''')\, dE''' dE'' dy''} \Bigg] d\mu dE dy\,.
\end{aligned}
$$

Eq. (7.31) is the condition that we require $\overline{D}_{2,g}$ to satisfy.

To calculate $\overline{D}_{2,g}$, we rewrite Eq. (7.31):

$$\begin{aligned}\sum_{g=1}^{G}\left(A_g + B_g\overline{D}_{2,g}\right) &= \int_0^{\infty} C(E)\,dE \\ &= \sum_{g=1}^{G}\int_{E_g}^{E_{g-1}} C(E)\,dE\,,\end{aligned} \tag{7.32}$$

where A_g, B_g and $C(E)$ are chosen such that Eqs. (7.31) and (7.32) are equivalent. This can be done in a number of ways; however, we restrict our discussion to the most logical formulations.

7.3 Defining $\overline{D}_{2,g}$

If we require that Eq. (7.32) hold for each individual energy group g, we obtain a straightforward expression for $\overline{D}_{2,g}$:

$$\overline{D}_{2,g} = \frac{\left(\int_{E_g}^{E_{g-1}} C(E)\,dE\right) - A_g}{B_g}\,. \tag{7.33}$$

Although there are numerous ways to define $\overline{D}_{2,g}$, we consider only two in this work. Both expressions for $\overline{D}_{2,g}$ are based on Eq. (7.33), but differ in their definition of the function $C(E)$.

The first definition is the most logical:

$$\overline{D}^{(1)}_{2,g} = \frac{\left(\int_{E_g}^{E_{g-1}} C^{(1)}(E)\,dE\right) - A^{(1)}_g}{B^{(1)}_g}\,, \tag{7.34a}$$

where

$$A_g^{(1)} = \overline{F}_{0,g}^{*}\Bigg[\frac{\overline{D}_{0,g}\overline{F}_{1,g}}{\left(\sum_{g'=1}^{G}\overline{F}_{0,g'}^{*}\overline{\chi}_{g'}\right)\left(\sum_{g''=1}^{G}\overline{\nu\Sigma}_{f,g''}\overline{F}_{0,g''}\right)} + \overline{\chi}_g\frac{\left(\sum_{g'=1}^{G}\overline{\nu\Sigma}_{f,g'}\overline{F}_{2,g'}\right)}{\left(\sum_{g''=1}^{G}\overline{F}_{0,g''}^{*}\overline{\chi}_{g''}\right)\left(\sum_{g'''=1}^{G}\overline{\nu\Sigma}_{f,g'''}\overline{F}_{0,g'''}\right)} - \overline{D}_{0,g}\overline{F}_{0,g}\frac{\left(\sum_{g'=1}^{G}\overline{\nu\Sigma}_{f,g'}\overline{F}_{1,g'}\right)}{\left(\sum_{g''=1}^{G}\overline{F}_{0,g''}^{*}\overline{\chi}_{g''}\right)\left(\sum_{g'''=1}^{G}\overline{\nu\Sigma}_{f,g'''}\overline{F}_{0,g'''}\right)^2} - \frac{\overline{D}_{0,g}\overline{F}_{2,g}}{\left(\sum_{g'=1}^{G}\overline{F}_{0,g'}^{*}\overline{D}_{0,g'}\overline{F}_{0,g'}\right)}\Bigg], \tag{7.34b}$$

$$B_g^{(1)} = \overline{F}_{0,g}^{*}\left[\frac{\overline{\chi}_g}{\left(\sum_{g'=1}^{G}\overline{F}_{0,g'}^{*}\overline{\chi}_{g'}\right)} - \frac{\left[\overline{D}_{0,g}\overline{F}_{0,g}\right]}{\left(\sum_{g'=1}^{G}\overline{F}_{0,g'}^{*}\overline{D}_{0,g'}\overline{F}_{0,g'}\right)} - \frac{\overline{\chi}_g}{\left(\sum_{g'=1}^{G}\overline{F}_{0,g'}^{*}\overline{\chi}_{g'}\right)}\right], \tag{7.34c}$$

and

$$C^{(1)}(E) = \int_0^h \int_{-1}^1 \Bigg[- \frac{\mu f_0^*(y,\mu,E) f_6(y,\mu,E)}{\int_0^h \int_0^\infty \int_{-1}^1 \mu' f_0^*(y',\mu',E') f_1(y',\mu',E') d\mu' dE' dy'} \tag{7.34d}$$
$$+ \frac{\mu f_0^*(y,\mu,E) f_5(y,\mu,E)}{\int_0^h \int_0^\infty F_0^*(y',E') \frac{1}{2}\chi(y',E') \int_0^\infty \nu\Sigma_f(y',E'') F_0(y',E'') dE'' dE' dy'}$$
$$+ \frac{F_0^*(y,E) \frac{1}{2}\chi(y,E) \int_0^\infty \nu\Sigma_f(y,E') F_3(y,E') dE'}{\int_0^h \int_0^\infty F_0^*(y',E'') \frac{1}{2}\chi(y',E'') \int_0^\infty \nu\Sigma_f(y',E''') F_0(y',E''') dE''' dE'' dy'}$$
$$- \frac{F_0^*(y,E) \frac{1}{2}\chi(y,E) \int_0^\infty \nu\Sigma_f(y,E') F_2(y,E') dE'}{\int_0^h \int_0^\infty F_0^*(y',E'') \frac{1}{2}\chi(y',E'') \int_0^\infty \nu\Sigma_f(y',E''') F_0(y',E''') dE''' dE'' dy'}$$
$$\times \frac{\int_0^h \int_0^\infty \int_{-1}^1 \mu' f_0^*(y',\mu',E') f_1(y',\mu',E') d\mu' dE' dy'}{\int_0^h \int_0^\infty F_0^*(y'',E'') \frac{1}{2}\chi(y'',E'') \int_0^\infty \nu\Sigma_f(y'',E''') F_0(y'',E''') dE''' dE'' dy''} \Bigg] d\mu dy .$$

The second definition is similar to the first, but with an alternate definition of the energy-dependent function $C(E)$:

$$\overline{D}_{2,g}^{(2)} = \frac{\left(\int_{E_g}^{E_{g-1}} C^{(2)}(E) dE \right) - A_g^{(2)}}{B_g^{(2)}} , \tag{7.35a}$$

where

$$A_g^{(2)} = A_g^{(1)} , \tag{7.35b}$$

$$B_g^{(2)} = B_g^{(2)} , \tag{7.35c}$$

and

$$C^{(2)}(E) = \int_0^h \int_{-1}^1 \Bigg[-\frac{\mu f_0^*(y,\mu,E) f_6(y,\mu,E)}{\int_0^h \int_0^\infty \int_{-1}^1 \mu' f_0^*(y',\mu',E') f_1(y',\mu',E') d\mu' dE' dy'} \tag{7.35d}$$
$$+ \frac{\mu f_0^*(y,\mu,E) f_5(y,\mu,E) d\mu dE dy}{\int_0^h \int_0^\infty F_0^*(y',E') \frac{1}{2}\chi(y',E') \int_0^\infty \nu\Sigma_f(y',E'') F_0(y',E'') dE'' dE' dy'}$$
$$+ \frac{\nu\Sigma_f(y,E) F_3(y,E) \int_0^\infty F_0^*(y,E') \frac{1}{2}\chi(y,E') dE'}{\int_0^h \int_0^\infty F_0^*(y',E'') \frac{1}{2}\chi(y',E'') \int_0^\infty \nu\Sigma_f(y',E''') F_0(y',E''') dE''' dE'' dy'}$$
$$- \frac{\nu\Sigma_f(y,E) F_2(y,E) \int_0^\infty F_0^*(y,E') \frac{1}{2}\chi(y,E') dE'}{\int_0^h \int_0^\infty F_0^*(y',E'') \frac{1}{2}\chi(y',E'') \int_0^\infty \nu\Sigma_f(y',E''') F_0(y',E''') dE''' dE'' dy'}$$
$$\times \frac{\int_0^h \int_0^\infty \int_{-1}^1 \mu' f_0^*(y',\mu',E') f_1(y',\mu',E') d\mu' dE' dy'}{\int_0^h \int_0^\infty F_0^*(y'',E'') \frac{1}{2}\chi(y'',E'') \int_0^\infty \nu\Sigma_f(y'',E''') F_0(y'',E''') dE''' dE'' dy''} \Bigg] d\mu dy .$$

The two $\overline{D}_{2,g}$ expressions presented in this chapter are very similar in form. However, the numerical results presented in Chapter 8 will demonstrate that the subtle differences between them have a significant effect on the multigroup SP_2 solution.

CHAPTER 8

Asymptotic Analysis of the Hypothesized 1-D Homogenized, Multigroup SP_2 Equation – Numerical Results

In this chapter, we present numerical results for the hypothesized homogenized, multigroup, 1-D SP_2 equation and asymptotic diffusion coefficients defined in Chapter 7.

Three sets of multigroup cross sections were used in our simulations. The first took a 56-group library, obtained from the MPACT code [31] with a homogeneous mixture of UO_2 and light water, and group-collapsed down to two energy groups. The second and third cross section sets are taken from the seven C5G7 reactor benchmark [30], for both UO_2 and 4.3% MOX fuel.

The results are generally inconsistent. When the 56-group library (collapsed to two groups) is used, each asymptotic diffusion coefficient set is outperformed by the standard diffusion coefficient set. However, for the C5G7 problems, there is no clear trend.

8.1 56-Group Library

The 56-group library was generated using the MPACT code [31] with a homogeneous mixture of UO_2 fuel and light water (borated) moderator, as described in Chapter 6. Number densities for the fine group library were obtained from the VERA benchmark [32] for

3.1% enriched fuel, 0.743 g/cc light water moderator, and 1300 ppm boron, then volume weighted to obtain the number densities shown in Table 6.1.

Each of the "continuous energy" (56-group) and multigroup (2-group) lattice functions and cross sections were calculated with a fine-mesh, 1-D S_{32} code, and input into Eqs. (7.34) and (7.35) to calculate $\overline{D}_{2,g}$. The 56-group library was used in the fine-mesh, 1-D S_{32} code to generate reference solutions.

8.1.1 Results

Similar to the results presented in Chapter 6, we obtained two-group cross sections and diffusion coefficients from an infinite homogeneous medium calculation. These values were then used in a series of homogeneous medium simulations for finite systems of varying widths L. Each simulation was performed with a 1-D, SP_2 and diffusion code with vacuum boundary conditions. The 56-group S_N results were used as the reference solution, with the eigenvalue error is reported in percent mille (pcm):

$$\Delta k_{eff} = \left(k_{eff,56G} - k_{eff,\text{Few Group}}\right) \times 10^5 (\text{pcm}) \,. \tag{8.1}$$

Table 8.1 compares the eigenvalue error for standard multigroup diffusion and SP_2 to the asymptotically defined multigroup diffusion and SP_2 equations. The two sets of asymptotic SP_2 results correspond to the definitions of $\overline{D}_{2,g}$ shown in Eqs. (7.34) and (7.35), respectively. It is disheartening to see that, aside from L = 12 cm case, the standard definitions of $D_{0,g}$ and $D_{2,g}$ are more accurate than the asymptotic definitions. The L = 12 cm case, as seen in previous chapters, is an outlier. For most problem lengths L, $\overline{D}^{(2)}_{2,g}$ appears to be the best of the asymptotic methods. However, it results in "inconsistent" errors, that do not change in a predictable manner as the problem size increases (unlike the asymptotic diffusion and $\overline{D}^{(1)}_{2,g}$ cases).

Table 8.1 Multigroup Eigenvalue Results

Length (cm)	56 Group S_N Reference k-eff	Standard Diffusion Δk (pcm)	Standard SP_2 Δk (pcm)	Asymptotic Diffusion Δk (pcm)	Asymptotic SP_2 (1) Δk (pcm)	Asymptotic SP_2 (2) Δk (pcm)
12	0.426928	-622.6	-2574.4	-536.6	-294.1	-4257.3
24	0.746386	901.9	272	958.1	1223	18.7
36	0.87009	582	355.4	615.8	756.6	327.1
48	0.926879	335.7	237.6	357.5	435.1	249.6
72	0.974806	130.4	103.5	141.3	171.2	119.5
96	0.993722	63.8	54.2	70.3	85.3	65.1
120	1.003005	37.3	34.1	41.6	51	41.4

For the 56-group cases presented here, the performance of the asymptotic multigroup SP_2 equation is mixed at best. We will see similar behavior the C5G6 results presented in section 8.2.

8.2 C5G7 Library

For the C5G7 cases, seven-group cross sections were taken directly from the benchmark document [30]. In the C5G7 benchmark specification, the cladding and fuel are spatially homogenized. The fuel and moderator for each pin were then spatially homogenized using volume weighting. This was performed with the idea that if the method proved unsuccessful at modeling a simple homogeneous medium, then it would require additional modification before application to more realistic problems. Only two fuel pin types were used, the UO_2 pin and 4.3% MOX pin.

For both cases, two sets of cross sections were obtained, a seven-group set and a two-group set. For each cross section set, diffusion coefficients were calculated in both the

standard way and using the asymptotic definitions from Chapter 7 (including both $\overline{D}_{2,g}$ formulations).

8.2.1 UO_2

Reference solutions were generated using a 1-D multigroup S_N code with the seven-group C5G7 cross sections. Eigenvalue errors for the seven-group cross sections, with problem lengths ranging from 5 to 40 cm, are presented (in pcm) in Table 8.2. Eigenvalue errors for the two-group cross sections are presented in Table 8.3.

Table 8.2 Seven-Group UO_2

Length (cm)	56 Group S_N Reference k-eff	Standard Diffusion Δk (pcm)	Standard SP_2 Δk (pcm)	Asymptotic Diffusion Δk (pcm)	Asymptotic SP_2 (1) Δk (pcm)	Asymptotic SP_2 (2) Δk (pcm)
		Standard		Asymptotic		
10	0.336736	3513.5	257.4	3513.5	-36.1	-8584.1
20	0.758444	2218	39.4	2218	1321.9	-2445.9
40	1.10299	588.4	-11.1	588.4	632.5	-217.9
80	1.259431	90.5	-2.1	90.5	132.4	15.3

For seven energy groups, standard SP_2 is clearly the most accurate. The standard and asymptotic diffusion results are identical, because the asymptotic diffusion coefficient reduces to the standard diffusion definition for a homogeneous medium. For larger systems (L = 40 or L = 80), $\overline{D}^{(2)}_{2,g}$ yields better results than both $\overline{D}^{(1)}_{2,g}$ and diffusion. However, for smaller problems (L = 10 or L = 20), $\overline{D}^{(1)}_{2,g}$ is superior. Neither of the asymptotic SP_2 definitions result in "consistent" error behavior, i.e. one that behaves semi-predictably as the system width increases.

Table 8.3 Two-Group UO_2

Length (cm)	56 Group S_N Reference k-eff	Standard Diffusion Δk (pcm)	Standard SP_2 Δk (pcm)	Asymptotic Diffusion Δk (pcm)	Asymptotic SP_2 (1) Δk (pcm)	Asymptotic SP_2 (2) Δk (pcm)
		Standard		Asymptotic		
10	0.336736	-3386.3	-5709.1	-3380.6	-6217.3	-8030.5
20	0.758444	-328.6	-1517.6	-345.6	-1774.2	-2001.5
40	1.10299	384.2	125.1	364.8	68.3	124.7
80	1.259431	117	85.4	108.4	78.3	98.2

For two energy groups, the results are even less consistent. $\overline{D}^{(2)}_{2,g}$ outperforms $\overline{D}^{(1)}_{2,g}$ for all problem sizes considered, while asymptotic diffusion proves superior to asymptotic SP_2 for smaller systems. This behavior is the opposite of what we would expect. Asymptotic diffusion is generally more accurate than standard diffusion, but not always, and standard SP_2 varies in accuracy.

8.2.2 4.3% MOX

For the MOX homogeneous medium case, reference solutions were once again generated using a 1-D multigroup S_N code with the seven group cross sections. Eigenvalue errors for the seven-group cross sections, with a problem sizes ranging from 5 to 40 cm, are presented (in pcm) in Table 8.4, while eigenvalue errors for the two-group cross sections are presented in Table 8.5.

Table 8.4 Seven-Group MOX 4.3%

Length (cm)	56 Group S_N Reference k-eff	Standard Diffusion Δk (pcm)	Standard SP_2 Δk (pcm)	Asymptotic Diffusion Δk (pcm)	Asymptotic SP_2 (1) Δk (pcm)	Asymptotic SP_2 (2) Δk (pcm)
		Standard		Asymptotic		
10	0.322132	3188.7	246.5	3188.7	-99.4	-5912.2
20	0.67115	1888.2	50.8	1888.2	890.4	-1582.6
40	0.947516	490.6	-3	490.6	417	-132.8
80	1.072275	75.1	-0.5	75.1	87.3	12.2

For this case, standard SP_2 is clearly more accurate than the other methods. The two definitions of $\overline{D}_{2,g}$ once more wavered in their accuracy, though it appears that $\overline{D}^{(1)}_{2,g}$ is more accurate for smaller problems, while $\overline{D}^{(2)}_{2,g}$ is more accurate for larger problems.

Table 8.5 Two-Group MOX 4.3%

Length (cm)	56 Group S_N Reference k-eff	Standard Diffusion Δk (pcm)	Standard SP_2 Δk (pcm)	Asymptotic Diffusion Δk (pcm)	Asymptotic SP_2 (1) Δk (pcm)	Asymptotic SP_2 (2) Δk (pcm)
		Standard		Asymptotic		
10	0.322132	-2891.4	-5410.3	-2854.5	-	-5906.3
20	0.67115	-91.1	-1295.6	-143.1	-	-1282.4
40	0.947516	408.5	152.7	346.6	-	162.8
80	1.072275	124.1	0	96.8	-	84.9

For the two-group case, use of the $\overline{D}^{(1)}_{2,g}$ formulation caused the simulation to become unstable ($\overline{D}^{(1)}_{2,1}$ was negative). Once more, standard SP_2 was the most consistently accurate method; both standard and asymptotic diffusion were more accurate than multigroup SP_2 with $\overline{D}^{(2)}_{2,g}$ for small problems and less accurate for larger problems.

8.3 Discussion

In this chapter, the asymptotic, multigroup SP_2 coefficients defined in Chapter 7 were numerically tested for a set of homogeneous medium problems. The multigroup SP_2 equation with asymptotically-defined coefficients proved inconsistent in its accuracy, and was frequently outperformed by both standard SP_2 and even diffusion. [The most likely explanation for these inconsistencies is our definition of $\overline{D}_{2,g}$. Eq. (7.31) does not lend itself to an unambiguous definition of $\overline{D}_{2,g}$.] Furthermore, we used the definition of $\overline{D}_{0,g}$ chosen by Trahan. While this proved accurate for asymptotic diffusion test cases, it may not be the best choice for a multigroup SP_2 equation. Future work is suggested to try an obtain a less ambiguous, more accurate definition for $\overline{D}_{2,g}$.

Because the method performed poorly for homogeneous medium problems, we were not able to investigate discontinuity factors or flux reconstruction, two important factors in any future asymptotic, multigroup SP_2 method.

CHAPTER 9

Conclusions and Future Work

In this chapter, we summarize our theoretical derivations and numerical results and discuss potential future work.

9.1 Summary of the Asymptotic, Homogenized, Monoenergetic SP_2 Equation

In Chapter 3, we considered a continuous energy, spatially periodic, 1-D system that is optically thick. By applying an asymptotic analysis to the system, we obtained a 1-D, monoenergetic, *homogenized* SP_2 equation. In the analysis, the lattice-geometry continuous energy neutron transport equation was subjected to an asymptotic expansion. The expansion involved a small parameter ϵ, which is inversely proportional to the thickness of the system. Our analysis was comparable to that performed by Trahan [25], but carried to higher order. While Trahan's result (a monoenergetic, homogenized diffusion equation) had $O(\epsilon^2)$ error, our work extended the analysis to $O(\epsilon^4)$ error. Additionally, we obtained a higher order flux reconstruction formula (for $\psi(x,\mu,E)$), with two more terms than Trahan's formula and three more terms than standard flux reconstruction. In a monoenergetic, homogeneous medium, these results reduce to the standard SP_2 equation and the SP_2 prescription for the angular flux.

In Chapter 4, we numerically evaluated the 1-D, monoenergetic, homogenized SP_2 equation

derived in Chapter 3. Reference solutions for a set of 1-D, monoenergetic transport problems were generated using a 1-D, discrete ordinates code with diamond difference spatial discretization. They were then solved with the homogenized SP_2 equation developed in Chapter 3, as well as with the asymptotic homogenized diffusion equation developed by Trahan [25], standard SP_2, and standard diffusion. The asymptotic, homogenized SP_2 equation showed a clear improvement in accuracy over the other three methods, particularly for small problems. This suggests that the asymptotic, homogenized SP_2 equation may improve the solution's accuracy in calculations for SMRs and other reactors with steep flux gradients. Furthermore, the additional flux reconstruction terms considerably improve the reconstructed flux in the fuel pins.

While the asymptotic derivation in Chapter 3 required the assumption that $\epsilon = 1/N \ll 1$, where N is the number of spatial cells, our numerical results showed that the asymptotic, homogenized SP_2 equations are still valid for larger values of ϵ. For problems with ϵ very small, we found standard homogenized diffusion theory to be accurate, asymptotic homogenized diffusion to be more accurate, and asymptotic homogenized SP_2 to be even more accurate. As ϵ increased (i.e. the optical width of the system decreased), all three methods degraded in accuracy; however, asymptotic homogenized SP_2 remained the most accurate of the three. Thus, there are "larger" values of ϵ in which standard diffusion theory produced unacceptable results, but asymptotic SP_2 results remained acceptable.

9.2 Summary of the Asymptotic Scaling Factor

In Chapter 5, we considered the problem of accurately defining cross sections for multigroup transport problems. The standard multigroup cross section generation procedure involved flux-weighting the cross sections over each energy group to preserve the multigroup infinite medium eigenfunction and eigenvalue. By performing an asymptotic analysis on both a continuous-energy and multigroup 1-D transport problem, we were able to apply a

simple modification to the standard multigroup cross sections to improve their accuracy. This modification involved multiplying the cross sections by a constant ρ_G that was chosen to preserve the asymptotic limit of the continuous-energy transport equation. Two different definitions of ρ_G were chosen - one that preserved the asymptotic diffusion limit of the continuous-energy transport equation, and one that preserved the asymptotic SP_2 limit of the continuous-energy transport equation.

In Chapter 6, we numerically evaluated the modified cross sections for several 1-D test problems. A fine-group structure was used for reference solutions (in the absence of a continuous energy cross section library), and group-collapsed cross section sets were calculated both with and without the scaling factor. We showed that for each case the scaling factor improved the accuracy of the few-group calculation. The difference between the diffusion- and SP_2- based scaling factors was small, particularly with large problems.

9.3 Summary of the Asymptotic, Homogenized, Multigroup SP_2 Equation

In Chapter 7, we applied an asymptotic analysis to a hypothesized, spatially homogenized, multigroup 1-D SP_2 equation. The hypothesized equation used standard homogenized cross section definitions while leaving the diffusion coefficients unspecified. An asymptotic analysis, similar to the one shown in Chapter 3, was performed, and the diffusion coefficients were chosen such that the hypothesized multigroup SP_2 equation has the same asymptotic limit as the continuous-energy lattice transport equation. The analysis was similar to the one performed by Trahan [25], and the same multigroup diffusion coefficient was chosen. While there were a number of ways to define the second multigroup diffusion coefficient ($\overline{D}_{2,g}$), two definitions were chosen for testing in Chapter 8.

In Chapter 8, the SP_2 equation hypothesized in Chapter 7 was tested for a series of homogeneous medium problem. The multigroup SP_2 equations with asymptotically-defined

coefficients proved inconsistent in their accuracy, and were frequently outperformed by both standard SP_2 and diffusion. The most likely explanation for these inconsistencies was the definition of $\overline{D}_{2,g}$. Eq. (7.31) does not lend itself to an unambiguous definition of $\overline{D}_{2,g}$. Furthermore, with multigroup cross sections, one is faced with the problem of a range of optical thicknesses. Even if the asymptotic analysis is valid for the thermal energy groups, it is possible that the large mean free paths seen in fast energy ranges violates the assumptions of the asymptotic analysis.

9.4 Future Work

To conclude this thesis, we discuss potential future work related to the three topics of this thesis.

In order to improve their applicability to real-life problems, all three methods can (and should) be extended to multiple spatial dimensions. While the 1-D results are an important stepping-stone, most practical applications (i.e. real reactors) require 3-D results. The one exception is the 2-D/1-D method, in which transport calculations are performed on discrete two-dimensional "slices" of the core, while lower-order one-dimensional calculations (typically diffusion) are performed in the axial direction. The two calculations are then linked via the transverse leakage terms. The 2-D/1-D method provides a computationally inexpensive alternative to full 3-D transport calculations, and has been used successfully in many modern transport codes [31].

Asymptotic SP_2 could potentially replace diffusion in the 2-D/1-D method. Asymptotic diffusion coefficients ($\overline{D}_0$ and $\overline{D}_2$) could be pre-calculated for every pin or assembly for use in the axial calculation. Because one is only interested in 1-D diffusion (in the axial direction), it would not be necessary to calculate more complicated diffusion tensors. Furthermore, the reconstructed flux formulas could be used to provide a shape function for adding the axial leakage source to the 2-D problem.

The scaling factors described in Chapters 5 and 6 have considerable potential in improving multigroup transport problems. If these are limited to asymptotic diffusion-based scaling factors, extension to multiple dimensions will be relatively simple. Furthermore, we focused on preserving the continuous-energy *homogenized* transport equation. Preserving the continuous-energy lattice transport equation would be comparable and simple to implement. Due to the lack of improvement from asymptotic diffusion-based to asymptotic SP_2-based scaling factors, we suggest using asymptotic diffusion scaling factors until a clear need for higher-order scaling arrives.

Considerable work will be required to make the hypothesized homogenized, multigroup SP_2 equation defined in Chapter 7 viable. More accurate definitions for the diffusion coefficients are required. Once these have been established, discontinuity factors and flux reconstruction must also be investigated.

Finally, we note that much of this work may be considered a higher-order extension of Trahan's work [25]. This implies (correctly) that our work may also be extended to even higher-order, resulting in a simplified P_N equation (with $N > 2$). However, due to the increasing number of lattice functions, this may be inadvisable, particularly when considering two or three spatial dimensions. Many of the lattice functions are space-dependent, and increase in number with spatial dimensions. As the number of lattice functions increases, any increase in accuracy may no longer be worth the corresponding increases in calculation time.

APPENDIX A

FREDHOLM ALTERNATIVE THEOREM (FAT)

A.1 Properties of the FAT

The Fredholm Alternative Theorem (FAT) [29] is useful for determining the existence of a solution to an inhomogeneous equation.

Assume we have an operator M and an adjoint operator M^*, with

$$Mh(x,\mu,E) = 0\,, \tag{A.1a}$$

$$M^*h^*(x,\mu,E) = 0\,, \tag{A.1b}$$

and inner product defined by

$$(f,g) = \int_0^h \int_0^\infty \int_{-1}^1 f(x,\mu,E)\, g(x,\mu,E)\, d\mu dE dx\,. \tag{A.2}$$

where h is the width of a cell. The FAT says that if non-trivial solutions to Eqs. (A.1a) and (A.1b) exist, then the following is true.

1. $Mh = 0$ and $M^*h^* = 0$ have the same number of linearly independent solutions.

2. $Mh = g$ has a particular solution if and only if g is orthogonal to all the solutions of

$M^* h^* = 0$, i.e. $(g, h^*) = 0$.

3. The general solution to $Mh = g$ is given by:

$$h = h_{particular} + \sum_{n=1}^{N} a_n h_{homogeneous,n}\,, \tag{A.3}$$

where N is the number of non-trivial linearly independent solutions to the homogeneous equation $Mh = 0$ and a_i are arbitrary constants.

In this work, $M = L$ and $M^* = L^*$ are the infinite-lattice and adjoint infinite-lattice operators, respectively, and the homogeneous solutions to $Mh = 0$ and $M^* h^* = 0$ are $h = f_0(x, mu, E)$ and $h^* = f_0^*(x, mu, E)$. The second item from the FAT list provides the solvability condition used in Chapters 3, 5, and 7. The third item provides the form of the solutions to Eqs. (3.9), (5.18) and (7.7).

A.2 Proof that $\lambda_1 = 0$

In Chapter 3 and 5, the result from [25] was used to claim that $\lambda_1 = 0$. A proof for this claim for the continuous-energy, lattice system described in Chapter 3 is presented here.

If we hypothesize that $\lambda_1 \neq 0$, then Eq. (3.7b) is

$$\lambda = \lambda_0 + \epsilon\lambda_1 + \epsilon^2\lambda_2\,, \tag{A.4}$$

and Eq. (3.9b) becomes

$$\begin{aligned} L\Psi_1(y,z,\mu,E) = &-\mu\frac{\partial}{\partial z}\Psi_0(y,z,\mu,E) \\ &+ \lambda_1\frac{\chi(y,E)}{2}\int_0^\infty \nu\Sigma_f(y,E')\int_{-1}^{1}\Psi_0(y,z,\mu',E')\,d\mu'\,dE'\,. \end{aligned} \tag{A.5}$$

Substituting Eq. (3.19) into Eq. (A.5), we have

$$\begin{aligned} L\Psi_1(y,z,\mu,E) &= -\mu\frac{\partial}{\partial z}(f_0(y,\mu,E)A_0(z)) \\ &\quad + \lambda_1\frac{\chi(y,E)}{2}\int_0^\infty \nu\Sigma_f(y,E')\int_{-1}^1 (f_0(y,\mu',E')A_0(z))d\mu' dE' \\ &= -\mu f_0(y,\mu,E)\frac{\partial}{\partial z}A_0(z) \\ &\quad + \lambda_1\frac{\chi(y,E)}{2}\int_0^\infty \nu\Sigma_f(y,E')F_0(y,E')A_0(z)dE', \end{aligned} \tag{A.6}$$

where F_0 is described by Eq. (3.37). By the FAT, $L\Psi_1(y,z,\mu,E) = g(y,z,\mu,E)$ has a particular solution if and only if g is orthogonal to $f_0^*(y,\mu,)$, or

$$\begin{aligned} \left(f_0^*(y,\mu,E), g(y,z,\mu,E)\right) &= \Big(f_0^*(y,\mu,E), -\mu f_0(y,\mu)\frac{\partial}{\partial z}A_0(z) \\ &\quad + \lambda_1\frac{\chi(y,E)}{2}\int_0^\infty \nu\Sigma_f(y,E')F_0(y,E')A_0(z)dE'\Big) \\ &= -\Big(f_0^*(y,\mu,E), \mu f_0(y,\mu,E)\Big)\frac{\partial}{\partial z}A_0(z) \\ &\quad + \lambda_1\frac{\chi(y,E)}{2}\int_0^\infty \nu\Sigma_f(y,E')F_0(y,E')A_0(z)dE' \\ &= 0. \end{aligned} \tag{A.7}$$

Because $f_0(y,\mu,E)$ and $f_0^*(y,\mu,E)$ are symmetric in y and μ,

$$\Big(f_0^*(y,\mu,E), \mu f_0(y,\mu,E)\Big) = 0 \tag{A.8}$$

(see Appendix B), leaving us with

$$\lambda_1\frac{\chi(y,E)}{2}\int_0^\infty \nu\Sigma_f(y,E')F_0(y,E')A_0(z)dE' = 0. \tag{A.9}$$

The inner product $\left(f_0^*(y,\mu,E), \frac{\chi(y,E)}{2}\int_0^\infty \nu\Sigma_f(y,E')F_0(y,E')\right) \neq 0$ (again, see Appendix B).

For Eq. (A.9) to be true, λ_1 must equal zero, or

$$\lambda_1 = 0\,. \tag{A.10}$$

APPENDIX B

PROPERTIES OF L AND f_n

B.1 Properties of L

The following analysis is performed for a monoenergetic medium. The same analysis can be done for a energy-dependent system, with similar results.

The infinite-lattice operator L from Chapter 3 is defined by:

$$\begin{aligned} L\Psi(y,z,\mu) =& \mu\frac{\partial}{\partial y}\Psi(y,z,\mu) + \Sigma_t(y)\Psi(y,z,\mu) \\ & - \frac{1}{2}\left(\Sigma_s(y) + \lambda_0\nu\Sigma_f(y)\right)\int_{-1}^{1}\Psi(y,z,\mu')\,d\mu' , \end{aligned} \tag{B.1}$$

and has the following properties:

1. L is independent of z. **Proof**: If $\Psi(y,z,\mu)$ is a separable function of z, i.e.

$$\Psi(y,z,\mu) = f(y,\mu)A(z) , \tag{B.2}$$

then Eq. (B.1) is

$$
\begin{aligned}
L\Psi(y,z,\mu) =& L(f(y,\mu)A(z)) \\
=& \mu\frac{\partial}{\partial y}(f(y,\mu)A(z)) + \Sigma_t(y)(f(y,\mu)A(z)) \\
& - \frac{1}{2}\left(\Sigma_s(y) + \lambda_0 \nu\Sigma_f(y)\right)\int_{-1}^{1}(f(y,\mu')A(z))d\mu' \\
=& \left(\mu\frac{\partial}{\partial y}f(y,\mu)\right)A(z) + \left(\Sigma_t(y)f(y,\mu)\right)A(z) \\
& - \left(\frac{1}{2}\left(\Sigma_s(y) + \lambda_0 \nu\Sigma_f(y)\right)\int_{-1}^{1}f(y,\mu')d\mu'\right)A(z) \\
=& \left[\mu\frac{\partial}{\partial y}f(y,\mu) + \Sigma_t(y)f(y,\mu)\right. \\
& \left. - \frac{1}{2}\left(\Sigma_s(y) + \lambda_0 \nu\Sigma_f(y)\right)\int_{-1}^{1}f(y,\mu')d\mu'\right]A(z) \\
=& \left[Lf(y,\mu)\right]A(z)\,.
\end{aligned}
\tag{B.3}
$$

It is clear that L acts only on y, μ, and E, and is independent of z.

2. L is symmetry-preserving. **Proof**: If we have a symmetric function f, such that $f(y,\mu) = f(-y,-\mu)$, then

$$
\frac{\partial}{\partial y}f(-y,-\mu) = -\frac{\partial}{\partial y}f(y,\mu)\,, \tag{B.4}
$$

and

$$
\begin{aligned}
Lf(-y,-\mu) =& \mu\frac{\partial}{\partial y}f(-y,-\mu)+\Sigma_t(y)f(-y,-\mu) \\
&-\frac{1}{2}\left(\Sigma_s(y)+\lambda_0\nu\Sigma_f(y)\right)\int_{-1}^{1}f(-y,-\mu')\,d\mu' \\
=& -\mu\left(-\frac{\partial}{\partial y}f(y,\mu)\right)+\Sigma_t(y)f(y,\mu) \\
&-\frac{1}{2}\left(\Sigma_s(y)+\lambda_0\nu\Sigma_f(y)\right)\int_{-1}^{1}f(y,\mu')\,d\mu' \\
=& \frac{\partial}{\partial y}f(y,\mu)+\Sigma_t(y)f(y,\mu) \\
&-\frac{1}{2}\left(\Sigma_s(y)+\lambda_0\nu\Sigma_f(y)\right)\int_{-1}^{1}f(y,\mu')\,d\mu' \\
=& Lf(y,\mu)\,.
\end{aligned}
\tag{B.5}
$$

Likewise, if we have an antisymmetric function g, i.e. $g(y,\mu) = -g(-y,-\mu)$, then

$$
\frac{\partial}{\partial y}g(-y,-\mu) = \frac{\partial}{\partial y}g(y,\mu)\,, \tag{B.6}
$$

and

$$
\begin{aligned}
Lg(-y,-\mu) =& \mu\frac{\partial}{\partial y}g(-y,-\mu)+\Sigma_t(y)g(-y,-\mu) \\
&-\frac{1}{2}\left(\Sigma_s(y)+\lambda_0\nu\Sigma_f(y)\right)\int_{-1}^{1}g(-y,-\mu')\,d\mu' \\
=& -\mu\frac{\partial}{\partial y}g(y,\mu)-\Sigma_t(y)g(y,\mu) \\
&+\frac{1}{2}\left(\Sigma_s(y)+\lambda_0\nu\Sigma_f(y)\right)\int_{-1}^{1}g(y,\mu')\,d\mu' \\
=& -\left(\frac{\partial}{\partial y}g(y,\mu)+\Sigma_t(y)g(y,\mu)\right. \\
&\left.-\frac{1}{2}\left(\Sigma_s(y)+\lambda_0\nu\Sigma_f(y)\right)\int_{-1}^{1}g(y,\mu')\,d\mu'\right) \\
=& -Lg(y,\mu)\,.
\end{aligned}
\tag{B.7}
$$

Eqs. (B.5) and (B.7) show that L is *symmetry-preserving*.

3. The solution to $Lf_0 = 0$ is the infinite-medium lattice solution, and it is both a periodic function of y and a symmetric function of y and μ. **Proof**: If we rewrite

$$\begin{aligned} Lf_0(y,\mu) =& \mu\frac{\partial}{\partial y}f_0(y,\mu) + \Sigma_t(y)\,f_0(y,\mu) \\ & - \frac{1}{2}\left(\Sigma_s(y) + \lambda_0\nu\Sigma_f(y)\right)\int_{-1}^{1} f_0(y,\mu')\,d\mu' = 0\,, \end{aligned} \tag{B.8}$$

as

$$\begin{aligned} & \mu\frac{\partial}{\partial y}f_0(y,\mu) + \Sigma_t(y)\,f_0(y,\mu) \\ & \qquad = \frac{1}{2}\left(\Sigma_s(y) + \lambda_0\nu\Sigma_f(y)\right)\int_{-1}^{1} f_0(y,\mu')\,d\mu'\,, \end{aligned} \tag{B.9}$$

then it is clear that Eq. (B.9) is the infinite-medium lattice equation with infinite-lattice eigenvalue λ_0.

If we take Eq. (B.8) and perform the substitution $y = y + h$, we have

$$\begin{aligned} Lf_0(y+h,\mu) =& \mu\frac{\partial}{\partial y}f_0(y+h,\mu) + \Sigma_t(y+h)\,f_0(y+h,\mu) \\ & - \frac{1}{2}\left(\Sigma_s(y+h) + \lambda_0\nu\Sigma_f(y+h)\right)\int_{-1}^{1} f_0(y+h,\mu')\,d\mu' = 0\,. \end{aligned} \tag{B.10}$$

In Section 3.1, the cross sections in Eq. (B.8) were stated to be periodic,

$$\Sigma_x(y) = \Sigma_x(y+h)\,. \tag{B.11}$$

Substituting Eq. (B.11) into Eq. (B.10)), we have

$$\begin{aligned} Lf_0(y+h,\mu) =& \mu\frac{\partial}{\partial y} f_0(y+h,\mu) + \Sigma_t(y) f_0(y+h,\mu) \\ & - \frac{1}{2}\left(\Sigma_s(y) + \lambda_0 \nu \Sigma_f(y)\right) \int_{-1}^{1} f_0(y+h,\mu')\, d\mu' = 0\,, \end{aligned} \tag{B.12}$$

which implies that f_0 is periodic, i.e. $f_0(y+h,\mu) = f_0(y,\mu)$.

To see that f_0 is symmetric, we consider $Lf_0(-y,-\mu)$:

$$\begin{aligned} Lf_0(-y,-\mu) =& \mu\frac{\partial}{\partial y} f_0(-y,-\mu) + \Sigma_t(y) f_0(-y,-\mu) \\ & - \frac{1}{2}\left(\Sigma_s(y) + \lambda_0 \nu \Sigma_f(y)\right) \int_{-1}^{1} f_0(-y,-\mu')\, d\mu' = 0\,. \end{aligned} \tag{B.13}$$

Also in Section 3.1, the cross sections were declared to be symmetric, or

$$\Sigma_x(y) = \Sigma_x(-y)\,. \tag{B.14}$$

Substituting Eq. (B.14) into Eq. (B.13), we have

$$\begin{aligned} Lf_0(-y,-\mu) =& \mu\frac{\partial}{\partial y} f_0(-y,-\mu) + \Sigma_t(-y) f_0(-y,-\mu) \\ & - \frac{1}{2}\left(\Sigma_s(-y) + \lambda_0 \nu \Sigma_f(-y)\right) \int_{-1}^{1} f_0(-y,-\mu')\, d\mu' = 0\,. \end{aligned} \tag{B.15}$$

Performing the change of variable

$$y' = -y\,, \tag{B.16a}$$

$$\frac{\partial}{\partial y'} = -\frac{\partial}{\partial y}\,, \tag{B.16b}$$

and

$$\mu' = -\mu\,, \tag{B.16c}$$

Eq. (B.15) becomes

$$\begin{aligned} Lf_0(-y,-\mu) =& -\mu'\Big(-\frac{\partial}{\partial y'}f_0(y',\mu')\Big)+\Sigma_t(y')\,f_0(y',\mu') \\ & -\frac{1}{2}\Big(\Sigma_s(y')+\lambda_0\nu\Sigma_f(y')\Big)\int_{-1}^{1}f_0(y',\mu'')\,d\mu'' \\ =&\mu'\frac{\partial}{\partial y'}f_0(y',\mu')+\Sigma_t(y')\,f_0(y',\mu') \\ & -\frac{1}{2}\Big(\Sigma_s(y')+\lambda_0\nu\Sigma_f(y')\Big)\int_{-1}^{1}f_0(y',\mu'')\,d\mu'' \\ =&Lf_0(y',\mu')\,, \end{aligned} \tag{B.17}$$

implying that f_0 is symmetric, such that $f_0(-y,-\mu) = f_0(y,\mu)$.

4. L has an adjoint, L^*, with a solution to $L^*f_0^* = 0$ that is also a periodic and symmetric function. Furthermore, $f_0^*(y,\mu) = f_0(y,-\mu)$.

   Proof: The adjoint operator L^* is

$$\begin{aligned} L\Psi^*(y,z,\mu) =& -\mu\frac{\partial}{\partial y}\Psi^*(y,z,\mu)+\Sigma_t(y)\,\Psi^*(y,z,\mu) \\ & -\frac{1}{2}\Big(\Sigma_s(y)+\lambda_0\nu\Sigma_f(y)\Big)\int_{-1}^{1}\Psi^*(y,z,\mu')\,d\mu'\,, \end{aligned} \tag{B.18}$$

   and

$$\begin{aligned} Lf_0^*(y,\mu) =& -\mu\frac{\partial}{\partial y}f_0^*(y,\mu)+\Sigma_t(y)\,f_0^*(y,\mu) \\ & -\frac{1}{2}\Big(\Sigma_s(y)+\lambda_0\nu\Sigma_f(y)\Big)\int_{-1}^{1}f_0^*(y,\mu')\,d\mu' = 0\,. \end{aligned} \tag{B.19}$$

   Periodicity and symmetry can be proven the same way they were proven for f_0. To prove that $f_0(y,\mu) = f_0^*(y,-\mu)$, we begin with Eq. (B.8) and make the change of

variable, $\mu = -\mu'$:

$$\begin{aligned} Lf_0(y,\mu) =& -\mu' \frac{\partial}{\partial y} f_0(y,-\mu') + \Sigma_t(y) f_0(y,-\mu') \\ & - \frac{1}{2}\left(\Sigma_s(y) + \lambda_0 \nu \Sigma_f(y)\right) \int_{-1}^{1} f_0(y,-\mu')\, d\mu' \\ =& L^* f_0(y,-\mu') = 0 \\ =& L^* f_0^*(y,\mu)\,, \end{aligned} \tag{B.20}$$

implying that $f_0(y,\mu) = f_0^*(y,-\mu)$.

5. The inner product has the property $(Lg,h) = (g,L^*h)$. **Proof**: If the inner product of two functions $g(y,\mu)$ and $h(y,\mu)$ is defined as

$$(g,h) = \int_0^h \int_{-1}^{1} g(y,\mu)\, h(y,\mu)\, d\mu dy\,, \tag{B.21}$$

then

$$\begin{aligned} (g,Lh) =& \int_0^h \int_{-1}^{1} g(y,\mu)\, Lh(y,\mu)\, d\mu dy \\ =& \int_0^h \int_{-1}^{1} g(y,\mu) \left[\mu \frac{\partial}{\partial y} h(y,\mu) + \Sigma_t(y) h(y,\mu)\right. \\ & \left. - \frac{1}{2}\left(\Sigma_s(y) + \lambda_0 \nu \Sigma_f(y)\right) \int_{-1}^{1} h(y,\mu')\, d\mu' \right] d\mu dy\,. \end{aligned} \tag{B.22}$$

By the chain rule,we have

$$\begin{aligned} & \int_0^h \int_{-1}^{1} \mu g(y,\mu) \frac{\partial}{\partial y} h(y,\mu)\, d\mu dy \\ & \quad = \int_0^h \int_{-1}^{1} \mu \left[\frac{\partial}{\partial y}\Big(g(y,\mu) h(y,\mu)\Big) - h(y,\mu) \frac{\partial}{\partial y} g(y,\mu)\right] d\mu dy \\ & \quad = \int_{-1}^{1} \mu \Big(g(h,\mu) h(h,\mu) - g(0,\mu) h(0,\mu)\Big) - \\ & \qquad \int_0^h \int_{-1}^{1} \mu h(y,\mu) \frac{\partial}{\partial y} g(y,\mu)\, d\mu dy\,, \end{aligned} \tag{B.23}$$

or, assuming $g(0,\mu) = g(h,\mu)$ and $h(0,\mu) = h(h,\mu)$,

$$\int_0^h \int_{-1}^1 \mu g(y,\mu) \frac{\partial}{\partial y} h(y,\mu)\, d\mu dy = -\int_0^h \int_{-1}^1 \mu h(y,\mu) \frac{\partial}{\partial y} g(y,\mu)\, d\mu dy\,. \tag{B.24}$$

Eq. (B.22) can be rewritten as

$$\begin{aligned}
(g, Lh) &= \int_0^h \int_{-1}^1 g(y,\mu) \Bigg[\mu \frac{\partial}{\partial y} h(y,\mu) + \Sigma_t(y) h(y,\mu) \\
&\qquad - \frac{1}{2}\Big(\Sigma_s(y) + \lambda_0 \nu \Sigma_f(y)\Big) \int_{-1}^1 h(y,\mu')\, d\mu' \Bigg] d\mu dy \\
&= \int_0^h \int_{-1}^1 h(y,\mu) \Bigg[-\mu \frac{\partial}{\partial y} g(y,\mu) + \Sigma_t(y) g(y,\mu) \\
&\qquad - \frac{1}{2}\Big(\Sigma_s(y) + \lambda_0 \nu \Sigma_f(y)\Big) \int_{-1}^1 g(y,\mu')\, d\mu' \Bigg] d\mu dy \\
&= \int_0^h \int_{-1}^1 h(y,\mu) L^* g(y,\mu)\, d\mu dy \\
&= (L^* g, h)\,.
\end{aligned} \tag{B.25}$$

B.2 Symmetry of f_n

We have proven that L is symmetry-preserving, and that f_0 is symmetric. Now we examine the symmetry of the higher order f_n functions. Before doing this, we must several identities.

First, if L is symmetry-preserving, then the symmetry of f_n, the solution to $L f_n(y,\mu) = g(y,\mu)$, must have the same as the symmetry of g.

Second, operating on any function by $(I - P)$ also preserves symmetry. The result of the operator P,

$$\begin{aligned}
Pg(y,\mu) = &\frac{f_0(y,\mu)}{\int_0^h \int_{-1}^1 f^*(y',\mu') f_0(y',\mu')\, d\mu' dy'} \\
&\times \int_0^h \int_{-1}^1 f_0^*(y',\mu') g(y',\mu')\, d\mu' dy'\,,
\end{aligned} \tag{B.26}$$

is a constant times f_0, and must be symmetric. The identity operator I is by definition symmetry-preserving. An antisymmetric function plus or minus a symmetric function yields a antisymmetric function, while a symmetric function plus or minus a symmetric function equals a symmetric function. Hence, $(I - P)$ is symmetry-preserving.

Third, integrating over all angles preserves symmetry. If $g(y,\mu)$ is an antisymmetric function, then

$$\begin{aligned} G(y) &= \int_{-1}^{1} g(y,\mu)\, d\mu \\ &= \int_{-1}^{1} \Big(- g(-y,-\mu) \Big) d\mu \\ &= \int_{1}^{-1} \Big(- g(-y,\mu') \Big) (-d\mu') \\ &= \int_{1}^{-1} g(-y,\mu')\, d\mu' \\ &= - \int_{-1}^{1} g(-y,\mu')\, d\mu' \\ &= -G(-y) \,, \end{aligned} \tag{B.27}$$

is an antisymmetric function. Similarly, if g is a symmetric function, then its integral

$$\begin{aligned} G(y) &= \int_{-1}^{1} g(y,\mu)\, d\mu \\ &= \int_{-1}^{1} g(-y,-\mu)\, d\mu \\ &= \int_{1}^{-1} g(-y,\mu') (-d\mu') \\ &= - \int_{1}^{-1} g(-y,\mu')\, d\mu' \\ &= \int_{-1}^{1} g(-y,\mu')\, d\mu' \\ &= G(-y) \,, \end{aligned} \tag{B.28}$$

is a symmetric function. Integrating a function over angle is therefore symmetry-preserving.

Next, we look at the multiplicative properties of symmetric and antisymmetric functions.

If $h(y,\mu)$ is the product of two symmetric functions $f(y,\mu)$ and $g(y,\mu)$, then

$$\begin{aligned} h(-y,-\mu) &= f(-y,-\mu)\,g(-y,-\mu) \\ &= f(y,\mu)\,g(y,\mu) \\ &= h(y,\mu)\ , \end{aligned} \tag{B.29}$$

is also symmetric. Likewise, if $h(y,\mu)$ is the product of two antisymmetric functions $f(y,\mu)$ and $g(y,\mu)$, then

$$\begin{aligned} h(-y,-\mu) &= f(-y,-\mu)\,g(-y,-\mu) \\ &= (-f(y,\mu))(-g(y,\mu)) \\ &= h(y,\mu)\ , \end{aligned} \tag{B.30}$$

is also symmetric. Finally, if $h(y,\mu)$ is the product of an antisymmetric function $f(y,\mu)$ and a symmetric function $g(y,\mu)$, then

$$\begin{aligned} h(-y,-\mu) &= f(-y,-\mu)\,g(-y,-\mu) \\ &= (-f(y,\mu))g(y,\mu) \\ &= -h(y,\mu)\ , \end{aligned} \tag{B.31}$$

is antisymmetric.

We will now consider $f_1 - f_6$:

1. f_1: antisymmetric

$$Lf_1(y,\mu) = \mu f_0(y,\mu) \tag{B.32}$$

f_0 is symmetric, and μ is antisymmetric. Therefore μf_0 and f_1 are antisymmetric.

2. f_2: symmetric

$$Lf_2(y,\mu) = (I-P)\frac{\nu\Sigma_f(y)}{2}F_0(y) \tag{B.33}$$

f_0 is symmetric, and so its integral over angle F_0 is also symmetric. $\nu\Sigma_f$, like all cross sections, is symmetric. Finally, because $(I-P)$ is symmetry-preserving, f_2 is symmetric.

3. f_3: symmetric

$$Lf_3(y,\mu) = (I-P)\mu f_1(y,\mu) \tag{B.34}$$

f_1 is antisymmetric, so the product μf_1 is symmetric. Again, $(I-P)$ preserves symmetry, and f_3 is symmetric.

4. f_4: antisymmetric

$$Lf_4(y,\mu) = \frac{\nu\Sigma_f(y)}{2}F_1(y) \tag{B.35}$$

The angular integral of the antisymmetric f_1 is an antisymmetric function (if it is not zero). $\nu\Sigma_f$ is symmetric, so $\frac{\nu\Sigma_f(y)}{2}F_1(y)$ is antisymmetric. Hence, f_4 is antisymmetric.

5. f_5: antisymmetric

$$Lf_3(y,\mu) = (I-P)\mu f_2(y,\mu) \tag{B.36}$$

f_2 is symmetric, so the product μf_2 is antisymmetric. Therefore, $(I-P)\mu f_2$ and f_5 are antisymmetric.

6. f_6:antisymmetric

$$Lf_3(y,\mu) = (I-P)\mu f_3(y,\mu) \tag{B.37}$$

f_3 is symmetric, so the product μf_3 is antisymmetric. Therefore, $(I - P)\mu f_3$ and f_6 are antisymmetric.

BIBLIOGRAPHY

[1] A. Hebert, *Applied Reactor Physics*, Presses Internationales Polytechnique (2009).

[2] E.E. Lewis and W.F. Miller, Jr., *Computational Methods of Neutron Transport*, American Nuclear Society, La Grange Park, Il, USA (1993).

[3] "AP1000 Design Control Document," http://www.nrc.gov/reactors/new-reactors/design-cert/ap1000/dcd/ Tier%202/Chapter%204/4-1_r14.pdf, (Accessed August 18, 2015).

[4] "Titan Cray XK7," https://www.olcf.ornl.gov/computing-resources/titan-cray-xk7/, (Accessed May 21, 2014).

[5] R. Black, "Bringing Small Modular Reactors (SMRs) to Commercial Markets," DOE SMR Workshop, June 29 (2010).

[6] "Introducing Nuclear Power Plants Into Electrical Power Systems of Limited Capacity: Problems and Remedial Measure," Technical Reports Series No. 271, International Atomic Energy Agency, Vienna (1987).

[7] W.M. Stacey, *Nuclear Reactor Physics*, John Wiley & Sons, Inc., New York, NY, USA (2001).

[8] R.J.J. Stamm'ler and M.J. Abbate, *Methods of Steady-state Reactor Physics in Nuclear Design*, Elsevier Science Publishing Co. Inc., San Diego, CA, USA (1983).

[9] N.Z. Cho, "Fundamentals and Recent Developments of Reactor Physics Methods," Nuclear Engineering and Technology, **37**, pp. 25 – 78 (2005).

[10] J.J. Duderstadt and L.J. Hamilton, *Nuclear Reactor Analysis*, John Wiley & Sons, Inc., New York, NY, USA (1976).

[11] K. Koebke, "Advances in Homogenization and Dehomogenization," *Proceedings of the International Topical Meeting on Advances in Mathematical Methods for the Solution of Nuclear Engineer Problems (M&C 1981)*, Munich, Germany, April, 1981.

[12] K. Smith, "Assembly Homogenization Techniques for Light Water Reactor Analysis," *Progress in Nuclear Energy*, **17**, 3, pp. 30 – 335 (1986).

[13] R. Sanchez, "Assembly Homogenization Techniques for Core Calculations," *Progress in Nuclear Energy*, **51**, 1, 14 – 31 (2009).

[14] P. Benoist, "Streaming Effects and Collision Probabilities in Lattices," *Nuclear Science and Engineering*, **34**, 285 – 307 (1968).

[15] T.J. Trahan, *An Asymptotic, Homogenized, Anisotropic, Multigroup Diffusion Approximation to the Neutron Transport Equation*, Ph.D. Thesis, University of Michigan, Ann Arbor, MI, USA (2014).

[16] E.M. Gelbard, "Anisotropic Neutron Diffusion in Lattices of the Zero-Power Plutonium Reactor Experiments," *Nuclear Science and Engineering*, **54**, 327 - 340 (1974).

[17] E.M. Gelbard, "Simplified Spherical Harmonics Equations and Their Use in Shielding Problems," WAPD-T-1182 (Rev 1), February 1961.

[18] E.W. Larsen, J.E. Morel and J.M. McGhee, "Asymptotic Derivation of the Simplified P_N Equations," Proc. ANS Topical Meeting, *Mathematical Methods and Supercomputing in Nuclear Applications, M&C + SNA 93*, April 19 – 23, 1993, Karlsruhe, Germany, **1**, 718 (1993).

[19] E.W. Larsen, "Asymptotic Derivation of the Multigroup P_1 and SP_N Equations," *Transactions of the American Nuclear Society*, **69**, 209 (1993).

[20] E.W. Larsen, J.E. Morel, and J.M. McGhee "Asymptotic Derivation of the Multigroup P_1 and SP_N Equations with Anisotropic Scattering," *Nuclear Science and Engineering*, **123**, 328 (1996).

[21] D. Tomašević and E.W. Larsen, "Variational Derivation of Simplified P_2 Equations with Boundary Conditions," *Transactions of the American Nuclear Society*, **70**, 159 (1994).

[22] D.I. Tomašević and E.W. Larsen, "Variational Derivation of the Simplified P_2 Equations with Boundary and Interface Conditions," Proc. ANS Topical Meeting, *International Conference on Mathematics and Computations, Reactor Physics, and Environmental Analyses*, April 30 – May 4, 1995, Portland, Oregon, **1**, 319 (1995).

[23] P.S. Brantley and E.W. Larsen, "Variational Derivation of the Simplified P_3 Approximation," Proc. ANS Topical Meeting, *Joint International Conference on Mathematical Methods and Supercomputing for Nuclear Applications*, October 5-10, 1997, Saratoga Springs, New York, **1**, 910 (1997).

[24] R.P. Rulko and E.W. Larsen, "Variational Derivation of Multigroup P_1 Equations and Boundary Conditions," *Proc. ANS Topical Meeting, Advances in Mathematics, Computations, and Reactor Physics*, April 29 - May 2, 1991, Pittsburgh, **4**, Sec. 17.1, p. 2-1 (1991).

[25] T.J. Trahan and E.W. Larsen, "An Asymptotic Homogenized Diffusion Approximation. I. Theory," *Proceedings of Advances in Reactor Physics Linking Research, Industry, and Education (PHYSOR 2012)*, Knoxville, TN, USA April 15-20 (2012).

[26] E.W. Larsen, "Course Notes for NERS 543: Numerical Reactor Theory II, University of Michigan," (2010).

[27] X-5 Monte Carlo Team, "MCNP - A General N-Particle Transport Code, Version 5, Volume I: Overview and Theory," Tech. Rep. LA-UR-03-1987, Los Alamos National Laboratory, 2003.

[28] M. H. Kalos and P. A., *Monte Carlo Methods*, 2nd edition, Wiley-Blackwell, Hoboken, NJ, USA (2008).

[29] A.G. Ramm, "A Simple Proof of the Fredholm Alternative and a Characterization of the Fredholm Operators," *American Mathematical Monthly*, **108**, 9, 855-860 (2001).

[30] "Benchmark on Deterministic Transport Calculations Without Spatial Homogenisation A 2-D/3-D MOX Fuel Assembly Benchmark," Tech. Rep. NEA/NSC/-DOC(2005)16 (2005).

[31] B. Kochunas, B. Collins, D. Jabaay, T.J. Downar, and W.R. Martin, "Overview of Development and Design of MPACT: Michigan Parallel Characteristics Transport Code," *Proceedings of International Conference on Mathematics and Computational Methods Applied to Nuclear Science and Engineering (M&C 2013)*, Sun Valley, ID, USA May 5-9 (2013).

[32] "VERA Core Physics Benchmark Progression Problem Specifications (Rev. 2)," Tech. Rep. CASL-U-2012-0131-002, Oak Ridge National Laboratory, Oak Ridge, TN, http://www.casl.gov/publications.shtml (2013).